Scientific Research

Journal of Modern Physics

www.scirp.org/journal/jmp

Scientific
Research

TABLE OF CONTENTS

Volume 1   Number 3   August 2010

Journal of Modern Physics (JMP)

Journal Information

SUBSCRIPTIONS

SERVICES

COPYRIGHT

PRODUCTION INFORMATION

Scientific
Research

Effect of Kind Rolling on the Properties of Plasma-Formed Nitride Layers on $Fe_{93}Ni_4Ti_3$

Fayez Mahomoud El-Hossary[1], Sayed Mohammed Khalil[1,2], Magdy Abdel Wahab Kassem[3], Khaled Lotfy[1]

[1]*Physics Department, Faculty of Science, Sohag University, Sohag, Egypt*
[2]*Physics Department, University of Colorado at Boulder, Boulder, USA*
[3]*Department of Materials and Metallurgical Engineering, Faculty of Petroleum and Mining Engineering,*
Suez Canal University, Suez, Egypt
E-mail: khalil_20002000@yahoo.com

Abstract

The nitriding behavior of cold rolled $Fe_{93}Ni_4Ti_3$ specimens was compared with that of hot rolled specimens of the same materials. Radio frequency (rf) nitriding was performed for 10 minutes in a 10^{-2} mbar nitrogen atmosphere. The continuous plasma power was varied from 300-550 W in steps 50 W or less. Results of optical microscopy (OM), x-ray diffraction (XRD) and microhardness measurements (Hv) are presented and discussed with regard to the influence of kind rolling on the nitriding behavior, particularly nitride formation and nitride layer growth on mechanical properties. The results show a remarkable increase of nitrogen diffusivity and microhardness of cold rolled nitride samples. These best results may be attributed to enhancement of the defect and/or a compressive stress.

1. Introduction

Surface plasma nitriding of steels is a well-established technique to produce a modified (hard) surface layer on steels or other iron based alloys with good anti-corrosive and wear resistance properties. Both the nitrogen case depth and the resulting nitride type commonly depend on the nitriding conditions as well as on the properties of material, such as composition, crystallographic structure and the density of various lattice defects. In particular, the thickness and the composition of the nitrided layer are strongly affected by the type of chemical reactions occurring at the specimen's surface as well as by the diffusivity of nitrogen in the treated material.

Nitrogen diffusivity in materials depends on many factors including lattice structure, grain size, chemical composition and defect density. In ultrafine-grained materials, which can be fabricated by consolidation of nanopowders [1,2], sever plastic deformation [3], hot rolling [4] and cold rolling [5], the increased grain boundary area and the dislocation density will promote the diffusion of alloying elements and nitrogen. Therefore, it can be expected that during a thermochemical treatment, e.g. plasma nitriding, such materials will develop a large thick-

ness of nitriding layer. Ferkel *et al*. [6] reported that sever deformation of X5CrNi1810 steel rf nitrided at 350°C can enhance the nitrogen diffusion. This enhancement may be attributed to an increased grain boundary area and dislocation density. In the present investigation, an attempt has been made to evaluate the effect of kind rolling prior to rf plasma nitriding mainly on the properties of $Fe_{93}Ni_4Ti_3$ samples. After rf plasma nitriding, the surface microhardness, nitrogen diffusion layer thickness, surface morphology and formed phases have been analyzed using a Vickers microhardness tester, optical microscopy (OM) and x-ray diffraction (XRD).

2. Experimental Procedure

The material studied was $Fe_{93}Ni_4Ti_3$ iron-based alloy. Cupon-shaped specimens 1 cm × 2 cm in diameter and 2 mm thick. The cupons were prepared by arc-melting pure metals with nominal purities of 99.99 wt.% in an induction furnace under an argon atmosphere (99.9999% purity). The produced castings were heated at 900°C for two hours. The heated specimens were hot rolled with about 10% reduction each time at 800°C up to 2mm thickness. After the initial hot rolling, these specimens

were divided into to two groups. One was rolled at room temperature (cold rolled) and the other was rolled at 900°C (hot rolled). Nitriding treatment of specimens was carried out using a radio frequency (rf) inductively coupled glow discharge, with a continuous mode of operation at 13.56 MHz. The nitriding system consists of a quartz reactor tube with 500 mm in length and 41.5 mm in diameter evacuated by a two-stage rotary pump to a base pressure of 10^{-2} mbarr. Iron-based alloy samples were supported on copper sample holder fitted which were equipped with water cooling pipes. Nitrogen (N_2) was introduced to establish a gas pressure of 8-8.4 × 10^{-2} mbar, measured with a pirani gauge. The distance between the sample holder surface and the rf coil was 2.9 cm and the water cooling rate for samples was 1500 cm^3/min. The discharge is generated by an induction copper coil energized by rf power generator (type HFS 2.5 KW, 13.65 MHz) via a tunable matching network. The surface morphologies and cross-sectional micrographs were examined using an optical microscope. The phase compositions of the surface region of the nitrided layer were studied by X-ray diffraction (XRD) using CuKα radiation in the Θ-2Θ gemoetry. The microhard-

ness was measured by using a Wetzlar microhardness tester with the load of 0.98 N (100 g).

3. Results and Discussion

3.1. Cross-Section Analysis by Optical Microscope

An optical micrograph (OM) cross-section study was employed to determine the thickness of the nitrided cross-section layer (compound layer) of cold and hot (at 900°C) rolled $Fe_{93}Ni_4Ti_3$ samples. The typical cross section views of nitrided samples treated for 10 minutes using different input plasma power levels of 300, 350, 400, 425, 450, 475, 500, 525 and 550 W are shown in **Figure 1** (for cold) and in **Figure 2** (for hot at 900°C) rolled treatments, respectively. From **Figures 1(a)** and **(b)** and **2(a)** and **(b)**, it can be seen that in both types of rolling, the two samples which were nitrided at 300 and 350 W do not contain any observed compound layer. This behavior can be attributed to low plasma processing power (from 300 W to 350 W) where the mobility of ni-
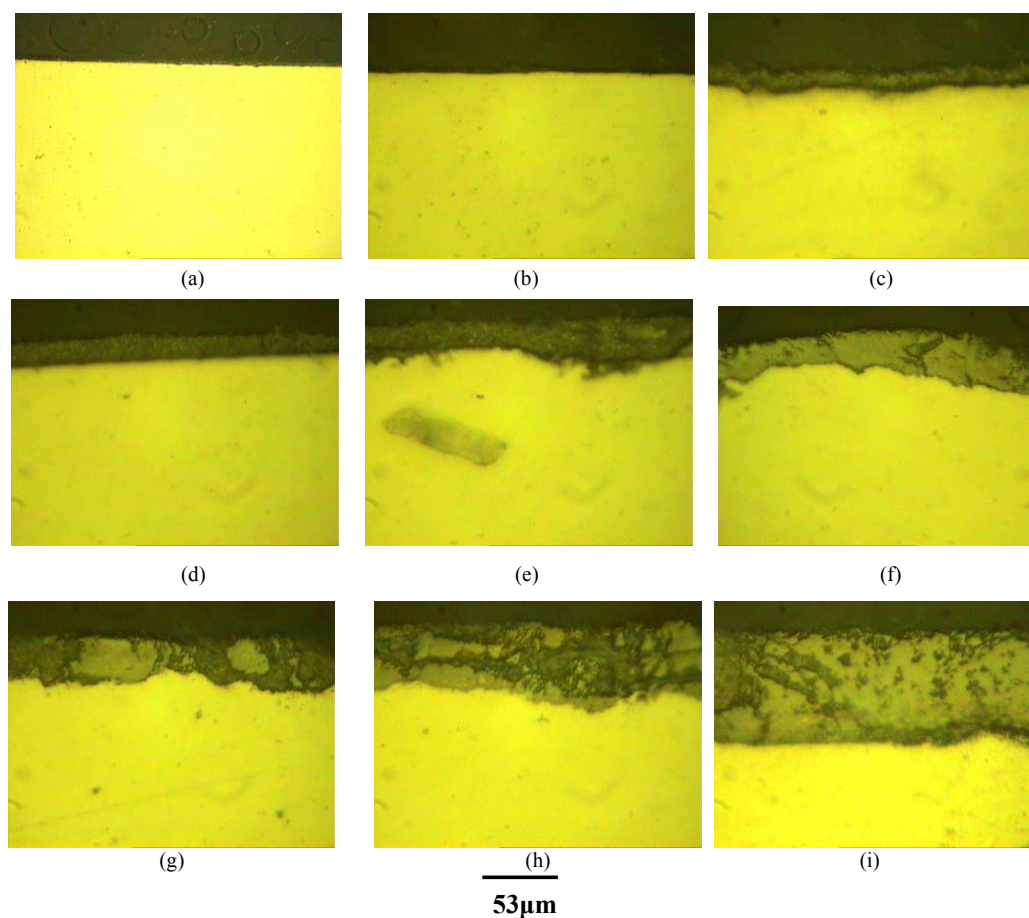
Figure 1. Optical micrographs of compound layer thickness of cold rolled samples $Fe_{93}Ni_4Ti_3$ treated at various plasma processing power input: (a) 300 W; (b) 350 W; (c) 400 W; (d) 425 W; (e) 450 W; (f) 475 W; (g) 500 W; (h) 525 W; (i) 550 W.
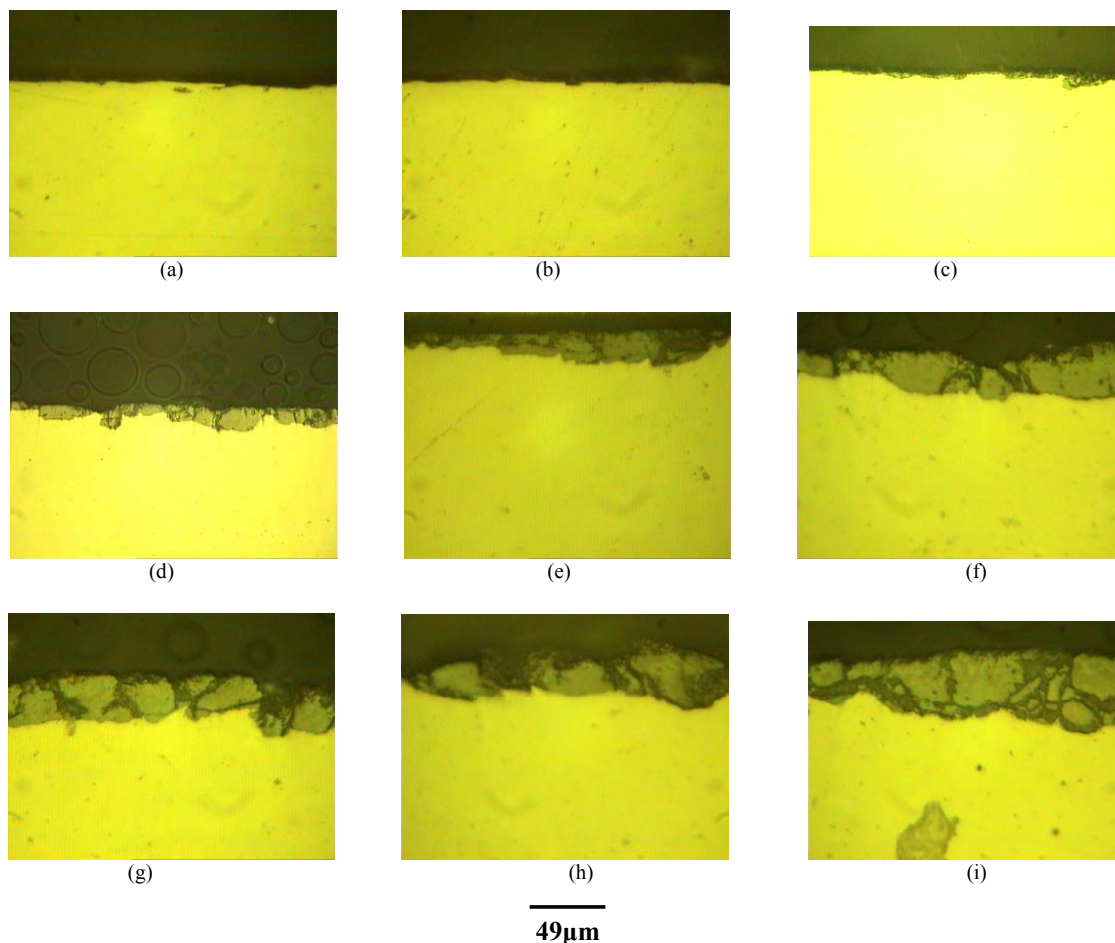
Figure 2. Optical micrographs of compound layer thickness of hot rolled samples $Fe_{93}Ni_4Ti_3$ at 900ºC treated at various plasma processing power input. (a) 300 W; (b) 350 W; (c) 400 W; (d) 425 W; (e) 450 W; (f) 475 W; (g) 500 W; (h) 525 W and (i) 550 W.

trogen atoms is low and penetration is done more easily-through grain boundaries [7]. When the plasma power input is increases with increasing the input plasma power from 400 W to 550 W for cold and hot rolled samples, respectively. The variation range of the layer thickness is 15 μm to 79 μm for cold rolled while from 11 μm to 56 μm for hot rolled at 900°C. This enhancement of thickness for the cold rolled samples is probably due to the promotion of nitrogen ionization, leading to high concentrations of high-energy ions supplied onto the specimen. However, this result agrees with Mahboubi *et al.* [7]. Also, Ferkel *et al.* [8] reported that, the cold high pressure torsion (HPT) processed material shows a thicker and more homogeneous compound layer than the material not subjected to HPT; the nitrogen uptake is largest in the HPT-processed material.

3.2. Compound Layer Thickness

The variation of the compound layer thickness of cold rolled $Fe_{93}Ni_4Ti_3$ and hot rolled $Fe_{93}Ni_4Ti_3$ at 900°C ni-

trided samples for different input plasma power are shown in the **Figures 3** and **4** respectively. However, these values of thickness are measured from the cross section morphology. From these figures, for both the kinds of rolling, one can see that the thickness increases continuously as the plasma power increases. The enhancement of thickness is probably due to the domination of lattice and the penetration of nitrogen atoms through the grains, which all enhance the formation of a more uniform compound layer [8].

3.3. Surface Morphology

Figure 5 shows typical OM micrograph of the surface features of untreated and treated cold rolled $Fe_{93}Ni_4Ti_3$ samples for different plasma processing power. The micrograph of the untreated sample is shown in **Figure 5(a)**. This figure appears to be a relatively coarse-grained structure composed of iron α–phase. The micrographs of treated samples at 300 W and 350 W are shown in **Figures 5(b)** and **(c)**, which reveal no observed change in
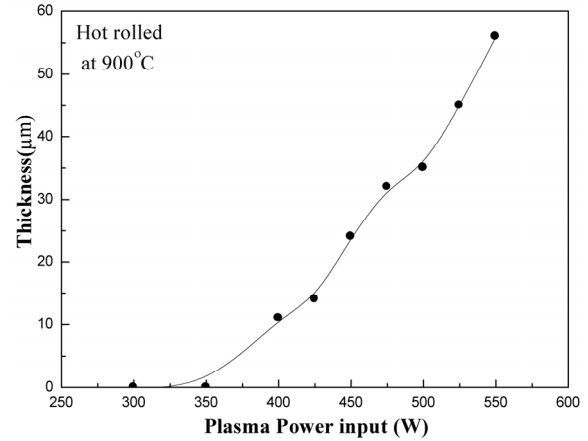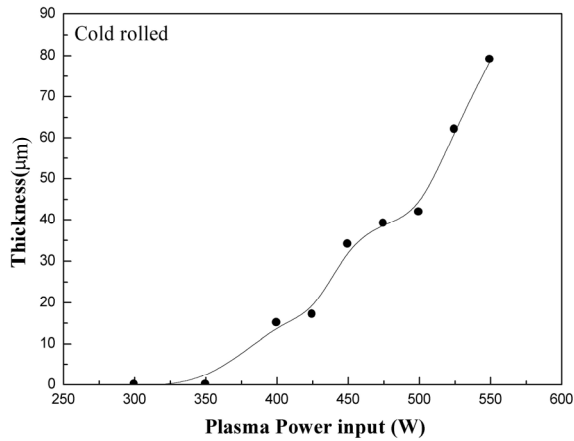
Figure 3. Thickness of compound layer as a function of plasma power for cold rolled samples of Fe$_{93}$Ni$_4$Ti$_3$.

Figure 4. Thickness of compound layer as a function of plasma power for hot rolled samples of Fe$_{93}$Ni$_4$Ti$_3$ at 900ºC.
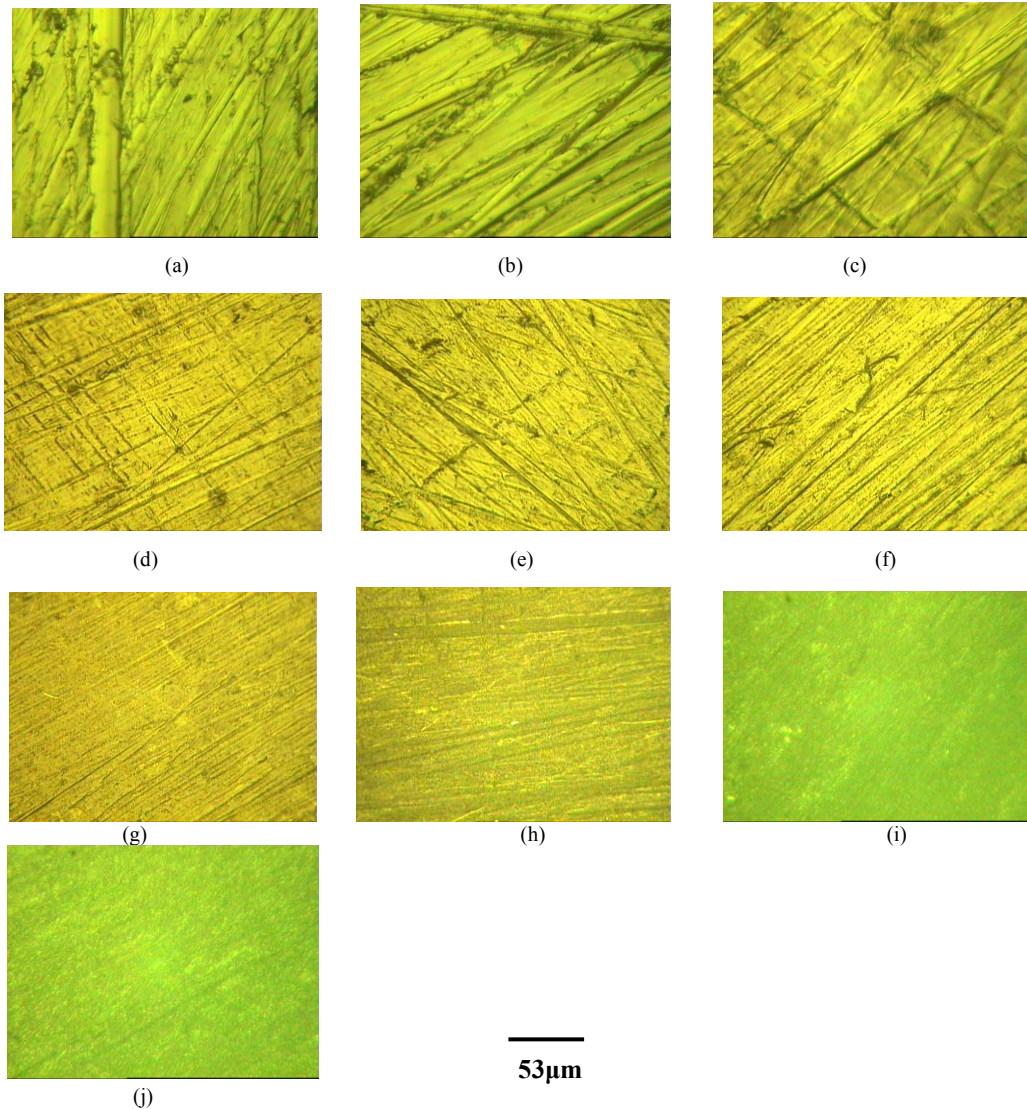
Figure 5. Optical micrographs of the surface morphology of cold rolled samples Fe$_{93}$Ni$_4$Ti$_3$ for plasma processing power input (a) 0.0 W; (b) 300 W; (c) 350 W; (d) 400 W; (e) 425 W; (f) 450 W; (g) 475 W; (h) 500 W; (i) 525 W; (j) 550 W.

the microstructure with respect to the native sample. It means that, this range of plasma processing power is not adequate to form a clear compound layer. **Figures 5(d-j)** shows a different microstructure with respect to the above samples as plasma power increases from 400 W to 550 W. This microstructure is finer and finer in scale, as a result of the increased nitrogen solubility and diffusivity produced by the rf plasma process. This observation agrees with Pantazopoulos *et al*. [9], in which they reported that the liquid nitrocarburised of cold work steel exhibits a very different microstructure with respect to native sample.

3.4. Phase Analysis by XRD Diffraction

The X-ray diffraction patterns with CuKα radiation was used to clarify the effect of kind rolling on the formed phases in the original and nitrided samples at different input plasma processing powers. **Figures 6(a)** and **7(a)** show the diffraction patterns of the original samples of cold and hot (at 900°C) rolled $Fe_{93}Ni_4Ti_3$, respectively. These figures reveal that all intense peaks are assigned to α-Fe-phase. The same diffractgrams can be seen in **Figures 6(b)** and **7(b)** for the nitrided samples of cold and hot rolled $Fe_{93}Ni_4Ti_3$ respectively, when the plasma power input is increased to 350 W. When plasma power input was increased to 450 W and 550 W for cold nitrided samples, the most intense peaks are assigned to ε-$Fe_{2-3}N$ and γ′-Fe_4N phases while the peaks of α-phase are disappeared as shown in **Figures 6(c-d)**. It is worth mentioning that hcp ε-nitride exhibits a higher hardness than fcc- γ-nitride [10]. **Figure 7(c)** shows the diffraction peaks of the hot nitrided sample when plasma power input was adjusted to 450W. From this figure, only ε-phase can be detected while the peaks of α and γ′ phases have disappeared. When plasma power input reached
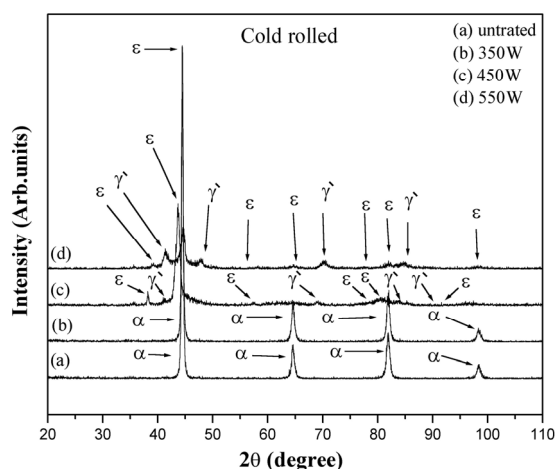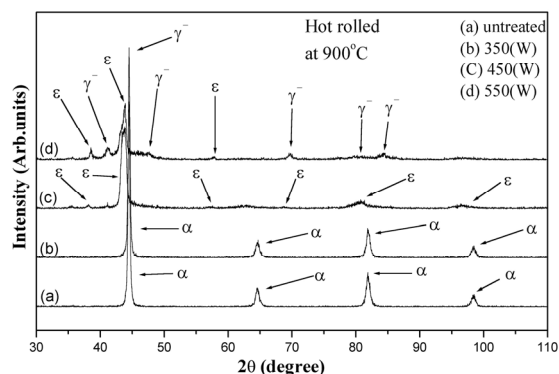
Figure 7. X-ray diffraction patterns for $Fe_{93}Ni_4Ti_3$ samples (a) untreated hot rolled at 900°C and treated for plasma processing powers; (b) 350 W; (c) 450 W; (d) 550 W.

550W for the same sample in **Figure 7(d)**, the intense peaks of γ′–phases emerge, while the peaks of ε-phase decrease significantly. From the above results, the following observations are made: 1) In both the types of rolled samples, the peaks of NiN and TiN cannot be detected. 2) The peak ratio of ε-phase to γ′-phase increases by increasing plasma power input from 450W to 550W for cold rolled samples, while it decreases at the same condition for hot rolled samples. It can be concluded that this is the reason for continuous increase in the microhardness for the cold rolled treated samples after nitrided for 450W, while the microhardness abruptly decreases for the hot rolled treated samples after nitrided for the same power (see the next paragraph). 3) The influence of the Ni present in the samples has not been considered, because the interaction of Ni with N that is even weaker than the interaction between N and Fe. However, these observations agree well with Chezan *et al*. [11], in which they reported that the severe deformation caused by cold rolling for Fe-Ni-Ti and Fe-Ni-Cr leads to formation of large density nucleation sites for new phases, *i.e.* γ′ and ε.

3.5. Microhardness Measurements

In order to clarify the influence of kind rolling on the mechanical properties of nitrided samples, microhardness measurements of nitrided cold rolled and hot rolled (at 900°C) $Fe_{93}Ni_4Ti_3$ samples were performed at a load of P = 100 g (0.89N).

Figure 8 displays the variation of microhardness values of untreated and nitrided cold rolled samples $Fe_{93}Ni_4Ti_3$ against the input plasma power. From this figure, one can notice that the microhardness value of the nitrided samples at 300, 350W equals nearly the same value of untreated sample 297 HV. This trend is probably due to the fact that at 350 W and below, there is not enough rf power to create precipitation, which would lead to significant hard phases. This result is confirmed by XRD analysis and OM observations. When plasma power in

Figure 6. X-ray diffraction patterns for $Fe_{93}Ni_4Ti_3$ samples (a) untreated cold rolled and treated for plasma processing powers; (b) 350 W; (c) 450 W; (d) 550 W.
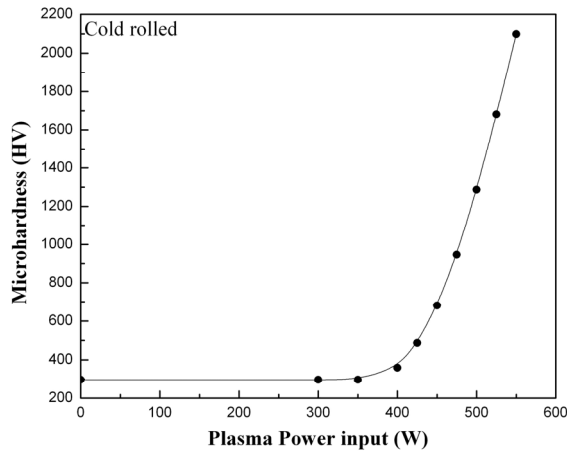
Figure 8. Microhardness values of untreated and treated cold rolled Fe$_{93}$Ni$_4$Ti$_3$ samples for different plasma power input.

put increases from 400 to 550W, the microhardness value increases exponentially to reach the value of 2098 HV. This represents a 7-fold increase in the surface-hardness comparing with the untreated sample (282 HV). The anomalously high microhardness values are due to the fact that high defect density in nitrided samples offers enough nucleation sites for nitrides and enough diffusion paths for nitrogen. In this case, a dense compound layer with high hardness can easily form [6]. Also, the dramatic increase of hardness is a result of compressive stresses, which is induced in the target surface by the cold rolling and a compound layer produced on the target surface by nitriding.

Figure 9 depicts the variation of microhardness values of untreated and nitrided hot rolled (at 900ºC) samples Fe$_{93}$Ni$_4$Ti$_3$ against the input plasma power. From this figure, one can notice that the microhardness values of the nitrided samples at 300 W and 350 W equal nearly the same value of untreated sample 274 HV. As plasma power input increases from 400 W to 450 W, the microhardness value increases continuously to reach the value of 572 HV; this represents a 2-fold increase in the surface hardness comparing with untreated sample. This trend may be credited to the formation of a compound layer thickness of 11 μm to 56 μm, which contains a high concentration of nitrogen [12]. Similar behavior has been observed by Devi and Mohanty [13], in which a microhardness value of 1478 HV in hot rolled D2 steel was achieved after plasma nitriding at 510ºC for 18 h. With the high input plasma power of 475 W or more, the microhardness value decreases. This reduction can be attributed to the decrease the ratio of ε-phase to γ'-phase [10]. However, this result agrees well with XRD analysis.

In light of the microhardness measurements, it can be concluded that a general hardness increase for cold rolled treated samples can be associated with enhancement of
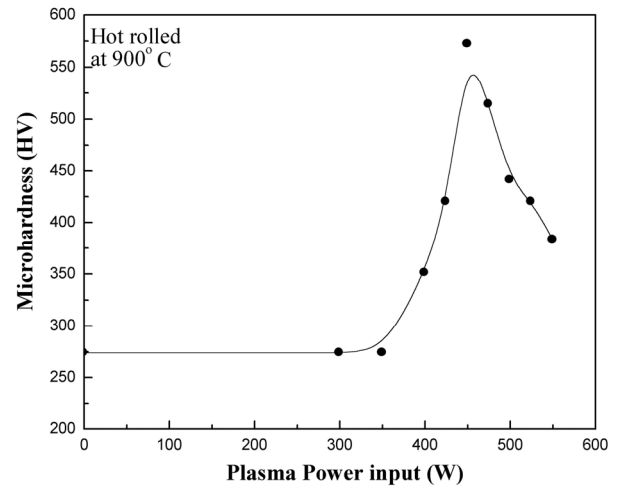
Figure 9. Microhardness values of untreated and treated hot rolled Fe$_{93}$Ni$_4$Ti$_3$ at 900°C samples for different plasma power input.

defect density and/or a compressive stress. *i.e.*, the hardness of the plasma nitrided sample shows a kind of rolling dependent behavior.

4. Conclusions

The thickness, hardness and phase composition of the modified layer formed on cold and hot rolled nitrided Fe$_{93}$Ni$_4$Ti$_3$ are investigated in this work. All of the samples were hardened by forming nitrided layers. The advantage of the pre-cold rolling is that a thicker nitrided layer with higher hardness is formed. The cold rolling process is a well-known technique applied to improve the mechanical properties of steel surfaces. Through this process, a large number of grain boundaries, dislocations and positive holes form through the surface of specimens, which all enhance the nitrogen diffusion. The surface hardness of nitrided cold-rolled Fe$_{93}$Ni$_4$Ti$_3$ samples represents a 3.7-fold increase with respect to the nitrided hot-rolled samples. This trend may be credited to the high defect density of nitrided cold rolled samples, which offers enough nucleation sites for nitrides and enough diffusion paths for nitrogen [12]. The modified surface of nitrided cold rolled samples is characterized with a finer microstructure. The phase analysis dictates that the peak ratio of ε to γ' phase increases by increasing plasma power input from 450 to 550 W for nitrided cold rolled samples, while it decreases at the same conditions for nitrided hot-rolled samples. This is the reason behind the continuous increase in the microhardness for the cold rolled treated samples after application of 450 W plasma power, with a decrease for the hot rolled treated samples after being nitrided for the same power. The most striking results of this work are the increased thickness of the nitrided cold rolled samples. Indeed, diffusion of nitro-

gen by the microcracks mechanism could be expected to be significantly affected by an increase in grain boundary area as a result of cold rolling. However, the experimental evidence demonstrates that the microstructure of cold rolled material does have a significant influence on nitrogen diffusion.

5. Acknowledgments

6. References

[1] F. M. El-Hossary, "The Influence of Surface Microcracks and Temperature Gradients on the Rf Plasma Nitriding Rate," *Surface and Coatings Technology*, Vol. 150, No. 2, 2002, pp. 277-281.

[2] F. M. EL-Hossary, N. Z. Negm, S. M. Khalil, A. M. Abd Elrahman and D. N. Mcllroy, "RF Plasma Carbonitriding of AISI Austenitic Stainless Steel," *Surface and Coatings Technology*, Vol. 141, No. 2-3, 2001, pp. 194-201.

[3] C. B. Craus, A. R. Chezan, N. G. Chechenin, D. O. Boerma and L. Niesen, "Soft Magnetism in Nitrided $Fe_{93}Ni_4Cr_3$ and $Fe_{94}Ni_4Ti_2$ Cold–Rolled Alloys," *Journal of Magnetism and Magnetic Materials*, Vol. 263, No. 1-2, 2003, pp. 47-56.

[4] G. Edrem and Y. Taptik, "Effect of Hot Rolling Conditions to Produce Deep Drawing Quality Steels for Continuous Annealing Process," *Journal of Material Processing Technology*, Vol. 170, No. 1-2, 2005, pp. 17- 23.

[5] H. Katoh, H. Takachi, N. Takahashi and M. Abe, "Cold Rolled Steel Sheets Produced by Continuous Annealing, Technology Continuously Annealed Cold-Rolled Steel," 1984, pp. 37-38.

[6] H. Ferkel, M. Glatzer, Y. Estrin and R. Z. Valiev, "RF Plasma Nitriding of Severely Deformed High Alloyed Steel," *Scripta Material Science*, Vol. 46, No. 9, 2002, pp. 623-628.

[7] F. Mahboubi and K. Abdolvahabi, "The Effect of Temperature on Plasma Nitriding Behavior of DIN 1.6959 Low Alloy Steel," *Vacuum*, Vol. 81, No. 3, 2006, pp. 239-243.

[8] H. Ferkel, M. Glatzer, Y. Estrin, R. Z. Valiev, C. Blawert and B. L. Mordike, "RF Plasma Nitriding of Severely Deformed Iron-Based Alloys," *Materials Science and Engineering A*, Vol. 348, No. 1-2, 2003, pp. 100-110.

[9] G. Pantazopoulos, P. Psyllaki, D. Kanakis, S. Antoniou, K. Papadimitriou and J. Sideris, "Tribological Properties of a Liquid Nitrocarburised Special Purpose Cold Work Tool Steel," *Surface and Coatings Technology*, Vol. 200, No. 20-21, 2006, pp. 5889-5895.

[10] H. Ferkel, Y. Estrin, C. Blawert and R. Z. Valiev, "RF Nitriding of Severely Deformed Armco Iron and St2 K50," *Surface and Coatings Technology*, Vol. 173-174, 2003, pp. 1164-1170.

[11] A. R. Chezan, C. B. Craus, N. G. Chechenin, T. Vystavel, L. Niesen, J. T. M. De Hosson and D. O. Boerma, "On the Formation of Ultra-Fine Grained Fe-Base Alloys Via Phase Transformations," *Materials Science and Engineering A*, Vol. 367, No. 1-2, 2004, pp. 176-184.

[12] F. M. El-Hossary, S. M. Khalil, K. Lotfy and M. A. Kassem, "The Influence of Hot-Rolled Temperature on Plasma Nitriding Behavior of Iron-Based Alloys," *Journal of Low Temperature Physics*, Vol. 156, No. 1-2, 2009, pp. 38-47.

[13] M. U. Devi and O. N. Mohanty, "Plasma-Nitriding of Tool Steels for Combined Percussive Impact and Rolling Fatigue Wear Applications," *Surface and Coatings Technology*, Vol. 107, No. 1, 1998, pp. 55-64.

Scientific
Research

A Model for the Quantization of the Hall Resistance in the Quantum Hall Effect

Paul Bracken

Department of Mathematics, University of Texas, Edinburg, USA
E-mail: *bracken@panam.edu*
Received January 25, 2010; *revised February* 26, 2010; *accepted March* 20, 2010

Abstract

Some aspects of anyon physics are reviewed with the intention of establishing a model for the quantization of the Hall conductance. A single particle Schrödinger model is introduced and coupled with a constraint equation formulated from the anyon picture. The Schrödinger equation-constraint system can be converted to a single nonlinear differential equation and solutions for the model can be produced.

Keywords: Anyon, Hall Resistance, Conductance, Composite Particles

1. Introduction

The quantum Hall effect is a recently discovered and now well known phenomenon which appears in a two-dimensional electron system which exhibits spectacular phenomena when subjected to an intense transverse magnetic field [1]. First encountered experimentally [2], the integer quantum Hall effect has received much study, and was subsequently followed by the fractional Hall effect [3,4]. Referring to these two effects as the quantum Hall effect, the Hall resistance is found experimentally to exhibit plateaus at the quantized values

$$R_H = \frac{h}{fe^2} \qquad (1)$$

where f is either an integer or a simple rational fraction. Thus (1) incorporates both of these effects. For the integer case, f takes on integer values $f = n = 1, 2, 3, \cdots$, and some prominent fractions for the fractional case appear in sequences such as $f = \dfrac{n}{2n \pm 1}, \ \dfrac{n}{4n \pm 1}$.
The two effects show remarkable similarities despite the differences in origin. In both effects, the localization of electrons and quasiparticles is believed to be responsible for the formation of the plateaus in the Hall conductivity. At the transitions between successive plateaus in the integer quantum Hall effect, scaling behavior has been observed. Theoretically, the aim in understanding this is to solve the many-body quantum mechanical problem defined by the many body Hamiltonian given by

$$H = \sum_j \frac{1}{2m_e}\left[\vec{p}_j + \frac{e}{c}\vec{A}(\vec{r}_j)\right]^2 + \frac{1}{2}\sum_{j \neq k}\frac{e^2}{\epsilon r_{jk}} + \sum_j U(\vec{r}_j) \quad (2)$$

The first term on the right-hand side is the kinetic energy in the presence of a constant external magnetic field; the second term is the Coulomb interaction energy; and the third term is a one-body potential due to a uniform positive background. The electrons are constrained to move in the two-dimensional xy-plane.

It is the intention here to set up and solve a simple version of (2) subject to a physical constraint. Such pictures occur often in this area, for example Landau levels are determined by solving the Schrödinger equation with a harmonic oscillator potential. Thus a simple physical model which emphasizes geometry in the problem is constructed for a Hall system and it is shown that solutions can be found. A wavefunction is obtained under some specific assumptions. It will be seen that some physical properties that are very relevant can be established from the model; in particular, the quantization of the Hall resistance, (1) can be obtained. To begin to set up the model some more physical concepts need to be introduced. Let us proceed to this [5,6].

2. Setting up the Model-Composite Particles

Let $\Psi(\vec{x})$ be the electron field. An anyon may be thought of as a flux carrying a boson or fermion quantum number. A composite-particle field $\phi(\vec{x})$ is defined by an operator phase transformation

$$\phi(\vec{x}) = e^{-im\Theta(\vec{x})}\Psi(\vec{x}). \qquad (3)$$

The phase field $\Theta(\vec{x})$ is defined by

$$\Theta(\vec{x}) = \int d^2y\, \vartheta(\vec{x} - \vec{y})\rho(\vec{y}), \qquad (4)$$

where m in (3) is an integer and $\vartheta(\vec{x} - \vec{y})$ in (4) is the angle made between the vector $\vec{x} - \vec{y}$ and the x-axis; ρ represents anyon density. The effect of the operator phase transformation (3) is to attach m flux quanta to each electron. Composite particles experience the effective magnetic field $B_{eff}(\vec{x})$ described by the potential $A_j(\vec{x})$, where $A_j(\vec{x})$ depends on the external vector potential $A_j^{ext}(\vec{x})$ and a field $C_k(\vec{x})$, which is an auxiliary field determined solely by the density $\rho(\vec{x})$,

$$A_j(\vec{x}) = A_j^{ext}(\vec{x}) + C(\vec{x}). \tag{5}$$

Therefore, from (5), it follows that

$$B_{eff}(\vec{x}) = -\epsilon_{ij}\partial_i A_j(\vec{x}) = B_\perp - m\phi_D \rho(\vec{x}), \tag{6}$$

and so the effective magnetic flux is the sum of the real magnetic flux and a term which can be regarded as a Chern-Simons flux.

Now suppose that $A_j(\vec{x})$ in (4) satisfies the Coulomb gauge condition

$$\partial_j A_j(\vec{x}) = 0. \tag{7}$$

It is possible to express $A_j(\vec{x})$ in terms of a scalar field $A(\vec{x})$ as

$$A_j(\vec{x}) = -\frac{\hbar}{e}\epsilon_{jk}\partial_k A(\vec{x}). \tag{8}$$

This conclusion is only possible in a planar geometry. Substituting (8) into $B_{eff}(\vec{x})$, the field $A(\vec{x})$ can be regarded as the scalar potential of the effective magnetic field,

$$B_{eff}(\vec{x}) = -\frac{\hbar}{e}\nabla^2 A(\vec{x}). \tag{9}$$

This is basically the type of constraint we would like to apply in order to solve (2); that is, by taking a particular reasonable form for $B_{eff}(\vec{x})$.

The state vector Ψ is assumed to fully or very nearly characterize the electronic state of the system. The total free charge is given by

$$Q = e\int_s |\Psi|^2 \, d^2x. \tag{10}$$

The steady state time-independent wavefunction is given by

$$\psi = e^{-iEt/\hbar}\psi_0,$$

where Ψ_0 is time-independent and will have to satisfy the time-independent Schrödinger equation

$$H\psi_0 = E\psi_0. \tag{11}$$

Let us incorporate an additional assumption into the

construction of this model here. Let us suppose that we can write $B_{eff}(\vec{x}) = B(\vec{x})$ in the following form

$$B(\vec{x}) = |k\Psi|^2, \tag{12}$$

where k is related to the total magnetic flux through the surface; that is, the number of flux quanta of the magnetic field and other constants. The magnetic flux density affects the electronic states as it modifies the Hamiltonian. Of course, the Hamiltonian is modified by the vector potential, which in a simply-connected domain is given by the usual formula $\nabla \times A = B(x)$. For example, suppose we write and use (12) in the form

$$B(\vec{x}) = a|\Psi_0|^2, \tag{13}$$

and a is a constant which satisfies

$$\Phi = \int_s B(\vec{x})d^2x = \int_s a|\Psi_0|d^2x = a\frac{Q}{e} = aN \tag{14}$$

In (14), N is the number of relevant current carrying charge quanta. Moreover, let M denote the number of magnetic flux quanta, which means the total flux can be written as

$$\Phi = M\frac{h}{2e}. \tag{15}$$

When the flux and charge are quantized, these results imply that a is a fraction which can be expressed in terms of the flux quantum

$$a = \frac{M}{N}\frac{h}{2e}. \tag{16}$$

On a simply connected region, the vector potential can be represented as a one-form given in terms of a single function φ, which stands for A here, as

$$A = \varphi_x dy - \varphi_y dx. \tag{17}$$

Using (17), the magnetic field can be calculated and then (13) yields a constraint equation

$$\varphi_{xx} + \varphi_{yy} = a|\Phi_0|^2. \tag{18}$$

3. Solution of the Schrödinger Equation

The main objective here is to solve the time-independent Schrödinger equation coupled with Equation (18) to obtain Ψ. Of course, vector potential (17) appears in the Schrödinger equation, as can be clearly seen from (2). This procedure will lead to a nonlinear equation; however, it will be found that solutions with the correct physical properties can be determined in closed form. Keeping the first term in (2), the left hand side without the overall multiplicative constant applying (17) leads to

$$-\left(\partial_x^2 + \partial_y^2\right)\Psi_0 + 2i\frac{e}{\hbar}\left(-\varphi_y\Psi_{0,x} + \varphi_x\Psi_{0,y}\right) + \frac{e^2}{\hbar^2}\left(\varphi_x^2 + \varphi_y^2\right)\Psi_0$$

Therefore (11) written out in full takes the form,

$$-\hbar^2\left\{-\left(\partial_x^2+\partial_y^2\right)\Psi_0+2\mathrm{i}\frac{e}{\hbar}\left(-\varphi_y\Psi_{0,x}+\varphi_x\Psi_{0,y}\right)+\frac{e^2}{\hbar^2}\left(\varphi_x^2+\varphi_y^2\right)\Psi_0\right\}$$
$$=2mE\Psi_0.$$

(19)

Now the problem takes the form of finding solutions to (19) subject to the condition (18) This will not be done in a completely general way, but with some assumptions which will lead to a physically relevant result.

Suppose the electron system describes a rectangular geometry in the xy plane. Moreover, let Ψ_0 have a plane wave dependence in the x direction, so solutions which have the structure

$$\Psi_0\left(x,y\right)=e^{ikx}\theta\left(y\right).$$

(20)

is sought where $\theta\left(y\right)$ is a real function of y. Let us take the function in the vector potential to be independent of x,

$$\varphi=\varphi\left(y\right)$$

(21)

The derivatives of Ψ_0 can be calculated based on (20) and then substituted into (19),

$$-\hbar^2\left(-k^2\theta\left(y\right)+\theta_{yy}\left(y\right)\right)+2e\hbar k\varphi\left(y\right)\theta\left(y\right)+e^2\varphi_y^2\theta\left(y\right)$$
$$=-2mE\theta\left(y\right).$$

(22)

This takes the form of a second order equation for $\theta\left(y\right)$, but it is coupled to $\varphi\left(y\right)$ in (17),

$$-\hbar^2\theta_{yy}\left(y\right)+\left(\hbar k+e\varphi_y\right)\theta\left(y\right)=-2mE\theta\left(y\right).$$

(23)

If φ is assumed to have the form (21), then $\varphi_{xx}=0$ and (18) assumes the simple form

$$\varphi_{yy}=a\theta^2\left(y\right).$$

(24)

Since the right-hand side of (24) depends only on y, (24) can be integrated once to obtain φ_y, which appears in (23), in terms of $\theta\left(y\right)$ as

$$\varphi_y\left(y\right)=a\int_{y_0}^{y}d\tau\theta^2\left(\tau\right).$$

(25)

Imposing $\varphi_y\left(0\right)=y_0$. Substituting (25) into (23), this coupled system is reduced to the following nonlinear eigenvalue problem

$$-\theta_{yy}\left(y\right)+(k+\frac{e}{\hbar}a\int_{y_0}^{y}d\tau\theta^2\left(\tau\right))^2\theta\left(y\right)=-\frac{2mE}{\hbar^2}\theta\left(y\right).$$ (26)

Therefore, the dependent variable in (26) is $\theta\left(y\right)$. In addition to (26), it is useful to write down a decoupled version which is obtained by introducing a new variable $\sigma\left(y\right)$ given by

$$\sigma\left(y\right)=k+\frac{e}{\hbar}a\int_{y_0}^{y}d\tau\theta^2\left(\tau\right).$$

(27)

Equation (26) can be written in the form of a pair of equations as follows,

$$\sigma_y\left(y\right)=\frac{e}{\hbar}a\theta^2\left(y\right),-\theta_{yy}\left(y\right)+\sigma^2\left(y\right)\theta\left(y\right)=-\frac{2mE}{\hbar^2}\theta\left(y\right).$$

(28)

The Hall resistance for this two-dimensional system can be calculated based on (28), in fact it can be written in terms of $\sigma\left(y\right)$. The geometry is that of a rectangular plate with edges which are parallel to the x and y-axes. To be consistent with (20), where the x-dependence in Φ_0 is assumed to be a plane wave, only the y dimension will be of significance here. The terminations for integration localized at fixed y-coordinates, are termed the left (L) and right (R) edges of the geometry. The Hall potential is defined as the difference of potentials between these two edges of the rectangle. In fact, the Hall potential can be obtained from (26), or better in terms of the solution for $\sigma\left(y\right)$ by means of

$$V_\mathrm{H}=\frac{\hbar^2}{2me}\left(\sigma^2\left(R\right)-\sigma^2\left(L\right)\right),$$

(29)

where R and L refer to right and left. Only the longitudinal x or plane wave component of the current density contributes

$$j_\mathrm{x}=\frac{e}{m}\mathrm{Re}\,\psi_0\left(i\hbar\vec{\nabla}+e\vec{A}\right)\psi_0=-\frac{e\hbar}{m}k+\frac{e}{\hbar}a\int_{y_0}^{y}d\tau\theta^2\left(\tau\right)\theta^2\left(y\right).$$

(30)

The potential V_H is transverse to the current. From (28), since θ^2 can be related to σ_y, the current density can be represented entirely in terms of the variable σ as

$$j_\mathrm{x}=-\frac{eh}{m}\sigma\theta^2=-\frac{\hbar^2}{am}\sigma\sigma_y=-\frac{\hbar^2}{2am}\left(\sigma^2\right)_y.$$

Integrating j_x and using the definition of V_H given in (29), I_x can be related to V_H as follows,

$$I_\mathrm{x}=\int_R^L j_\mathrm{x}dy=-\frac{\hbar^2}{2am}\int_R^L\left(\sigma^2\right)_y\,dy=\frac{\hbar^2}{2am}\left(\sigma^2\left(R\right)-\sigma^2\left(L\right)\right)=\frac{e}{a}V_\mathrm{H}.$$

(31)

By means of (16), the quantity a can be eliminated from (31) to produce the following remarkable formula,

$$I_\mathrm{x}=\frac{N}{M}\frac{2e^2}{h}V_\mathrm{H}.$$

(32)

The result in (32) immediately implies the Hall resistance is quantized according to,

$$R_\mathrm{H}=\frac{V_\mathrm{H}}{I_\mathrm{x}}=\frac{M}{N}\frac{h}{2e^2}.$$

(33)

Finally, it will be shown that a wavefunction ψ_0 can be determined based on the coupled system (28). In fact, the coupled equations in (28) can be combined into a single nonlinear differential equation for the function $\sigma(y)$, from which $\theta(y)$ can be determined. To begin to do this, differentiate the first equation in (28) and then divide this by σ_y to obtain

$$\frac{\sigma_{yy}}{\sigma_y} = 2\frac{\theta_y}{\theta}. \qquad (34)$$

Differentiating both sides of this, there follows

$$2\frac{\theta_{yy}}{\theta} - 2\frac{\theta_y^2}{\theta^2} = \frac{\sigma_{yyy}}{\sigma} - \frac{\sigma_{yy}^2}{\sigma_y^2}. \qquad (35)$$

Squaring both sides of (34), an additional expression for θ_y^2/θ^2 is obtained. Substituting this into the right hand side of (35),

$$\frac{\theta_{yy}}{\theta} = \frac{\sigma_{yyy}}{2\sigma_y} - \frac{1}{4}\left(\frac{\sigma_{yy}}{\sigma_y}\right)^2. \qquad (36)$$

From the second equation in (28), upon dividing by θ, it follows that

$$\frac{\theta_{yy}}{\theta} = \sigma^2 + \frac{2mE}{\hbar^2}. \qquad (37)$$

Substituting (37) into (36), a third order nonlinear equation in terms of the independent variable σ results,

$$\frac{\theta_{yyy}}{\theta_y} = \frac{1}{2}\left(\frac{\sigma_{yy}}{\sigma_y}\right)^2 + 2\sigma^2 - 2\hat{E}, \qquad (38)$$

where we put

$$\hat{E} = -\frac{2mE}{\hbar^2}. \qquad (39)$$

A general solution to (38) may not be possible, however, something can be done. Note that upon omitting $(2\sigma^2 - 2\hat{E})$ from (38), the equation can be integrated. Thus, we have $\left(\ln(\sigma_{yy})\right)_y - \frac{1}{2}\left(\ln(\sigma_y)\right)_y = 0$, and integrating gives $(\sigma_{yy})^2 - \hat{c}\,\sigma_y = 0$. This can be integrated as well to give $\sigma(y) = \frac{1}{3c_1}(c_1 y + c_2)^3 + c_3$. A specific physically realistic solution to the general form of (38) can be approached as follows. The first equation in (28) implies that the sign of $\sigma(y)$ is determined by a, therefore, when θ does not vanish, σ must be a monotonic function. Consequently, one way in which a class of solution can be obtained is to consider the case in which σ_y is only a function of σ,

$$\sigma_y = w(\sigma). \qquad (40)$$

In fact, $g(\sigma)$ can be determined explicitly. Differentiating both sides of (40) with respect to y, we get

$$\sigma_{yy} = \sigma_y w_\sigma = w w_\sigma, \sigma_{yyy} = w\left(w_\sigma^2 + w w_{\sigma\sigma}\right). \qquad (41)$$

Substituting (40) and (41) into (38) gives rise to the following equation for w,

$$w w_{\sigma\sigma} + \frac{1}{2}w_\sigma^2 = 2\left(\sigma^2 - \hat{E}\right), \qquad (42)$$

Clearly (42) is nonlinear, however, there is a way to produce a solution which is physically reasonable. There exists a quadratic polynomial solution for w which can be expressed in terms of σ as

$$w(\sigma) = \alpha\sigma^2 + \beta\sigma + \gamma$$

These constants can be specified upon substitution in (42), and it will constitute a solution provided that $\beta = 0$ and

$$w(\sigma) = \pm\frac{1}{\sqrt{2}}\sigma^2 - \sqrt{2}\,\hat{E}. \qquad (43)$$

Taking (43) and replacing the result in (40), it is clear the resulting equation can be separated to give

$$\int \frac{\sqrt{2}\,d\sigma}{\pm\sigma^2 - 2\hat{E}} = y + c. \qquad (44)$$

The negative sign gives a tangent function solution which will be prone to have poles and can be written

$$\sigma(y) = -\sqrt{2\hat{E}}\,\tan\left(\sqrt{2}\,(y + c)\right).$$

However, the other choice of sign in (44) gives rise to the result,

$$-\frac{1}{\sqrt{\hat{E}}}\,\text{arctan}(\frac{\sigma}{\sqrt{2\hat{E}}}) = y + c.$$

This can be solved explicitly for the function $\sigma(y)$,

$$\sigma(y) = -\sqrt{2\hat{E}}\,\tanh\left(\sqrt{\hat{E}}\,(y + c)\right) = -\sqrt{2\hat{E}}\,\frac{1 - Ce^{-2\sqrt{\hat{E}y}}}{1 + Ce^{-2\sqrt{\hat{E}y}}}. \qquad (45)$$

By differentiating (45), an expression for $\theta^2(y)$ is obtained. The function $\theta(y)$ which we need to write the wavefunction (20) is found from the square root of this, namely

$$\theta(y) = \pm 2 \cdot 2^{\frac{1}{4}}\left(C_1\frac{\hbar\hat{E}}{ea}\right)^{\frac{1}{2}}\frac{e^{-\sqrt{\hat{E}y}}}{1 - C_1 e^{-2\sqrt{\hat{E}y}}}. \qquad (46)$$

The wavefunction is then determined using (46) by means of,

$$\Psi = e^{-iEt/\hbar} e^{ikx} \theta(y).$$

This is a bounded function on any right half axis and square integrable over the rectangular area. Thus there exists a solution with the desired physical properties.

Therefore, it has been seen how (1) emerges and that physical classes of solutions to (2) can be investigated. Most importantly, a link between the wavefunctions implied by the model and the calculation of a corresponding resistence for the model has been shown.

4. Conclusions

An elementary model for the quantum Hall effect has been developed. It is known in this field that simple models based on Schrödinger equations can be very useful in studying the effect. For example, the equation is solved with the harmonic oscillator potential to describe and obtain the energies of Landau levels. The model emphasizes several aspects of the geometry of the system in obtaining the results (32,33). It is quite interesting that a single particle Schrödinger equation can be obtained and solved in closed form, and which incorporates a significant amount of the physics involved.

5. References

[1] J. K. Jain, "Composite Fermions, Perspectives in Quantum Hall Effects," In: S. D. Sarma and A. Pinczuk Eds., J. Wiley and Sons, New York, 1987.

[2] K. von Klitzing, G. Dorda and M. Pepper, "New Method for High-Accuracy Determination of the Fine Structure Constant Based on Quantized Hall Resistance," *Physics Review Letters*, Vol. 45, No. 6, 1980, pp. 494-497.

[3] R. B. Laughlin, "Quantized Hall conductivity in Two dimensions," *Physical Review B*, Vol. 23, No. 10, 1981, pp. 5632-5633.

[4] R. E. Prange and S. M. Girvin, "The Quantum Hall Effect," Springer Verlag, New York, 1987.

[5] Z. F. Ezawa, "The Quantum Hall Effects, Field Theoretical Approach and Related Topics," World Scientific, Singapore, 2000.

[6] R. B. Laughlin, "Fractional Quantization," *Reviews of Modern Physics*, Vol. 71, No. 4, 1999, 863-874.

Scientific
Research

Quantum Statistical Properties of Resonant Radiation Scattered on Excited Systems

Boris A. Veklenko

Joint Institute for High Temperature of Russian Academy of Science, Moscow, Russia
E-mail: VeklenkoBA@yandex.ru

Abstract

The scattering of resonant radiation on an excited atom is considered. It is shown that the scattering cross section calculated with the help of quantum theory of radiation is five times larger than the one calculated using semi-classical theory. The quantum theory predicts, in general, the change in internal quantum statistical properties of light due to the scattering processes on excited atoms.

1. Introduction

The quantum excited systems possess remarkable properties. They manifest themselves most prominently in lasers and masers, which were created in the middle of the last century. The theory of these devices was elaborated by W. Lamb [1] on the base of a semi classical theory of radiation which deals with classical electromagnetic field. Later the quantum theory was proposed [2]. It is possible to state omitting the fluctuations properties that both the semi classical and the quantum theories result practically in the same results for quantum means values. Such a fact resulted in overestimation of the applicability of the semi-classical theory. In 1966 year, Ch. Koester predicted the effect of light enhancement [3] by selective reflection of resonant radiation from excited media. All efforts of quantitative explaining this effect on the base of semi-classical theory of radiation discussed in monograph [4] were unsuccessful [5,6]. It was shown later that quantum field theory should be used instead [7], but the mathematically problems on this way occurred very difficult [8]. The consequences of such a theory manifest themselves on a macroscopic level. The correct description of stimulated radiation plays an especial role when the resonant reflection of light from excited media is considered. Nevertheless, there are recent works [9] which make use the semi-classical theory and Fresnel's formulae to describe the reflection of light from enhanced media.

Much attention has been paid recently to the effect of the enhanced transmission of light through the metallic films [10,11]. There is no agreement between theory and experiment. It is believed that the enhancement of radiation may be explained through the interaction of light with induced standing surface—plasmon waves. Thus we deal with effects of stimulate radiation, which means that one should use the quantum field theory.

Examples shown above made us revise the theory of resonant radiation scattering on excited systems. The conventional perturbation technique is not adequate to describe the resonant scattering and it is necessary to sum up (Dyson summation) the infinitely long subsets of Feynman's ladder diagrams. It was V. Weisskopff and E. Wigner who constructed such a theory for the first time by considering the interaction of resonant radiation with atomic systems [12]. Such a summation of Feynman's diagram proved to be useful for the shape of spectrum line of resonant radiation and effects of resonant light scattering on non excited systems. The difficulties emerge in the theory of combined resonant scattering processes when one of the photons after stimulation emission of excited atom undergoes of elastic scattering on the ground state of the same atom. Such combined scattering is non-analytic in charge. The summation of the Feynman's diagrams like this one is not performed up to now [8]. We propose indirect way to estimate this sum.

Present work demonstrates insufficiency Weisskopff-Wigner's method and Dyson's method of summation Feynman's ladder diagrams for the calculations the cross-sections of light scattering on resonant excited systems and failure of semi-classical theory of radiation.

Let the resonant radiation scatters on some system the initial state of which in interaction representation is described by wave function ψ_0. The total wave function of electromagnetic field and scattering system is denoted as Ψ. The expansion of such function over a base of scattering system wave function ψ_i is

$$\Psi = f_0 \psi_0 + \sum_{i \neq 0} f_i \psi_i = f_0 \psi_0 + \left(\Psi - f_0 \psi_0 \right).$$

The term containing ψ_0 is written separately. The scalar product due to orthogonality of scatter's wave functions

$$\left\langle f_0 \psi_0 \middle| \Psi - f_0 \psi_0 \right\rangle = 0$$

is equal to zero. Assume that the incident light is in quantum coherent state [13] and its quantum mean electrical strength is not equal to zero $\left\langle \hat{\mathcal{E}}^\nu (\mathbf{r}, t) \right\rangle \neq 0$ in all space points $\mathbf{r}$ at arbitrary instant of time t. We are interesting in quantum mean value of operator $\hat{\mathcal{E}}^\nu$ of the reflected light

$$\left\langle \hat{\mathcal{E}}^\nu (\mathbf{r}, t) \right\rangle = \left\langle \Psi \middle| \hat{\mathcal{E}}^\nu (\mathbf{r}, t) \middle| \Psi \right\rangle =$$

$$\left\langle f_0 \psi_0 \middle| \hat{\mathcal{E}}^\nu (\mathbf{r}, t) \middle| f_0 \psi_0 \right\rangle + \left\langle \Psi - f_0 \psi_0 \middle| \hat{\mathcal{E}}^\nu (\mathbf{r}, t) \middle| \Psi - f_0 \psi_0 \right\rangle \quad (1)$$

$$= \mathcal{E}^{\nu(c)} + \mathcal{E}^{\nu(n)}$$

We state that the first term of the right hand side of Equation (1) describes the so-called coherent scattering channel with medium returning to the initial quantum state after scattering (e.g. elastic scattering). The second term of the right hand side of Equation (1) describes the non-coherent scattering processes with the medium changing initial quantum state (Compton scattering, Raman scattering and induced radiation of light). The latter is very important. We stress once again that the coherent Heisenber-Kramers scattering and induced radiation of light are described by different scattering channels. It means that if the scattering media consisted only of the non-excited atoms the first term of Equation (1) would describe the coherent Heisenberg-Kramers scattering while the second one would describe the diffusion scattering. If the excited atoms are present in the medium then due to the induced radiation processes it is impossible to avoid the presence of the non-coherent channel even if only the selective scattering is under our investigation. The total measured electrical strength $\left\langle \hat{\mathcal{E}}^\nu (\mathbf{r}, t) \right\rangle$, that is the left hand part of Equation (1), may be evaluated separately using the semi-classical theory of radiation if one neglects the fluctuation optical processes and their influence on $\left\langle \hat{\mathcal{E}}^\nu (\mathbf{r}, t) \right\rangle$. The region of validity of the semi-classical theory of radiation is very large but it does not mean that $\left\langle \hat{\mathcal{E}}^\nu (\mathbf{r}, t) \right\rangle$ describes the bilinear field characteristics.

Let us consider the energy characteristics of electromagnetic field described by normal operator product $\left\langle \hat{N} \left(\hat{\mathcal{E}}^\nu \right)^2 \right\rangle$. Such value should be estimated from below

using the following procedure. One takes into account that

$$\hat{\mathcal{E}}^\nu (\mathbf{r}, t) = i \sum_{\mathbf{k}\lambda} \sqrt{\frac{\hbar c k}{2V}} e^\nu_{\mathbf{k}\lambda} \left(\hat{\alpha}_{\mathbf{k}\lambda} e^{i\mathbf{k}\mathbf{r} - ickt} - \hat{\alpha}^+_{\mathbf{k}\lambda} e^{-i\mathbf{k}\mathbf{r} + ickt} \right),$$

where $\hat{\alpha}_{\mathbf{k}\lambda}$ and $\hat{\alpha}^+_{\mathbf{k}\lambda}$ are the annihilation and creation photon operators in states describing by wave vector $\mathbf{k}$ and polarization index λ. These operators obey the conventional commutation relations

$$\left[\hat{\alpha}_{\mathbf{k}\lambda} ; \hat{\alpha}^+_{\mathbf{k}'\lambda'} \right] = \delta_{\mathbf{k}\mathbf{k}'} \delta_{\lambda\lambda'}$$

Consider electromagnetic field as a transverse one $(\lambda = 1, 2)$, $\mathbf{e}_{\mathbf{k}\lambda}$ denotes the unite linear polarization vectors, V is the quantization volume. Since the operators $\hat{\alpha}_{\mathbf{k}\lambda}$ and $\hat{\alpha}^+_{\mathbf{k}\lambda}$ are mutual conjugate than

$$\left\langle \sum_{\mathbf{k}'\lambda'} e^\nu_{\mathbf{k}'\lambda'} \sqrt{k'} \left(\hat{\alpha}^+_{\mathbf{k}'\lambda'} - \left\langle \hat{\alpha}^+_{\mathbf{k}'\lambda'} \right\rangle \right) \sum_{\mathbf{k}\lambda} e^\nu_{\mathbf{k}\lambda} \sqrt{k} \left(\hat{\alpha}_{\mathbf{k}\lambda} - \left\langle \hat{\alpha}_{\mathbf{k}\lambda} \right\rangle \right) e^{i(\mathbf{k}-\mathbf{k}')\mathbf{r} - ic(k-k')t} \right\rangle \geq 0$$

Now

$$\sum_{\mathbf{k}\mathbf{k}'\lambda\lambda'} \sqrt{kk'} e^\nu_{\mathbf{k}\lambda} e^\nu_{\mathbf{k}'\lambda'} \left\langle \hat{\alpha}^+_{\mathbf{k}'\lambda'} \hat{\alpha}_{\mathbf{k}\lambda} \right\rangle e^{i(\mathbf{k}-\mathbf{k}')\mathbf{r} - ic(k-k')t} \geq$$

$$\sum_{\mathbf{k}\mathbf{k}'\lambda\lambda'} \sqrt{kk'} e^\nu_{\mathbf{k}\lambda} e^\nu_{\mathbf{k}'\lambda'} \left\langle \hat{\alpha}_{\mathbf{k}\lambda} \right\rangle \left\langle \hat{\alpha}^+_{\mathbf{k}'\lambda'} \right\rangle e^{i(\mathbf{k}-\mathbf{k}')\mathbf{r} - ic(k-k')t}$$

If the electromagnetic field possesses the characteristic frequency ω_0 and characteristic wave length λ_0 and we are interesting in time and space values much larger then $1/\omega_0$ and λ_0 the following inequality occurs

$$\sum_{\mathbf{k}\mathbf{k}'\lambda\lambda'} \sqrt{kk'} e^\nu_{\mathbf{k}\lambda} e^\nu_{\mathbf{k}'\lambda'} \left\langle \hat{\alpha}^+_{\mathbf{k}'\lambda'} \hat{\alpha}_{\mathbf{k}\lambda} \right\rangle e^{i(\mathbf{k}-\mathbf{k}')\mathbf{r} - ic(k-k')t} +$$

$$\sum_{\mathbf{k}\mathbf{k}'\lambda\lambda'} \sqrt{kk'} e^\nu_{\mathbf{k}\lambda} e^\nu_{\mathbf{k}'\lambda'} \left\langle \hat{\alpha}^+_{\mathbf{k}\lambda} \hat{\alpha}_{\mathbf{k}'\lambda'} \right\rangle e^{-i(\mathbf{k}-\mathbf{k}')\mathbf{r} + ic(k-k')t} \gg$$

$$\sum_{\mathbf{k}\mathbf{k}'\lambda\lambda'} \sqrt{kk'} e^\nu_{\mathbf{k}\lambda} e^\nu_{\mathbf{k}'\lambda'} \left\langle \hat{\alpha}_{\mathbf{k}\lambda} \hat{\alpha}_{\mathbf{k}'\lambda'} \right\rangle e^{i(\mathbf{k}+\mathbf{k}')\mathbf{r} - ic(k+k')t} +$$

$$\sum_{\mathbf{k}\mathbf{k}'\lambda\lambda'} \sqrt{kk'} e^\nu_{\mathbf{k}\lambda} e^\nu_{\mathbf{k}'\lambda'} \left\langle \hat{\alpha}^+_{\mathbf{k}\lambda} \hat{\alpha}^+_{\mathbf{k}'\lambda'} \right\rangle e^{-i(\mathbf{k}+\mathbf{k}')\mathbf{r} + ic(k+k')t}$$

Now it is non difficult to see that

$$\left\langle \hat{N} \left(\hat{\mathcal{E}}^\nu (\mathbf{r}, t) \right)^2 \right\rangle \approx$$

$$\sum_{\mathbf{k}\mathbf{k}'\lambda\lambda'} \frac{\hbar c}{V} \sqrt{kk'} e^\nu_{\mathbf{k}\lambda} e^\nu_{\mathbf{k}'\lambda'} \left\langle \hat{\alpha}^+_{\mathbf{k}\lambda} \hat{\alpha}_{\mathbf{k}'\lambda'} \right\rangle e^{-i(\mathbf{k}-\mathbf{k}')\mathbf{r} + ick(t-t')} \geq$$

$$\sum_{\mathbf{k}\lambda} \frac{\hbar c}{V} \sqrt{kk'} e^\nu_{\mathbf{k}\lambda} e^\nu_{\mathbf{k}'\lambda'} \left\langle \hat{\alpha}^+_{\mathbf{k}\lambda} \right\rangle \left\langle \hat{\alpha}_{\mathbf{k}'\lambda'} \right\rangle e^{-i(\mathbf{k}-\mathbf{k}')\mathbf{r} + ick(t-t')}$$

$$\approx \left\langle \hat{\mathcal{E}}^\nu (\mathbf{r}, t) \right\rangle^2 \quad (2)$$

Thus $\left\langle \hat{\mathcal{E}}^\nu \right\rangle$ proposes the opportunity to estimate

$\left\langle \hat{N}\left(\hat{\mathcal{E}}^{\nu}\right)^{2}\right\rangle$ from below. The validity of obtained inequality does not depend on particular quantum state on which the averaging is performed and does nothing to do with perturbation theory. But if such inequality is applied to each term of right hand site of

$$\left\langle \hat{N}(\hat{\mathcal{E}}^{\nu})^{2}\right\rangle = \left\langle f_{0}\psi_{0}\left|\hat{N}(\hat{\mathcal{E}}^{\nu})^{2}\right|f_{0}\psi_{0}\right\rangle + \\ \left\langle \Psi - f_{0}\psi_{0}\left|\hat{N}(\hat{\mathcal{E}}^{\nu})^{2}\right|\Psi - f_{0}\psi_{0}\right\rangle \tag{3}$$

We find that

$$\left\langle \hat{N}(\hat{\mathcal{E}}^{\nu})^{2}\right\rangle \geq \\ \left\langle f_{0}\psi_{0}\left|\hat{\mathcal{E}}^{\nu}\right|f_{0}\psi_{0}\right\rangle^{2} + \left\langle \Psi - f_{0}\psi_{0}\left|\hat{\mathcal{E}}^{\nu}\right|\Psi - f_{0}\psi_{0}\right\rangle^{2}$$

The last formula can be rewritten in as

$$\left\langle \hat{N}(\hat{\mathcal{E}}^{\nu})^{2}\right\rangle \geq \\ \left\langle f_{0}\psi_{0}\left|\hat{\mathcal{E}}^{\nu}\right|f_{0}\psi_{0}\right\rangle^{2} + \left(\left\langle \Psi\left|\hat{\mathcal{E}}^{\nu}\right|\Psi\right\rangle - \left\langle f_{0}\psi_{0}\left|\hat{\mathcal{E}}^{\nu}\right|f_{0}\psi_{0}\right\rangle\right)^{2} \tag{4}$$

That stresses the importance of the coherent scattering channel when the scattered light is not classical and.

$$\left\langle \hat{N}(\hat{\mathcal{E}}^{\nu})^{2}\right\rangle \neq \left\langle \hat{\mathcal{E}}^{\nu}\right\rangle^{2} .$$

Inequality (4) allows to estimate $\left\langle \hat{N}(\hat{\mathcal{E}}^{\nu})^{2}\right\rangle$ in the semi-classical approximation. The value $\left\langle \Psi\left|\hat{\mathcal{E}}^{\nu}\right|\Psi\right\rangle = \mathcal{E}^{\nu}$ can be calculated using the conventional semi-classical theory operating with non quantum electromagnetic field. The calculation $\left\langle f_{0}\psi_{0}\left|\hat{\mathcal{E}}^{\nu}\right|f_{0}\psi_{0}\right\rangle = \mathcal{E}^{\nu(c)}$ can be performed using only the coherent scattering channel. Even in extensive media such procedure may be performed with the help of wave functions [14]. Thus one can avoid of matrix density formalism specific for non coherent scattering channel.

2. Principal Equations

Let the electromagnetic field scatters on an atom situated at a point with radius-vector $\mathbf{R}$ and for the sake of simplicity possesses only one orbital electron with coordinate $\mathbf{r}$. Let the atom possesses only two energy levels. Zeeman`s sublevels with different magnetic numbers are possible. Let the frequency of incident radiation ω is in a quasi resonance $\left|\omega_{o} - \omega\right| << \omega_{0} + \omega$ with the atom transition frequency ω_{0}. Let Schroedinger equation for atom and radiation is as follows

$$i\hbar\frac{\partial\Psi}{\partial t} = \left(\hat{H}_{a} + \hat{H}_{ph} + \hat{H}'\right)\Psi ,$$

where

$$\hat{H}_{a} = \int\hat{\psi}^{+}(\mathbf{r})\left(\frac{\hat{p}_{\mathbf{r}}^{2}}{2m} + U(\mathbf{r} - \mathbf{R})\right)\hat{\psi}(\mathbf{r})d\mathbf{r}$$

$$\hat{H}' = -\frac{e}{mc}\int\hat{\psi}^{+}(\mathbf{r})\hat{p}_{\mathbf{r}}^{\nu}\hat{A}^{\nu}(\mathbf{r})\hat{\psi}(\mathbf{r})d\mathbf{r}$$

are the Hamiltonian of the non-interacting atoms and an interaction Hamiltonian in Schroedinger representation. Than

$$\hat{\psi}(\mathbf{r}) = \sum_{j}\psi_{j}(\mathbf{r} - \mathbf{R})\hat{b}_{j} , \quad \hat{\psi}^{+}(\mathbf{r}) = \sum_{j}\psi_{j}^{*}(\mathbf{r} - \mathbf{R})\hat{b}_{j}^{+} ,$$

$$\hat{p}_{\mathbf{r}}^{\nu} = -i\hbar\nabla_{\mathbf{r}}^{\nu} .$$

The following communication relations are assumed

$$\left[\hat{b}_{j};\hat{b}_{j'}^{+}\right] = \delta_{jj'}$$

for the electron creation operator $\hat{b}_{j}^{+}$ and annihilation operator $\hat{b}_{j}$ in the state described by wave function ψ_{j}. The particular form of communication relations in our case of one electron in the atom does not play any role. By $U(\mathbf{r} - \mathbf{R})$ we denote the potential energy of atom electron. The Einstein summation rule is assumed over all repeating indices ν throughout the paper. The Hamiltonian of free electromagnetic field and vector-potential operator are as follows

$$\hat{H}_{ph} = \sum_{\mathbf{k}\lambda}\hbar ck\hat{\alpha}_{\mathbf{k}\lambda}^{+}\hat{\alpha}_{\mathbf{k}\lambda}$$

$$\hat{A}^{\nu}(\mathbf{r}) = \sum_{\mathbf{k}\lambda}\sqrt{\frac{\hbar c}{2kV}}e_{\mathbf{k}\lambda}^{\nu}\left(\hat{\alpha}_{\mathbf{k}\lambda}e^{i\mathbf{k}\mathbf{r}} + \hat{\alpha}_{\mathbf{k}\lambda}^{+}e^{-i\mathbf{k}\mathbf{r}}\right)$$

In order to realize the calculation project mentioned in introduction we switch to the interaction representation with the help of unitary operator

$$\hat{U}(t) = \exp\left(\frac{1}{i\hbar}(\hat{H}_{a} + \hat{H}_{ph})t\right).$$

In this picture

$$\Psi(t) = \hat{S}(t,t_{0})\Psi_{0} , \quad \hat{S}(t,t_{0}) = \hat{T}\exp\left(\frac{1}{i\hbar}\int_{-\infty}^{t}\hat{H}'(t')dt'\right) \tag{5}$$

$$\hat{H}'(t) = -\frac{e}{mc}\int\hat{\psi}^{+}(x)\hat{p}_{\mathbf{r}}^{\nu}\hat{A}^{\nu}(x)\hat{\psi}(x)d\mathbf{r} , \quad x = \{\mathbf{r},t\} ,$$

$$\hat{\psi}(x) = \sum_{j}\psi_{j}(\mathbf{r} - \mathbf{R})e^{-i\frac{\varepsilon_{j}}{\hbar}t}\hat{b}_{j}$$

$$\hat{\psi}^{+}(x) = \sum_{j}\psi_{j}^{*}(\mathbf{r} - \mathbf{R})e^{i\frac{\varepsilon_{j}}{\hbar}t}\hat{b}_{j}^{+} .$$

where $\hat{S}(t,t_{0})$ is the scattering operator, ε_{j} is the atomic energy in state ψ_{j}, $\hat{T}$ is the time-ordering operator and

$$\hat{A}^\nu(x) = \hat{A}^{\nu(+)}(x) + \hat{A}^{\nu(-)}(x) =$$

$$\sum_{\mathbf{k}\lambda}\sqrt{\frac{\hbar c}{2kV}}e^\nu_{\mathbf{k}\lambda}\hat{\alpha}_{\mathbf{k}\lambda}e^{i\mathbf{kr}-ikct} + \sum_{\mathbf{k}\lambda}\sqrt{\frac{\hbar c}{2kV}}e^\nu_{\mathbf{k}\lambda}\hat{\alpha}^+_{\mathbf{k}\lambda}e^{-i\mathbf{kr}+ikct} \quad (6)$$

3. Coherent Scattering Channel

Suppose that the initial state of the field was described by $(\mathbf{k}_0, \lambda_0)$ and was in quantum coherent state [13]

$$\overset{0}{f_0} = e^{-\frac{1}{2}|\alpha|^2}\sum_n \frac{(\alpha\hat{\alpha}_{\mathbf{k}_0\lambda_0})^n}{\sqrt{n!}}|0\rangle.$$

The amplitude of initial radiation was

$$\langle\Psi_0|\hat{A}^\nu(x)|\Psi_0\rangle = \left\langle \overset{0}{f_0}\psi_0\left|\hat{A}^\nu(x)\right|\overset{0}{f_0}\psi_0\right\rangle =$$

$$e^\nu_{\mathbf{k}_0\lambda_0}\left(a_{\mathbf{k}_0\lambda_0}e^{i\mathbf{k}_0\mathbf{r}-ik_0ct} + a^*_{\mathbf{k}_0\lambda_0}e^{-i\mathbf{k}_0\mathbf{r}+ik_0ct}\right),$$

$$a_{\mathbf{k}_0\lambda_0} = \sqrt{\frac{\hbar c}{2kV}}\alpha.$$

We are interested in the radiation amplitude after scattering in second order of perturbation technique. The problem of Feynman's diagrams summation will be discussed below. In Equation (5) it is sufficient to consider the sum

$$\hat{S} = 1 + \hat{S}^{(1)} + \hat{S}^{(2)} + \hat{S}^{(3)},$$

where

$$\hat{S}^{(1)} = \frac{1}{i\hbar}\int \hat{H}'(t')dt'$$

$$\hat{S}^{(2)} = \frac{\hat{T}}{2(i\hbar)^2}\left(\int\hat{H}'(t')dt'\right)^2,$$

$$\hat{S}^{(3)} = \frac{\hat{T}}{3!(i\hbar)^3}\left(\int\hat{H}'(t')dt'\right)^3.$$

If the photon scatters in the coherent channel then the atom rests in initial state. So in second order of perturbation technique we are interested in the construction

$$\mathscr{A}^{\nu(c)}(x) = \left\langle\Psi_0\left|\hat{A}^\nu(x)\hat{S}^{(2)}\right|\Psi_0\right\rangle + c.c. \quad (7)$$

We change the time-ordering product of the atom operators by the normal ordering one. For the scattering operator $\hat{S}^{(2)}$ we get

$$\hat{S}^{(2)} =$$

$$\left(\frac{e}{mc}\right)^2\frac{\hat{T}_A}{i\hbar}\int\hat{\psi}^+(x_1)\hat{p}^{\nu_1}_{\mathbf{r}_1}\hat{A}^{\nu_1}(x_1)G_r(x_1,x_2)\hat{p}^{\nu_2}_{\mathbf{r}_2}\hat{A}^{\nu_2}(x_2)\hat{\psi}(x_2)dx_1dx_2$$

where $\hat{T}_A$ is the time-ordering operator acting only on the electromagnetic field operators and

$$\left(\hat{T}-\hat{N}\right)\hat{\psi}(x)\hat{\psi}^+(x') = i\hbar G_r(x_1,x_2),$$

$$G_r(x_1,x_2) =$$

$$\sum_j\int\psi_j(\mathbf{r}_1-\mathbf{R})\psi^*_j(\mathbf{r}_2-\mathbf{R})e^{-\frac{E}{\hbar}(t_1-t_2)}G^j_r\left(\frac{E}{\hbar}\right)\frac{dE}{2\pi\hbar}$$

$$G^j_r\left(\frac{E}{\hbar}\right) = \frac{1}{E-\varepsilon_j+i0} \quad (8)$$

If the atom undergoes the action of external random fields the finite width of its energy levels can be taken into account by replacing the term $+i0$ by $+i\gamma_j/2$ with the same sign because it is governed by the causality principle. The same result follows from summing up (Dyson summation) the ladder Feynman's diagrams for excited atoms due to their interaction with electromagnetic vacuum. For the same reason formula (8) can be written as

$$G^j_r\left(\frac{E}{\hbar}\right) = \frac{1}{E-\varepsilon_j+i\dfrac{\gamma_j}{2}}.$$

without specifying the value γ_j. We take into account that,

$$\hat{T}_A\hat{A}^{\nu_1}(x_1)\hat{A}^{\nu_2}(x_2) =$$
$$i\hbar D^{\nu_1\nu_2}(x_1,x_2) + \hat{N}\hat{A}^{\nu_1}(x_1)\hat{A}^{\nu_2}(x_2) \quad (9)$$

where $D^{\nu_1\nu_2}(x_1,x_2)$ is not the operator function. The first term in (9) does not play any role in electromagnetic field scattering process. Finitely

$$\hat{S}^{(2)} = \frac{1}{i\hbar}\left(\frac{e}{mc}\right)^2\int\hat{\psi}^+(x_1)\hat{p}^{\nu_1}_{\mathbf{r}_1}G_r(x_1,x_2)\hat{p}^{\nu_2}_{\mathbf{r}_2}$$

$$\left[\hat{A}^{\nu_2(-)}(x_2)\hat{A}^{\nu_1(+)}(x_1) + \hat{A}^{\nu_1(-)}(x_1)\hat{A}^{\nu_2(+)}(x_2)\right]\hat{\psi}(x_2)dx_1dx_2$$

$$(10)$$

The right hand side terms of this equality are responsible on scattering processes of electromagnetic field by both the non excited atom and excited one.

3.1. Scattering on Non-Excited Atom

Substituting (6) and (8) into Equation (10) and taken the limit $t\to\infty$, we find

$$\hat{S}^{(2)}\left|\overset{0}{f_0}\psi_0\right\rangle = \frac{\pi c}{iVk_0}\left(\frac{e}{mc}\right)^2\sum_{j_2\mathbf{k}_1\lambda_1}p^{\nu_1}_{j_0j_2}p^{\nu_2}_{j_2j_0}\hat{b}^+_{j_0}\hat{b}_{j_0}\frac{\delta(k_1c-k_0c)}{\varepsilon_{j_0}+\hbar k_0c-\varepsilon_{j_2}+i\dfrac{\gamma_{j_2}}{2}}e^{-i\mathbf{R}(\mathbf{k}_1-\mathbf{k}_0)}e^{\nu_1}_{\mathbf{k}_1\lambda_1}e^{\nu_2}_{\mathbf{k}_0\lambda_0}\hat{\alpha}^+_{\mathbf{k}_1\lambda_1}\alpha\left|\overset{0}{f_0}\psi_0\right\rangle$$

Through j_0 one denote here the quantum number of initial state of atom. In dipole approximation

$$p_{j_0 j_2}^\nu = \int \psi_{j_0}^*(\boldsymbol{\rho}) \hat{p}_{\boldsymbol{\rho}}^\nu \psi(\boldsymbol{\rho}) d\boldsymbol{\rho} \ .$$

The limit $t \to \infty$ is not necessary but it makes the calculations simpler. According to (7) we need to calculate the construction

$$\mathscr{A}^{\nu(c)}(x) = \left\langle \overset{0}{f_0} \psi_0 \left| \hat{A}^{\nu(+)}(x) \hat{S}^{(2)} \right| \overset{0}{f_0} \psi_0 \right\rangle + c.c.$$

Let us use the following equalities connecting any smooth function $f(k)$ and limits $V \to \infty$, $|\mathbf{r} - \mathbf{R}| \to \infty$

$$\sum_{\mathbf{k}_1 \lambda_1} e_{\mathbf{k}_1 \lambda_1}^\nu e_{\mathbf{k}_1 \lambda_1}^{\nu_1} \delta(k_1 c - k_0 c) e^{i\mathbf{k}_1(\mathbf{r}-\mathbf{R})} f(k_1) =$$

$$\frac{V}{(2\pi)^3} \int \left(\delta_{\nu\nu_1} + \frac{\partial}{\partial r^\nu} \frac{\partial}{\partial r^{\nu_1}} \right) e^{i\mathbf{k}_1(\mathbf{r}-\mathbf{R})} \delta(k_1 c - k_0 c) f(k_1) d\mathbf{k}_1 =$$

$$\frac{V}{2\pi^2} k_0 f(k_0) \frac{\sin k_0 |\mathbf{r} - \mathbf{R}|}{|\mathbf{r} - \mathbf{R}|} \left(\delta_{\nu\nu_1} - n^\nu n^{\nu_1} \right)$$

where

$$n^\nu = \frac{(\mathbf{r} - \mathbf{R})^\nu}{|\mathbf{r} - \mathbf{R}|}$$

Here we take into account only the term describing diverge wave. The neglected term turns into zero by infinitely small interval of integration over k_0 that is supposed. Finitely

$$\mathscr{A}^{\nu(c)}(x) = -\frac{1}{4\pi} \left(\frac{e}{mc} \right)^2 \frac{\delta(\delta_{\nu\nu_1} - n^\nu n^{\nu_1})}{|\mathbf{r} - \mathbf{R}|} a_{\mathbf{k}_0 \lambda_0} e^{i\mathbf{k}_0 \mathbf{R}} \sum_{j_2} p_{j_0 j_2}^{\nu_1} p_{j_2 j_0}^{\nu_2} \frac{1}{\hbar c k_0 - \omega_0 \hbar + i\frac{\gamma_{j_2}}{2}} e_{\mathbf{k}_0 \lambda_0}^{\nu_2} e^{ik_0|\mathbf{r}-\mathbf{R}|-ik_0 ct} + c.c. \qquad (11)$$

3.2. Scattering on Excited Atom

$$\mathscr{A}^{\nu(c)}(x) = -\frac{1}{4\pi} \left(\frac{e}{mc} \right)^2 \frac{(\delta_{\nu\nu_2} - n^\nu n^{\nu_2})}{|\mathbf{r} - \mathbf{R}|} a_{\mathbf{k}_0 \lambda_0} e^{i\mathbf{k}_0 \mathbf{R}} \sum_{j_2} p_{j_0 j_2}^{\nu_1} p_{j_2 j_0}^{\nu_2} \frac{1}{\omega_0 \hbar - \hbar c k_0 + i\frac{\gamma_{j_2}}{2}} e_{\mathbf{k}_0 \lambda_0}^{\nu_1} e^{ik_0|\mathbf{r}-\mathbf{R}|-ik_0 ct} + c.c. \qquad (12)$$

If one takes into account the width of atom's energy level in state described by ψ_{j_0} than it is necessary to replace $\gamma_{j_2} \to \gamma = \gamma_{j_0} + \gamma_{j_2}$ in Equation (12). The validity of Equations (11) and (12) are restricted by domain $\gamma_r / \gamma \ll 1$ where γ_r is the radiation width of excited state of atom.

The second term in Equation (10) after the same type of transformation shown in part 3.1 yields

4. Non Coherent Scattering Channel

The second order perturbation technique gets

$$\mathscr{A}^{\nu(n)}(x) = \left\langle \overset{0}{f_0} \psi_0 \left| \hat{S}^{(1)+} \hat{A}^\nu(x) \hat{S}^{(1)} \right| \overset{0}{f_0} \psi \right\rangle \cdot$$

Or by taken into account only the scattering processes we have in explicit form

$$\mathscr{A}^{\nu(n)}(x) = \frac{1}{(i\hbar)^2} \left(\frac{e}{mc} \right)^2 \left\langle \overset{0}{f_0} \psi_0 \left| \int \hat{\psi}^+ \hat{p}_{\mathbf{r}_1}^{\nu_1} \hat{A}^{\nu_1(+)} \hat{\psi} dx_1 \hat{A}^{\nu(+)} \int \hat{\psi}^+ \hat{p}_{\mathbf{r}_2}^{\nu_2} \hat{A}^{\nu_2(-)} \hat{\psi} dx_2 \right| \overset{0}{f_0} \psi_0 \right\rangle + c.c.$$

Following the procedures described in part 3.1 we have

$$\mathscr{A}^{\nu(n)}(x) = \frac{i}{2\hbar} \left(\frac{e}{mc} \right)^2 \frac{(\delta_{\nu\nu_2} - n^\nu n^{\nu_2})}{|\mathbf{r} - \mathbf{R}|} a_{\mathbf{k}_0 \lambda_0} e^{i\mathbf{k}_0 \mathbf{R}} \sum_{j_2} p_{j_0 j_2}^{\nu_1} p_{j_2 j_0}^{\nu_2} \delta\left(\frac{\varepsilon_{j_0} - \varepsilon_{j_2}}{\hbar} - k_0 c \right) e_{\mathbf{k}_0 \lambda_0}^{\nu_1} e^{ik_0|\mathbf{r}-\mathbf{R}|-ik_0 ct} + c.c. \qquad (13)$$

If we take into account the finite width of atom energy level than in formula (13) it is necessary to change

$$\delta\left(\frac{\varepsilon_{j_0} - \varepsilon_{j_2}}{\hbar} - k_0 c \right) \to -\frac{\hbar}{2\pi i} \left(\frac{1}{\varepsilon_{j_0} - \varepsilon_{j_2} - k_0 c + i\frac{\gamma}{2}} - \frac{1}{\varepsilon_{j_0} - \varepsilon_{j_2} - k_0 c - i\frac{\gamma}{2}} \right)$$

Let us find now the total amplitude of electromagnetic field scattered by excited atom

$$\mathcal{A}^{\nu}(x) = \mathcal{A}^{\nu(c)}(x) + \mathcal{A}^{\nu(n)}(x) = -\frac{1}{4\pi}\left(\frac{e}{mc}\right)^2 \frac{\left(\delta_{\nu\nu_2} - n^{\nu}n^{\nu_2}\right)}{|\mathbf{r}-\mathbf{R}|} a_{\mathbf{k}_0\lambda_0} e^{i\mathbf{k}_0\mathbf{R}} \sum_{j_2} p_{j_0 j_2}^{\nu_1} p_{j_2 j_0}^{\nu_2} \frac{1}{\omega_0\hbar - \hbar ck_0 - i\frac{\gamma}{2}} e_{\mathbf{k}_0\lambda_0}^{\nu_1} e^{ik_0|\mathbf{r}-\mathbf{R}|-ik_0ct} + c.c.$$

(14)

5. Semi-Classical Theory of Radiation

The set equations for field operators $\overset{\vee}{\psi}(x)$ and $\overset{\vee}{A}^{\nu}(x)$ in Heisenberg representation is the following

$$i\hbar\frac{\partial\overset{\vee}{\psi}(x)}{\partial t} = \left(\frac{\hat{p}_{\mathbf{r}}^2}{2m} + U(\mathbf{r}-\mathbf{R}) - \frac{e}{mc}\overset{\vee}{A}^{\nu}(x)\hat{p}_{\mathbf{r}}^{\nu}\right)\overset{\vee}{\psi}(x)$$,

$$\overset{\vee}{A}(x) = -\frac{1}{c}\overset{\vee}{j}^{\nu}(x), \quad \overset{\vee}{j}^{\nu}(x) = \frac{e}{2m}\left(\overset{\vee}{\psi}^{+}\hat{p}_{\mathbf{r}}^{\nu}\overset{\vee}{\psi} + \hat{p}_{\mathbf{r}}^{\nu*}\overset{\vee}{\psi}^{+}\cdot\overset{\vee}{\psi}\right).$$

This set equations is equivalent to the one mentioned at part 3. Now

$$\overset{\vee}{A}^{\nu}(x) = \overset{\vee}{A}^{\nu 0}(x) - \frac{e}{mc}\int\Delta_r^{\nu\nu_1}(x,x_1)\overset{\vee}{\psi}^{+}(x_1)\hat{p}_{\mathbf{r}_1}^{\nu_1}\overset{\vee}{\psi}(x_1)dx_1 .$$ (15)

Here $\overset{\vee}{A}^{\nu 0}(x)$ is given by the formula (6) and

$$\Delta_r^{\nu\nu_1}(x,x_1) = \frac{1}{i\hbar}\left[\overset{\vee}{A}^{\nu 0}(x);\overset{\vee}{A}^{\nu_1 0}(x_1)\right]\vartheta(t-t_1) = $$
$$-\frac{c}{4\pi}\frac{\delta_{\nu\nu_1} - n^{\nu}n^{\nu_1}}{|\mathbf{r}-\mathbf{r}_1|}\delta\left(|\mathbf{r}-\mathbf{r}_1| - c(t-t_1)\right) \quad , |\mathbf{r}-\mathbf{r}_1|\to\infty .$$

(16)

We are interested in the second order perturbation expansion. This mean that the $\overset{\vee}{\psi}(x)$ operator has be evaluated in the first order of perturbation technique

$$\overset{\vee}{\psi}(x) = \overset{\vee}{\psi}^0(x) - \frac{e}{mc}\int G_r(x,x_1)\hat{p}_{\mathbf{r}_1}^{\nu_1}\overset{\vee}{A}^{\nu_1}(x_1)\overset{\vee}{\psi}(x_1)dx_1 .$$ (17)

Substituting (16) and (17) into (15) we find

$$\overset{\vee}{A}^{\nu}(x) = \overset{\vee}{A}^{\nu 0}(x) + \left(\frac{e}{mc}\right)^2 \int\Delta_r^{\nu\nu_1}(x,x_1)\hat{\psi}^{+}(x_1)\hat{p}_{\mathbf{r}_1}^{\nu_1}G_r(x_1,x_2)\hat{p}_{\mathbf{r}_2}^{\nu_2}\hat{A}^{\nu_2}(x_2)\hat{\psi}(x_2)dx_1 dx_2 + H.c.$$ (18)

For the mean values, the same result can be obtained either by averaging (18) with subsequent breaking up the correlators, or using the semi-classical theory. After realizing in (18) the substitution

$$\left\langle\overset{\vee}{A}^{\nu_2}(x_2)\right\rangle \to \overset{0}{\mathcal{A}}^{\nu_2}(x_2) = \left\langle\Psi_0\left|\overset{\vee}{A}^{\nu_2}(x_2)\right|\Psi_0\right\rangle = e_{\mathbf{k}_0\lambda_0}^{\nu_2}\left(a_{\mathbf{k}_0\lambda_0}e^{i\mathbf{k}_0\mathbf{r}_2-ik_0ct_2} + a_{\mathbf{k}_0\lambda_0}^{*}e^{-i\mathbf{k}_0\mathbf{r}_2+ik_0ct_2}\right)$$

for the scattered field we have

$$\mathcal{A}^{\nu}(x) = -\frac{1}{4\pi}\left(\frac{e}{mc}\right)^2 \frac{\left(\delta_{\nu\nu_1} - n^{\nu}n^{\nu_1}\right)}{|\mathbf{r}-\mathbf{R}|} a_{\mathbf{k}_0\lambda_0} e^{\pm i\mathbf{k}_0\mathbf{R}} \sum_{j_2} p_{j_0 j_2}^{\nu_1} p_{j_2 j_0}^{\nu_2} \frac{1}{\varepsilon_{j_0} - \varepsilon_{j_2} \pm \hbar ck_0 + i0} e_{\mathbf{k}_0\lambda_0}^{\nu_2} e^{\pm ik_0|\mathbf{r}-\mathbf{R}|\mp ik_0ct} + c.c.$$ (19)

The upper sign describes the scattering of electromagnetic field on the non-excited atom while the low one describes the scattering on excited atom. One should take into account the width of atomic energy level by replacing in dominator $+i0$ with $+i\gamma/2 = +i(\gamma_{j_0} + \gamma_{j_2})/2$.

By comparing Equation (19) with Equations (11) and (14) we find that in the approximation we used both the quantum theory and the semi-classical theory result in the same expressions for the scattered amplitude $\mathcal{A}^{\nu}(x)$. Namely the necessary coinciding in such results leads to the equality of constants γ in Formulas (19), (11) and (14).

6. Bilinear Field Charasteristics

In this part we are interesting in the following construction shown in introduction

$$\left\langle\Psi\left|\hat{N}\hat{\mathcal{E}}^{\nu}(x)\hat{\mathcal{E}}^{\nu'}(x')\right|\Psi\right\rangle .$$

In order to calculate this value in forth order of perturbation expansion it should use the Formula (3). But it is not worth to do it. The strait calculation shows that for resonant field scattering $(\omega = \omega_0)$ the construction

$$\left\langle\Psi_0\left|\hat{S}^{(1)+}\hat{N}\hat{A}^{\nu}(x)\hat{A}^{\nu}(x)\hat{S}^{(3)}\right|\Psi_0\right\rangle ,$$

which appears in such approximation at non-coherent channel results in negative value. This fact evidently contradicts with the positive definition of expression

$$\left\langle \Psi - f_0\psi_0 \left| \hat{N}(\hat{\mathcal{E}}^\nu)^2 \right| \Psi - f_0\psi_0 \right\rangle > 0$$

Such contradiction was found before in Reference [25] where different model has been considered. In order to reconstruct the positive definition of the non-coherent channel using perturbation set it is necessary to average the product $\hat{\mathcal{E}}^\nu(x)\hat{\mathcal{E}}^\nu(x)$ over the wave function $\left(1 + \hat{S}^{(1)} + \hat{S}^{(2)} + \hat{S}^{(3)}\right)\Psi_0$. But doing this we find the terms proportional to the sixth order of charge. It means that such reconstruction may be achieved only by using higher order terms of perturbation technique. Thus one

can not restrict oneself here by the terms of lover order of perturbation technique. So the conventional perturbation theory for $\left\langle \Psi \left| \hat{N}\hat{\mathcal{E}}^\nu(x)\hat{\mathcal{E}}^\nu(x) \right| \Psi \right\rangle$ is problematic. For these reasons we estimate the contribution of non-coherent processes using inequality (2)

$$\left\langle \Psi - f_0\psi_0 \left| \hat{N}\hat{\mathcal{E}}^\nu\hat{\mathcal{E}}^\nu \right| \Psi - f_0\psi_0 \right\rangle^2 \geq$$
$$\left\langle \Psi - f_0\psi_0 \left| \hat{\mathcal{E}}^\nu \right| \Psi - f_0\psi_0 \right\rangle^2 \qquad (20)$$

Then we use the same method to estimate the contribution of coherent channel. Thus according to the quantum theory using Equation (12), Equation (13) and Equation (20) one gets for the scattering by excited atom in two level approximation the following formula;

$$\left\langle \hat{N}\hat{\mathcal{E}}^\nu\hat{\mathcal{E}}^\nu \right\rangle_{qu} \geq 2\left| \frac{1}{4\pi}\left(\frac{e}{mc}\right)^2 \frac{\left(\delta_{\nu\nu_2} - n^\nu n^{\nu_2}\right)}{|\mathbf{r}-\mathbf{R}|} a_{\mathbf{k}_0\lambda_0} e^{\nu_1}_{\mathbf{k}_0\lambda_0} \sum_{j_2} p^{\nu_1}_{j_0 j_2} p^{\nu_2}_{j_2 j_0} \right|^2 \frac{1}{\left(\hbar\omega_0 - \hbar ck_0\right)^2 + \frac{\gamma^2}{4}}\left(1 + \frac{\gamma^2}{\left(\hbar\omega_0 - \hbar ck_0\right)^2 + \frac{\gamma^2}{4}}\right)$$

While according to the semi classical theory one gets

$$\left\langle \hat{N}\hat{\mathcal{E}}^\nu\hat{\mathcal{E}}^\nu \right\rangle_{scl} \geq 2\left| \frac{1}{4\pi}\left(\frac{e}{mc}\right)^2 \frac{\left(\delta_{\nu\nu_2} - n^\nu n^{\nu_2}\right)}{|\mathbf{r}-\mathbf{R}|} a_{\mathbf{k}_0\lambda_0} e^{\nu_1}_{\mathbf{k}_0\lambda_0} \sum_{j_2} p^{\nu_1}_{j_0 j_2} p^{\nu_2}_{j_2 j_0} \right|^2 \frac{1}{\left(\hbar\omega_0 - \hbar ck_0\right)^2 + \frac{\gamma^2}{4}}$$

The ratio of results of these two calculation methods for the resonant scattering frequency $\omega = \omega_0$ is equal to

$$\frac{\left\langle \hat{N}\hat{\mathcal{E}}^\nu\hat{\mathcal{E}}^\nu \right\rangle_{qu}}{\left\langle \hat{N}\hat{\mathcal{E}}^\nu\hat{\mathcal{E}}^\nu \right\rangle_{scl}} = 5.$$

The same value characterizes the ratio of scattering cross sections σ_{qu}/σ_{scl}. This result does not depend on γ. We note that for the scattering of electromagnetic field on non-excited atoms this ratio is equal to one. The dependence of ratio σ_{qu}/σ_{scl} for scattering on excited atom as a function of scattering frequency by $\omega \neq \omega_0$ is shown in the **Figure 1**.

7. Conclusions

The evaluations the scattered field amplitude of resonance scattering electromagnetic field on an excited atom can be performed equally well using both the Heisenberg representation and Schroedinger one. In our approximation the both calculations lead to the same results. The same results follow also from the semi-classical theory of radiation, which deals with classical electromagnetic field. In general, the perturbation technique is not suffi-

cient to describe the resonance scattering process and we need to sum up the ladder Feynman diagrams. Such procedure is not difficult to be performed using any of theories mentioned above.

In the other case we deal with calculation of the quantum mean values of bilinear products of the field operators $\left\langle \hat{\mathcal{E}}^\nu\hat{\mathcal{E}}^\nu \right\rangle$. Here it is more convenient to deal with Sch-
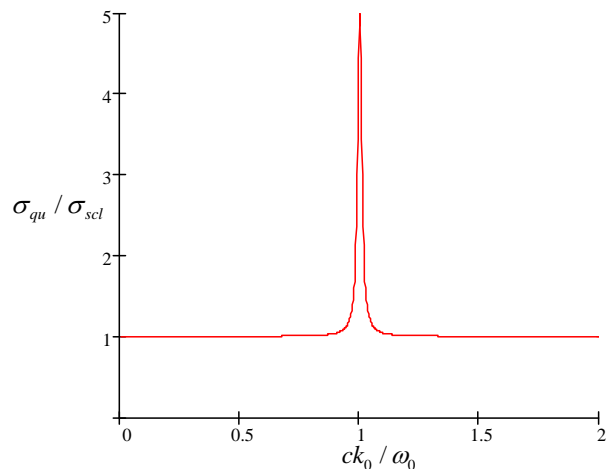
Figure 1. The typical dependence of ratio σ_{qu}/σ_{scl} for scattering of electromagnetic field on excited atom as a function of scattering frequency ck_0/ω_0.

rödinger representation or with interaction representation, which give additional opportunities to sum up the Feynman diagrams. The letter representations allow us to present the scattering process with the help of two components: coherent (elastic) and non-coherent. Such components could be evaluated independently. The analysis of non-coherent channel shows that the Dyson's summation of ladder Fynman's diagrams by scattering of resonant electromagnetic field on excited atoms is not sufficient. Other summation methods are very unwieldy [8]. In present work we propose the simple method of estimation from below the results of the non-coherent scattering channel. As a result we find that the semi-classical theory of radiation essentially underestimates the cross section of resonance scattering. The quantum theory in its turn shows the violation of equality $\left\langle \hat{N} \hat{\mathcal{E}}^{\nu} \hat{\mathcal{E}}^{\nu} \right\rangle =$

$\left\langle \hat{\mathcal{E}}^{\nu} \right\rangle \left\langle \hat{\mathcal{E}}^{\nu} \right\rangle$ in scattered radiation even if such equality took place in the incident electromagnetic field. So the quantum theory results in a change of quantum statistical structure of electromagnetic field due to scattering. This can not be obtained with the help of semi-classical theory of radiation. This change of internal quantum field structure by its scattering on excited atom manifests itself on macroscopic level. Namely such effect makes impossible using here the semi-classical theory of radiation.

8. References

[1] W. E. Lamb, "The Theory of Optical Masers," In: C. DeWitt, A. Blandin and C. Cohen-Tannoudji, Eds., *Quantum Optics and Electronics*, University of Grenoble, Houches, New York-London-Paris, 1965.

[2] M. O. Scully and W. E. Lamb, "Quantum Theory of a Optical Masers," *Physical Review Letters*, Vol. 159, No. 2, 1967, pp. 208-226.

[3] C. J. Koester, "9A4-Laser Action by Enhanced Total Internal Reflection," *IEEE Journal of Quantum Electronics*, Vol. QE-2, No. 9, 1966, pp. 580-584.

[4] B. B. Boyko and N. S. Petrov, "Reflection of Light from Enhanced and Non Linear Media," Nauka and Technika, Minsk, 1988.

[5] R. F. Cybulski and C. K. Carniglia, "Internal Reflection from fn Exponential Amplifying Region," *Journal of the Optical Society of America*, Vol. 67, No. 12, 1977, pp. 1620-1627.

[6] T. C. Biba, N. S. Petrov and I. Z. Djilavdary, "The Reflection of the Light from Non-Homogeneous Medium with Limited Region of Enhancement," *Journal of Applied Spectroscopy*, Vol. 32, No. 2, 1980, pp. 226-271.

[7] B. A. Veklenko, "Action of the Noise Processes on Interference Properties in Resonance Spektroscopy," Izvestija Vouzov Physika, No. 9, 1983, pp. 71-75.

[8] B. A. Veklenko, R. B.Gusarov and Y. B. Sherkunov, "Selective Reflection of Resonance Radiation from Excited Media," *Journal of Experimental and Theoretical Physics*, Vol. 86, No. 2, 1998, pp. 289-298.

[9] J. Skaar, "Fresnel Function and the Refractive Index of Active Media," *Physical Review E*, Vol. 73, No. 2, 2006. pp. 1-7.

[10] I. I. Smolyaninov and Y.-J. Hung, "Enhanced Transmition of Light through a Gold Film due to Excitation of Standing Surface-Plasmon Bloch Waves," *Physical Review B*, Vol. 75, No. 3, 2007, pp. 1-4.

[11] T. W. Ebbesen, H. G. Lezec, H. F. Ghaemi, T. Thio and P. A. Wolff. "Extraordinary Optical Transmission through Sub-Wavelength Hole Arrays," *Nature* (*London*), Vol. 391, No. 6668, 1998, pp. 667-669.

[12] V. Weisskopf and E. Wigner, "Berechnung der Naturlichen Linienbreit und Grund der Diracschen Lichttheory," *Zeitschrift fur Physik*, Vol. 63, No. 1/2, 1930, pp. 54-73.

[13] R. Glauber, "Optical Coherence and Photon Statistics," In: C. DeWitt. Ed., University of Grenoble, Houches, New York-London-Paris, 1965.

[14] B. A. Veklenko, "Remarks on Kramers—Heisenberg Formula and some Properties of induced Radiation," *Izvestija Vuzov. Physika*, No. 6, 1987, pp. 132-142.

❖❖ Scientific
❖❖ Research

Statistical Modeling of the Influence of Electron Degeneracy on the Interatomic Interactions

Anatoly M. Dolgonosov

Vernadsky Institute of Geochemistry and Analytical Chemistry, Russian Academy of Sciences, Moscow, Russia
E-mail: amdolgo@mail.ru

Abstract

It is shown that electrons forming simple and multiple covalent bonds may have different contributions to the interatomic interactions due to the degeneracy of electron states. A simple relationship between the length of covalent bond, its order and atomic numbers of the interacting atoms is deduced.

Keywords: Interatomic Interactions, Covalent Bond, Degeneracy of Electron States, Theory of Generalized Charges, Bond Length Ratio

1. Introduction

In the semiempirical methods describing interatomic interactions, the contribution to the interaction energy of π-bond is assumed to be larger than that of σ-bond [1,2]. The ratio of π- to σ-electron weight factors equal to 1.41 was empirically determined in [3,4] and checked many times for the adsorption of unsaturated hydrocarbons. We will show that this ratio can be evaluated from the characteristics of covalent bonds (and vice versa).

It follows from the theoretical and empirical equations found by London, Heitler, Lennard-Jones, and others that the parameters of atoms symmetrically enter the expression for interatomic bond energy [5]. A quasi-classical method for describing the self-consistent field of multi-component electron gas was developed in [6]. This method enables us to express the interatomic interaction energy. In particular it is shown that this energy is associated with the volume V of each atom through a symmetrical operation – volumes product

$$E_{12} = f\left(X_{12}, r_{12}\right);$$
$$X_{12} = V_1 V_2 = \sum_{i(1)} v_i \sum_{j(2)} v_j \tag{1}$$

where r_{12} is the internuclear distance; v is a "volume" of one electron, or the elementary volume, which is equal to unity for a nondegenerate electron; V is the electronic volume of the atom equal to the sum of elementary volumes of its electrons; the indices enumerate all electrons participating in bonding; and the figures at the summation symbol indicate summation over every electron of the corresponding atom.

According to [6], the shielding radius, which is inversely proportional to the square root of the height of

the potential barrier that the electron overcomes, can be used as a criterion of the participation of the electron in interatomic interactions. A sphere centered at the atomic nucleus with radius equal to the shielding radius of electrons (the shielding sphere) bounds the electrons that participate in bonding. An electron contributes to the electronic volume of its atom only if the nucleus of the atom with which the interaction is considered is situated within the electron shielding sphere.

It is very important to distinguish between the electronic volume, the key concept of the theory of generalized charges developed in [6], and the corresponding number of electrons, though these characteristics often quantitatively coincide. It will be shown below that the elementary volume of a degenerate electron larger than that of a nondegenerate one, *i.e.* larger than unity.

2. Theory

Let us consider the sums in (1) in detail

$$V_1 V_2 = \sum_{i(1)} v_i \sum_{j(2)} v_j =$$
$$= \frac{1}{2}\left(\sum_{ij} v_i v_j - \sum_{ij(1)} v_i v_j - \sum_{ij(2)} v_i v_j\right) \tag{2}$$

where $v_i = v_j = 1$. The summation is over all possible pairs of electrons. The coefficient ½ appears because there are no limitations on the permutation of indices.

Let us apply (2) to pairs of π- and σ-bond electrons. For a σ-bond, the orbital moment projection (*m*) of its electrons onto the internuclear axis has a single (zero) value. A pair of σ-electrons has therefore one state only

$$v_\sigma^2 \equiv \frac{1}{2}\left(v_{i(1)} v_{j(2)} + v_{j(1)} v_{i(2)}\right) = 1 \cdot$$

For π-bond electrons, the orbital moment projections onto the same axis take equal values, either $+1$ or -1 (depending on whether the right- or left-handed coordinate system is used; here we use atomic units of moment). We therefore have four terms for π-bond electrons

$$v_\pi^2 \equiv \frac{1}{2}[v_{i(1)}v_{j(2)}\big|_{m=+1} + v_{j(1)}v_{i(2)}\big|_{m=+1} + v_{i(1)}v_{j(2)}\big|_{m=-1} +$$

$$v_{j(1)}v_{i(2)}\big|_{m=-1}] = 2$$

This gives $v_\pi = \sqrt{2}$. It follows that the n-fold state of degeneracy corresponds to the n-fold increase in the sum of pair electronic products, that enhances the elementary volume of the pair of bond electrons, $v_e = \sqrt{n}$. It is necessary to bear in mind that the electron balance condition imposes the following restriction: if $\sum V_a = \sum Z_a$, then $v_e \equiv 1$ and, vice versa, if at least one v_e value is larger than 1, then $\sum V_a < \sum Z_a$.

The role of the product of volumes in describing the interaction of atoms is clarified by the following identity:

$$\sqrt{V_1 V_2} = \frac{1}{2}\left[\left(\sqrt{V_1} + \sqrt{V_2}\right)^2 - V_1 - V_2\right] \quad (3)$$

The appropriately normalized electronic volume of an atom corresponds to the probability of that its electrons belong to the bond under consideration. In terms of probability, the expression in brackets is the excess value, which appears as a result of bond formation.

On the other hand, the covalent bond energy is a function of the excess electron density in the internuclear space

$$\overline{\rho}(r_{12}) \propto (Z_1 + Z_2)\left[\int_{(l=r_{12})} \Psi^*\Psi\, d\tau - \int_{(l=\infty)} \Psi^*\Psi\, d\tau\right] =$$

$$= (Z_1 + Z_2)\left[\overline{\psi}^*(r_{12})\overline{\psi}(r_{12}) - A\right], \quad (4)$$

$$A = \overline{\psi}^*(\infty)\overline{\psi}(\infty) = \frac{1}{2}$$

where Z_1, Z_2 are the charges of nuclei in the elementary charge units; $d\tau$ is the space volume element; l is the interatomic distance; and the bars denote the averaging over the scale indicated in parentheses, which coincides with one of the arguments of the functional relation. The first integral equals the probability for an atomic electron to occur between the planes passing through the nuclei normally to the interatomic axis at distance r_{12} from each other. The second integral gives the same probability at infinite interatomic distance. The integration in (4) is performed taking into account that the electronic wave function in the internuclear space depends on bond length. When atoms are infinitely separated, the excess electron density is zero, and exactly one-half of

all the electrons occur in the internuclear space.

We can therefore write $E_{12} = F\left(\overline{\rho}(r_{12})\right) = f\left(X_{12}, r_{12}\right)$ that gives

$$\overline{\rho}(r_{12}) = g(V_1 V_2) \quad (5)$$

Comparing (3) and (4) by their sense and taking into account (5), we obtain

$$\sqrt{V_1 V_2} = (Z_1 + Z_2)\left(\psi(r_{12})\psi^*(r_{12}) - \frac{1}{2}\right) \propto \overline{\rho}(r_{12}) \quad (6)$$

According to (6), the excess density in the internuclear space is proportional to the geometric mean of the probabilities for atomic electrons to take part in the bond under consideration.

To simplify (6), let us make the substitution

$$\overline{\psi}(r_{12}) = \frac{1}{\sqrt{2}}\frac{\sqrt{Z_1}}{\sqrt{Z_1 + Z_2}}\overline{\psi}_1(r_{12}) + \frac{1}{\sqrt{2}}\frac{\sqrt{Z_2}}{\sqrt{Z_1 + Z_2}}\overline{\psi}_2(r_{12})$$

$$(7)$$

where $\overline{\psi}_a(r_{12}) \equiv \psi_a = \exp(i\varphi_a);\ a = 1, 2$. We obtain:

$$\frac{1}{2}\left(\psi_1^*\psi_2 + \psi_1\psi_2^*\right) \equiv \cos(\varphi_1 - \varphi_2) = \sqrt{\frac{V_1 V_2}{Z_1 Z_2}} \equiv \alpha \quad (8)$$

Let us clear the combinatorial meaning of α: its square is the relative part of the cases when a pair of the particles belonging to two nonoverlapping sets of Z_1 and Z_2 particles occurs among the set of $V_1 + V_2$ particles, where V_1 particles belong to the first set and V_2 particles, to the second one. This interpretation suffers from the shortcoming that the electronic volume is a more complex concept that the number of electrons.

The above-mentioned quantity $\overline{\psi}_a(r_{12}) \equiv \psi_a$ is the characteristic of atom depending on bond length. In such a case the φ_a phase is a function of the scalar product of the wave vector of atomic electrons ($\mathbf{k}_a$) and the internuclear vector

$$\varphi_a = \varphi(\mathbf{k}_a \mathbf{r}_{aa'}) = \sum_i A_i (\mathbf{k}_a \mathbf{r}_{aa'})^i;$$

$$a, a' = 1, 2;\ a' \neq a;\ i = 0, \pm 1, \pm 2, \ldots \quad (9)$$

The presence of even exponents in expansion (9) is inessential because of their zero contribution to the difference of phases in (8) when the atoms are identical. For the same reason, at least one of the odd constants A_i in (9) is nonzero. When the internuclear distance in its tending to zero falls beneath a certain value, the number of electrons forming the bond becomes nonzero. Negative exponents are therefore absent in (9). The absolute term ($i = 0$) in (8) is annulled and therefore does not play any role. Thus, we can keep in (9) only the linear term, and set, without loss of generality, the constant A_1 equal to

unity

$$\varphi_a = (\mathbf{k}_a \mathbf{r}_{aa'}); \quad \varphi_1 - \varphi_2 = (\mathbf{r}_{12}(\mathbf{k}_1 + \mathbf{k}_2)) \qquad (10)$$

Rewrite expression (8) taking into account (10):

$$\alpha = \cos(\mathbf{r}_{12}(\mathbf{k}_1 + \mathbf{k}_2)) = \cos(r_{12}\textstyle\sum k_r), \qquad (11)$$

where $\sum k_r$ is the sum of projections of the wave vectors of bond electrons on the bond axis. Finding this sum from (11), we get

$$\sum k_r = \pm r_{12}^{-1} \arccos \alpha \qquad (12)$$

The remarkable feature of $\sum k_r$ is its independence of π-electrons of the bond, because the limit value of π-electron moment projection on the bond axis corresponds to the zero projection of its wave vector in this direction

$$\sum k_r = k_{\sigma 1r} + k_{\sigma 2r}, \quad \sum k_{\pi r} \equiv 0 \qquad (13)$$

Combining (11) with (12) and (13), we find the general expression for a covalent bond

$$\alpha' = \cos(r_{12}'\textstyle\sum k_r) = \cos\left(\frac{r_{12}'}{r_{12}} \arccos \alpha\right) \qquad (14)$$

where primed and unprimed values relate to different cases of the bond between the same atoms. Note that (14) is valid for both double and triple bonds. Similar to (8), we can write

$$\alpha' = \sqrt{\frac{V_1' V_2'}{Z_1 Z_2}},$$

where V' differs from the single bond property V by the replacement of one or two electrons by π-electrons of double or triple bond, correspondingly. Thus, the number of electrons forming a covalent bond is independent of its order and, due to the above-introduced normalization of electronic volume, is equal to the electronic volume of atom for the case of single bond (V_a). Taking into account the value $v_\pi = \sqrt{2}$ obtained above, we find

$$V_a' - V_a = (\sqrt{2} - 1)(n - 1) \qquad (15)$$

where $n = 1, 2, 3$ is the bond order. In particular, it follows from (14) that for homo-nuclear bonds

$$V' = Z \cos\left(\frac{r_{12}'}{r_{12}} \arccos \frac{V}{Z}\right) \qquad (16)$$

It is quite natural to assume that V_a can differ from Z_a by the number of closed shell electrons (for which the shielding radius is smaller than that for outer shell electrons), equal to two for the second-period atoms that yields $V_a = Z_a - 2$. This expression in combination with (15) and (16) gives after simple transformations (see

Appendix)

$$\frac{r_{12}'}{r_{12}} = \arcsin \sqrt{\frac{2 - (\sqrt{2} - 1)(n - 1)}{2Z}} \Big/ \arcsin \sqrt{\frac{1}{Z}} \approx \qquad (17)$$

$$\approx \sqrt{1 - \frac{(\sqrt{2} - 1)(n - 1)}{2}} \qquad (18)$$

The last result valid for large atomic numbers is valuable due to its independence of the kind of atoms, displaying only the dependence of the bond order.

The calculation using (18) gives $\dfrac{r_{12}'}{r_{12}} = 0.890$ for double bond and $\dfrac{r_{12}''}{r_{12}} = 0.765$ for triple bond. Formula (18) is approximately valid for hetero-nuclear compounds as well.

The comparison of the theoretical result obtained with experimental data is given in the **Table.**

For some possible compounds there is no information on bond length. This lack of knowledge can be eliminated by theoretical forecast. For example, the triple bond of boron with carbon or nitrogen is possible in principle. Its length will be about 24% shorter than the corresponding single bond.

3. Conclusions

Thus, there is good compliance between experimental and theoretical values that confirms the necessity to distinguish in interatomic interactions the contributions of differently degenerated electrons. The contribution of π-electron to such an additive property of the interactive atom as its electronic volume is in $\sqrt{2}$ times larger than that of σ-electron. This effect can be explained by different symmetries of the states with different degeneracy of σ- and π-electrons. In present work, the simple expression (17, 18) for covalent bond length ratio which shows strong influence of bond orders and weak dependence on atomic numbers is obtained.

Table. Ratios of the bond lengths for compounds of the second-period elements: reference data [7,8] *versus* calculation results.

Atoms bonded	Bond length ratio: *double to single*	Bond length ratio: *triple to single*
C-C	0.865	0.778
N-N	0.862	0.757
O-O	0.813(O_2); 0.861(O_3)	0.766(O_2^+)[8]
C-N	0.910	0.786
C-O	0.852	0.791
N-O	0.897	0.779(NO^+)[8]
Theory: formula (18)	0.890	0.765

4. References

[1] E. V. Kalashnikova, A. V. Kiselev, D. P. Poshkus and K. D. Shcherbakova, "Retention Indices in Gas-Solid Chromatography," *Journal of Chromatography A*, Vol. 119, No. 41, 1976, pp. 233-242.

[2] J. A. Pople and D. L. Beveridge, "Approximate Molecular Orbital Theory," McGraw-Hill, New York, 1970.

[3] A. M. Dolgonosov, "Energy and Molecular Area of the Adsorbate on a Uniform Adsorbent," *Doklady Physical Chemistry*, Vol. 358, No. 1-3, 1998, pp. 26-30.

[4] A. M. Dolgonosov, "Calculation of Adsorption Energy and Henry Law Constant for Nonpolar Molecules on a Nonpolar Uniform Adsorbent," *The Journal of Physical Chemistry B*, Vol. 102, No. 24, 1998, pp. 4715-4730.

[5] S. Lundquist and N. H. March (Eds.), "Theory of the Inhomogeneous Electron Gas," Plenum Press, New York -London, 1983.

[6] A. M. Dolgonosov, "Electron Gas Model and Theory of Generalized Charges for Description of Interatomic Forces and Adsorption," Librokom/Urss, Moscow, 2009.

[7] A. J. Gordon and R. A. Ford, "The Chemist Companion," Wiley, New York, 1972.

[8] V. A. Rabinovich and Z. Ya. Havin, "Brief Chemical Handbook," Khimia, St-Petersburg, 1994

5. Appendix

<u>Deduction of (17).</u>

Let us denote

$$s_1 = \frac{2 - (\sqrt{2} - 1)(n-1)}{2Z}, s_2 = \frac{1}{Z}.$$

It is necessary to transform the expression

$$x = \frac{\arccos(1 - 2s_1)}{\arccos(1 - 2s_2)}.$$

Using the formula $\arccos t = \arcsin\sqrt{1 - t^2}$ yields

$$x = \frac{\arcsin\sqrt{2s_1(2 - 2s_1)}}{\arcsin\sqrt{2s_2(2 - 2s_2)}} = \frac{\arcsin 2\sqrt{s_1(1 - s_1)}}{\arcsin 2\sqrt{s_2(1 - s_2)}}.$$

Substitution of $s_i = \sin^2 \varphi_i$ leads to

$$x = \frac{\arcsin 2\sqrt{\sin^2 \phi_1 \cos^2 \phi_1}}{\arcsin 2\sqrt{\sin^2 \phi_2 \cos^2 \phi_2}} = \frac{\arcsin(\sin 2\phi_1)}{\arcsin(\sin 2\phi_2)} =$$

$$= \frac{\phi_1}{\phi_2} = \frac{\arcsin\sqrt{s_1}}{\arcsin\sqrt{s_2}}.$$

The inverse substitutions of the expressions for s_1, s_2 give formula (17).

Scientific
Research

The Phenomenon of Proton Dissolving in Vacuum and of Proton Condensation from Vacuum. Two Forms of Protons, Structure of Nuclei, Electrons and Atoms

Kristina Zubow[2], Anatolij Zubow[1], Viktor A. Zubow[2]*

[1]*Department of Computer Science, Humboldt University Berlin, Johann von Neumann Haus, Berlin, Germany*
[2]*A IST Handels- und Consulting GmbH, Department of Research & Development, Groß Gievitz, Germany*
E-mail: *zubow@informatik.hu-berlin.de, aist@zubow.de*
Received April 18, 2010; revised May 15, 2010; accepted May 22, 2010

Abstract

It was investigated how react molecular clusters in water, starch, bio-matrices, polymers and in quartz on gravitation radiation from planets. Gravitation radiation (GR) was found to influence the proton jumping in hydrogen bonds that stabilize the cluster structure. There was given a method calculating parameters of GR as well as a mechanism of its resonance interaction with weak GR from molecular matter (WGR). WGR has been defined as the result of proton dissolving in vacuum connected with its simultaneous condensation in the nearest free space. Both dissolving and condensation proceed with super light velocity. The gravitation wave length has been determined experimentally and it depends on the planet masses (between Earth and Sun $\lambda \geq 62$ km, between Earth and Milky Way center $\lambda \geq 330$ km). GR has been characterized with super light velocity. After analyzing the Sun influence on water two forms of protons were found: in a condensed and dissolved state. A new model for the atomic nucleus has been suggested according to which the protons in the nucleus oscillate between condensed and dissolved state, where in the case of isotopes this state is partially destroyed. The models for H_2 and Be shall be given. Electron orbitals in atoms and molecules were found to be caused by a stationary front of shock waves from condensing protons.

Keywords: Gravitation Waves, Proton, Dissolving, Vacuum, Planets, Electron, Form of Matter

1. Introduction

The proton jumping via hydrogen bridges (H-bonds) or via even a group of atoms in a molecule has been illustrated as follows:
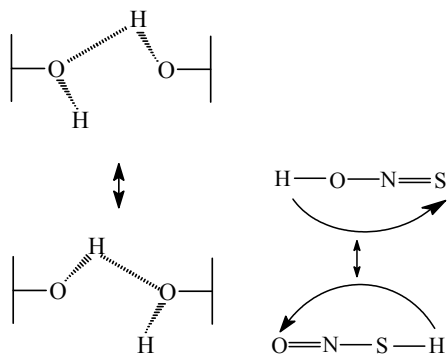
Scheme 1

The hydrogen atom that is linked with an oxygen atom builds simultaneously a H-bond (~0.2 nm) with an other molecule fragment or an other molecule and it is able to

jump to the second oxygen atom. Instead of oxygen other atoms like nitrogen; sulfur etc. can be applied to this scheme. Inner molecular jumps in low molecular substances can proceed at distances longer than 0.2 nm but in high molecular ones the talk is even on umpteen nm.

This effect has been observed for many organic and inorganic substances and it is well described [1-3] though a proton jumping through electron orbitals of atoms and molecules seems to be more or less unprobably. Furthermore, because of unavailable mechanism models and analysis methods it is difficult to understand this effect. On the other side hydrogen bridges were found important for the stabilisation of the conformation of synthetic macromolecules and biomolecule coils (proteins, starch). Destruction of hydrogen bridges leads to a change of the conformation of protein macromolecules, to changed directions of biochemical reactions and finally to another behaviour of the organisms. In our earlier publications we informed on fields of unknown nature that are present in moleculare systems with hydrogen bridges. For instance, in [4] we described the "wall effect": near the wall there

is a special gravitation excitation (water, salt solutions), that seems to be connected with hydrogen bonds and proton jumping. We developed the idea about the proton jumping via the vacuum to the nearest energy vacancy place in space. According to this hypothesis the proton jumping is connected with acceleration and breaking of masses in the proton leading to weak gravitation radiation. To identify a gravitation wave in a real time it is necessary to shift "the interference of the gravitation pair (mutual compensation) at the time or to expand the events in the space. For that we have to look for the resonance of gravitation waves between micro and macro objects for example, in gravitation pairs—between clusters in the molecular matter and masses of planets. To proof this hypothesis we developed a gravitation mass spectrometer (GMS) by which help we registered molecular mass clusters as well as their interaction with the surroundings [5,7].

It was the aim of the present work to understand the mechanism of proton jumping in molecular matter as well as to find out the reasons that cause unknown fields in it.

2. Experimentally

As investigation objects the following substances were chosen: water, agarose hydrogel (97 wt.% water), salt solutions (NaCl, 3.5 wt.%), starch, polyethylene, atactic polystyrene (aPS, average molecular mass of 15 kDa) as well as bio matrices of eggs and potato tubers. The GMS-sensor was placed directly in the bio-matrices, pressed (1-2 kPa) to powders or films or installed in aged

for 6 month liquids. The GMS method is ascribed in [5-8]. Masses and oscillation frequencies of clusters in the samples were calculated by the Zubow equations using the Zubow constant 6.4×10^{-15} N/m for biomatrices, water and 6.8×10^{-15} N/m for starch and 5.2×10^{-15} N/m for aPS. Samples were placed in an iron (grounded) box that was isolated from light, anthropogeneous noises and heat/mechanical fields. The box itself was in a building far from industrial centers. Some curves, reflecting the energy flow (sum of cleaned signals) that achieves the GMS-sensor in the samples between August the 15th and 16th 2008, are shown in **Figure 1**. The base line (dotted line) was obtained as follows. After noises were registered by GMS-sensor in vacuum (10^{-4} N/m^2) the real signals (first) were extracted where an analogous procedure was done for the sample without vacuum (second). The real sample signals were calculated by subtracting the second signals from the first ones [6]. 265784 represents the sum of all signals in the mass interval up to 4.3 billion Da.

3. Results and Discussion

The existence of cluster ensembles in molecular matter showing both wave and corpuscle properties are undoubtedly [9]. Clusters oscillate and noise. These oscillations e.g. in liquids are similar to "structure transfusion" and it is connected with a constant virtual mass jumping in the dynamic balance between noise energy stabilizing clusters [10] and heat (kT), that destroy clusters.

In **Figure 1**, the planet influence on the energy of cluster ensembles in molecular matter shall be shown. As
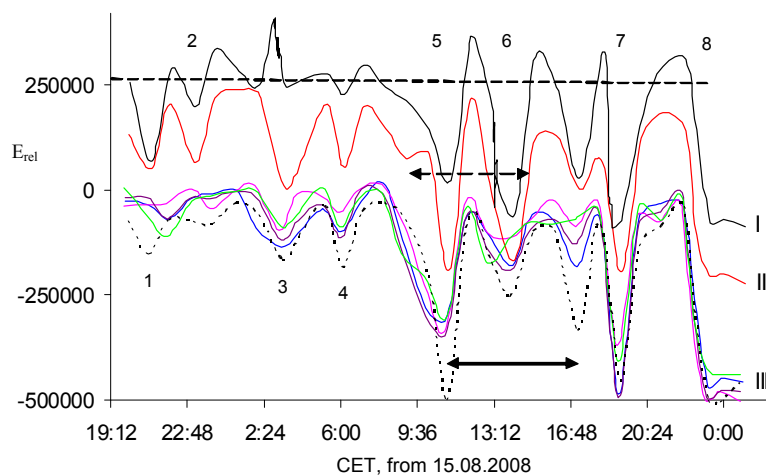
Figure 1. Energy flows in different substances: I—bio-matrix of fresh potato tuber, II—melted quartz (glass), III—water, methanol, bio-matrix of a hen's egg (egg white), polymers (dotted line), water solution of 3.5 wt.% NaCl, 1—sundown, 2—full Moon before the moon was covered by Earth 24 h later (8), 3—Uranus culmination, 4—Sunrise, 5—Mars culmination, 6—nearly simultaneous culmination of Mercury, Venus and Saturn, 7—Jupiter rise, 8—moon eclipse. By horizontal arrows the effects of interference of gravitation noises from Sun are given (dotted line: from 09:00 until 15:00) and Galaxy centre (dotted line: from 11:00 until 17:00). The curve is formed from points in which every point is a statistical value which isn't worse than 95%. The base horizontal line corresponds to 265,784 relative units (state, on August 15th, 2008, at 19:12).

visible the molecular cluster ensemble energy is sensitive to the planet constellation and this energy, for instance of gravitation nature, was found to be detectable by the GMS method.

Let us discuss two pairs of peaks at 09:00 and 15:00, and at 11:00 and 17:00, both peaks are on a line, that is perpendicularly to the line connecting the centers of the Sun and the Earth, and of the Milky Way and the Earth, accordingly. The peaks can be interpreted as interference of gravitation waves and with the help of the Junge equation the wave length can be calculated and compared with literature references. The calculation was made using

$$\lambda \geq D \cdot S / R$$

where λ – average gravitation wave length, R – distance from the gravitation source to sample (until Sun 150 mio km, until Milky Way center 10,000 pc), D – distance between peaks, amounting to $D = 2 \cdot r \cdot \sin(90° − 53°) \cdot \sin(120°/2)$, $r = 6370$ km (radius of Earth), S – diameter of source (Sun, 1,392,000 km, Galaxy center 500 pc), here the role of two slits played the Earth atmosphere and the role of display – area which connects the peaks with each other and stands vertically to the gravitation source. Thus, $\lambda \geq 62$ km (gravitation waves of Sun) and $\lambda \geq 330$ km (gravitation waves of the Galaxy center). The gravitation wave length calculated by Hickey [11] was found to be

~100 km furthermore Smirnov described a device for the registration of gravitation excitation in the frequency interval 10 Hz…40 kHz [12], which includes all investtigated cluster oscillations in molecular matter. We can therefore notice with a great probability that the GMS device registers directed gravitation radiation (GR). Now we want to analyze how GR influences the long range order in water whose structure was already proved experimentally [8]. Inside the clusters, the water molecules are linked with each other by two hydrogen bridges but on the cluster surface the water molecules possess only one hydrogen bridge (HB) for their interaction with the surroundings. If the proton jumping in HB proceeds with emission of weak GR then we have to expect a resonance between weak GR of molecular matter and GR of planets. The proof of this assumption is given in **Figure 2**.

As visible from **Figure 2** the number of clusters in water reacts on the planets' GR where this effect is shown most strongly at full moon (23:16, point M) and eclipse of the moon (the moon is covered to 80% by the Earth). The GR of Jupiter at its rise has a strong influence on the cluster number in water too. To understand the structure of GR we investigated GR of Jupiter (**Figure 3**). GR of Jupiter consists of two parts which were ascribed to signals of "gravitation Jupiter" and of "visible Jupiter". The
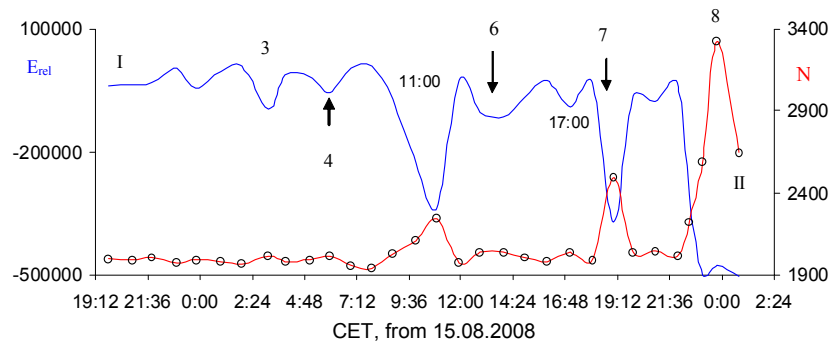
Figure 2. Behavior of the GR energy curve registered by GMS-sensor in water (I) and of the number of cluster kinds (II) in dependence on events in the near space, cluster ensembles up to 4.3 billion Da. Comments see in Figure 1.
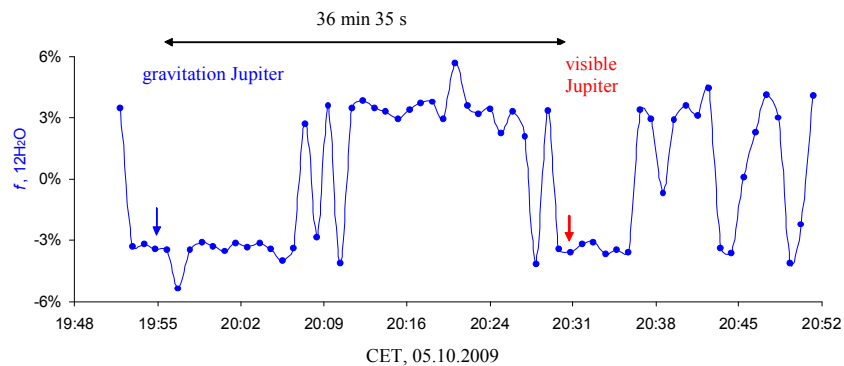
Figure 3. Signal intensities of the base water cluster in agarose hydrogel when the flows of both Jupiter gravitation energy kinds are in the slide plane of gravitation proton resonance (SPGPR). Distance to Jupiter—658,629,000 km; altitude 19.7°. SPGPR—plane going through the Earth rotating axis and the sample place on the Earth surface.

sample was fully protected from visible light therefore, the signal of "visible Jupiter" can be interpreted as ripples of main Jupiter GR [7,11]. That means we have the right to use the correlation between the visible and gravitation constellation of planets.

In **Figure 4**, computer models for the simplest water clusters, consisting of the base water cluster $(H_2O)_{11\pm1}$ [13,14], and experimentally observed methanol clusters are given [8]. The base water cluster belongs to an ensemble of dominating clusters which were formed forced in the white noises: $(H_2O)_{11\pm1}$, $(H_2O)_{100}$, $(H_2O)_{178}$, $(H_2O)_{280}$, $(H_2O)_{545}$, $(H_2O)_{903}$, $(H_2O)_{1351}$, $(H_2O)_{1601}$, $(H_2O)_{1889}$ etc.. Jupiter at rise (**Figure 1**) and culmination (**Figure 4**) strongly influences by its gravitation radiation the long range order in water and destroys the cluster ensemble temporarily. On the other side, the destruction of the water cluster ensemble has been observed during the gravitation interference (signal at 11:00) and even at GR of Uranus and sunrise (**Figure 2**).

Cluster ensembles in methanol react analogously to GR flow of planets where the highest destruction of hydrogen bridges takes place at Jupiter rise. However, the behavior of polyethylene, which doesn't have any hydrogen bridges, is something differently the strongest cluster ensemble destruction is at Moon eclipse and at GR interference of the Galaxy center and WGR of polyethylene (11:00 and 17:00).

In the **Table 1**, the GR frequencies of planets and water molecular clusters that were calculated by the Zubow

equation are given.

Let us now discuss the hydrogen bridges (HB) in the amorphous part of starch (**Figure 5**). As shown in **Figure 5** HB, reflecting conformation changes in the starch coils, react on GR of planets. In **Figure 6**, the review GM-spectra of starch powder at Jupiter rise will be given (see **Figure 1** too), the destruction of the hydrogen bridges that form the globular structure of this polymer can be seen. This destruction process proceeds reversibly and is an indication for a special resonance interaction between gravitation radiations. On the other side the dominating influence of planets' GR on a cluster ensemble in molecular matter often leads to a simultaneous energy inversion of the density of all clusters. In starch, the conformation of macromolecule coils are known to be stabilized by HB and its destruction, which is caused by resonance with planets' GR, should be modelable by a forced compression. At pressure the length of HB shall be changed and the oxygen influence on the "naked" proton becomes stronger. We found, that by pressing the starch powder mechanically (1…5 kPa) the hydrogen bonds were forced and reversibly destroyed too conesquently, mechanical pressure is comparable with planets' GR.

Thus, the existence of weak gravitation radiation in molecular matter, which is caused by super light mass transfer in hydrogen bridges, has been concluded. It is hard to imagine this process, as a simple jump on a dis-hard to imagine this process, as a simple jump on a dis-
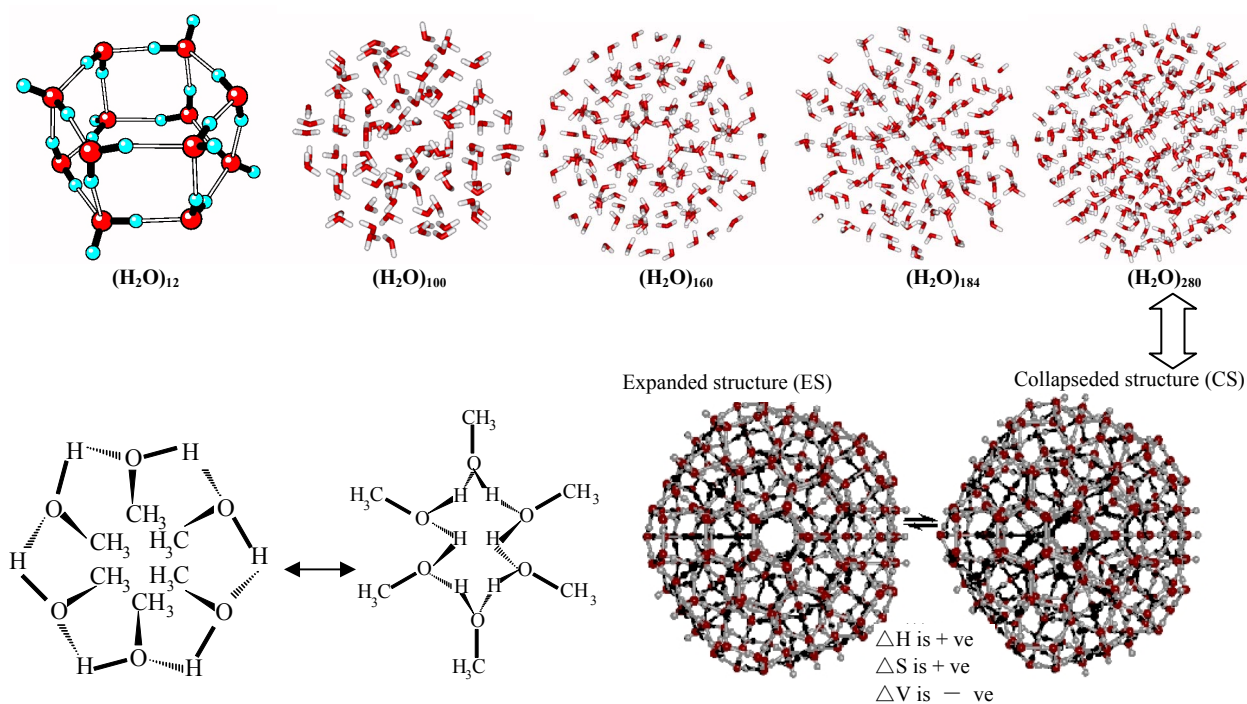
Figure 4. Calculated water cluster models (with kind permission of the professors Chaplin (http://www.lsbu.ac.uk/water/index.html) and Lenz [14]) and methanol clusters, experimentally observed by the authors [8].

　　　　　　　　　　　　　　　　　　　　　　　　　　　JMP
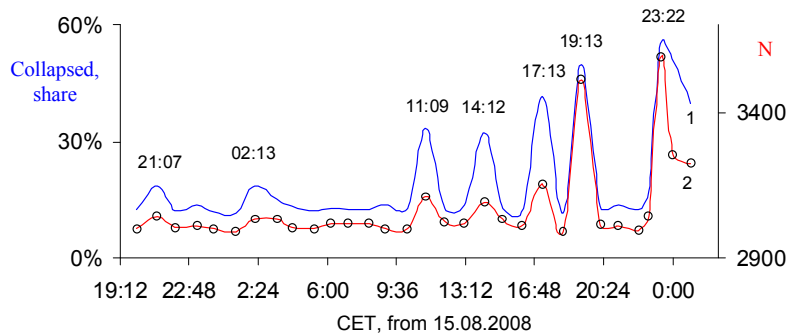
Figure 5. Share of collapsed clusters (1) and of cluster kinds' numbers (2) in the amorphous part of potato starch observed at GR influence of planets (Figure 1).
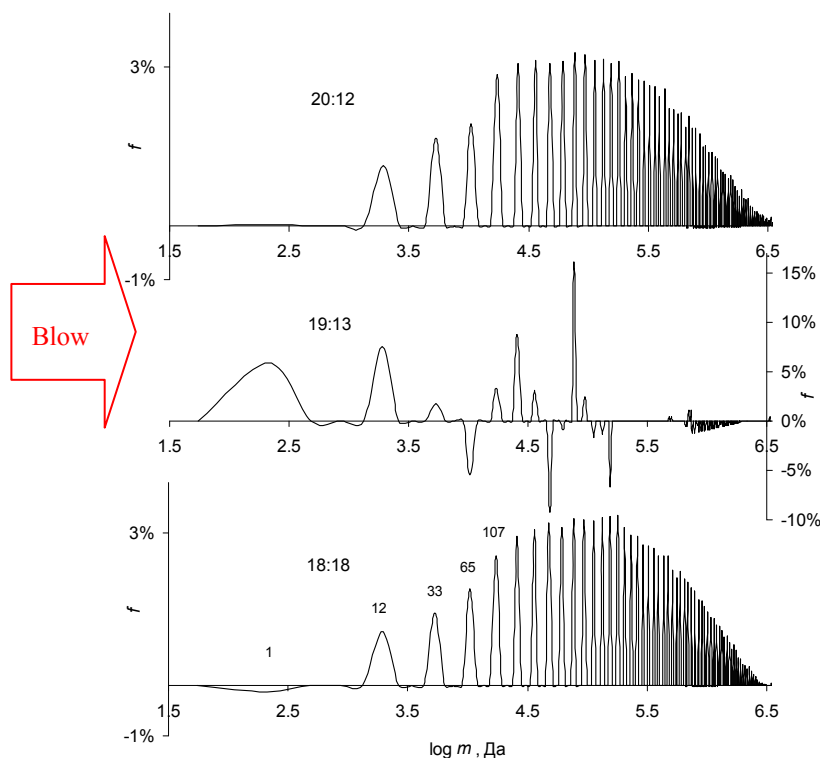
Figure 6. FNS of potato starch (powder 1.55 mmol, 0.5 cm^3) at Jupiter rise (Figure 5). Weak shock wave ($p < 1$ N/m^2), Zubow constant is equal to 6.8×10^{-15} N/m. The numbers over the signals correspond to the number of α-D-glycopyranose in a cluster. The number of cluster kinds (signals) in the investigated mass ensemble amounts to: 102 at 18:18, 59 at 19:13 and 104 at 20:12 (Central European Time, 16.08.2008). The distance between Jupiter and Earth is 655×10^6 km.

Table 1. The main noise frequencies of planets and of the sun, that were calculated according to $m = N_A \cdot 10^{11} \cdot \omega^{-2}$, where compared with the frequencies of water clusters in a potato bio-matrix, $m = 10^{11} \cdot \omega^{-2}$.

	Characteristics		Molecule clusters*	
Planet	**m, g**	**ω, Hz**	**ω, Hz**	**Formula**
Mercury	3.40E + 26	13309 ± 2000	11111 ± 2000	$(H_2O)_{45}$
Venus	4.87E + 27	3517 ± 200	3431 ± 200	$(H_2O)_{472}$
Earth	5.97E + 27	3176 ± 200	3193 ± 200	$(H_2O)_{545}$
Mars	6.40E + 26	9700 ± 1500	7454 ± 1500	$(H_2O)_{100}$
Jupiter	1.90E + 30	178 ± 20	178 ± 20	$(H_2O)_{174420}$
Saturn	5.69E + 29	325 ± 30	333 ± 30	$(H_2O)_{50124}$
Uranus	8.70E + 28	832 ± 50	827 ± 50	$(H_2O)_{8131}$
Neptune	1.03E + 29	765 ± 40	769 ± 40	$(H_2O)_{9385}$
Moon	7.35E + 25	28624 ± 4000	21517 ± 4000	$(H_2O)_{11\pm1}$
Sun	1.99E + 33	5.5 ± 1	5.5 ± 1	$(H_2O)_{36453036}$

tance of 0.2 nm or longer, a process in which the proton must penetrate a "net" from electron clouds of atoms and molecules. However, there are another way, namely the transition of the proton into the vacuum (dissolving) connected with the arising of his equivalent simultaneously in the next free energy place. This process of super fast dissolving and condensation of mass could cause WGR from molecular matter [15]. Under the examined substances stand out the ones, those don't have any HB (aPS, polyethylene). The proton jump in HB is therefore a special case of the general phenomenon for the proton jump from the atomic nucleus into vacuum and reversed.

To evaluate the velocity of the proton jumping in vacuum the results of GR wave length analysis were applied (**Figure 1**) using in the first approximation the Planck equation $E = h \cdot c_\Gamma \cdot /\lambda$, where h –Planck constant, λ –wave length, m, c_Γ – velocity, m/s. The energy value (E) can be considered as the disintegration energy of starch coils [16]. We assume that this value amounts to ~2 kJ/mole, then

$$c_\Gamma = E \cdot \lambda/h > 15 \times 10^{35} \text{ m/s.}$$

This velocity is 5×10^{27} times higher than the light velocity and the GR frequency is equal to $c_\Gamma \cdot 1/\lambda = 2.32 \times 10^{31}$ s^{-1} which doesn't agree with the gravitation frequencies published in [17-20] as well as with the conclusions on the GR influence on the long range order in molecular matter. However, this situation can be cleared with the results of Kokkotas [21] according to whom at moving of masses their gravitation waves initiate ripples of smaller ones (gravitation noise), that spread with light velocity. The gravitation noise we observed to be the reason for the forced oscillation of clusters in molecular matter and matter in space but the clusters themselves are the result of stationary gravitation waves. Then, the energy dependence of the main gravitation waves on their wave length can be given as:

$$E = z \cdot \lambda,$$

where $z \sim (2...3) \cdot 10^{-2}$ J/m, $\lambda \sim 65,000...100,000$ m.

Of course, the proton moving with super light velocity has to understand as a short living time at the level of proton dissolving in vacuum (P_p) and proton condensation from vacuum ($P_\text{к}$). Then, the model for the proton jumping can be shown as follows.

In this scheme, the distance between dissolving and
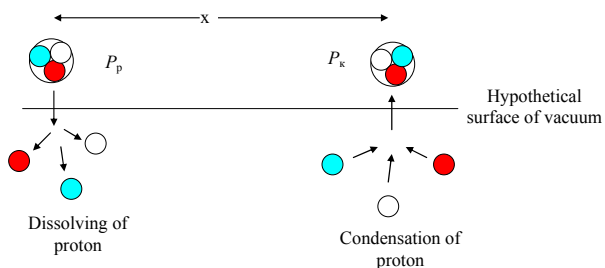
Scheme 2

condensing proton can be forced changed for example, by a simple sample compressing [7] or by the resonance with analogous processes from planets.

This nucleus model doesn't contradict the idea about the cluster formation in boson matter, according to which the mass transformation proceeds to strictly deterministic gravitation laws [7]. The physicists have unbelievable done, to explain the stability of great and thick accumulations of positively charged particles in a very small volume of the nucleus. One tried to find a force which holds these particles together however it wasn't found. Now as we understand the proton as an oscillating substance (dissolving and condensing) the nucleus formation of chemical elements and their isotopes should be clearer. In nuclei, the proton dissolving proceeds in the energy balance with the condensation of the neighboring proton (see scheme). In this case, the probability that two positive charges are besides each other, gets lower but the gravitation interaction in the nucleus becomes more dominant.

The instability of radioactive isotopes has been explained by the destruction of the oscillation harmony in the nucleus. Radioactive isotopes are characterized by a high potential energy of their nuclei (as a pendulum system) and its minimization is connected with nucleus disintegration.

The molecule stability of hydrogen (H-H) can be better explained by this model according to which the protons alternately dissolve and condense and the electrons permanently catch up with the positive charges (condensed proton). Here the electrons permanently rotate around the condensed proton and its Fata Morgana "(dissolved proton) leading to multiple canonical structures for instance H-H.

For the beryllium nucleus, two canonical structures shall be shown, for example (**Figure 7**) this scheme is analogous to the one which describes the formation of clusters in molecular matter [9].

The electron clouds around the nuclei can be understood as stationary shock waves arose from condensing protons from vacuum. The shock wave front is in balance with the energy state of the vacuum 1.4×10^{16} kJ/m^3 [7,9]. This front (electron orbital) is permanently generated by high frequency shock waves from the condensing proton and at proton dissolution; it doesn't manage to dissipate in vacuum and saves therefore its spherical form (model for hydrogen atom, **Figure 8**) because of a higher inertia of the dissipation process, probably. A proof for this model could be that the electron orbital in the hydrogen atom oscillates (known as electron transition from one energy state to the other one). In accordance with this logic the energy released at proton condensation should correspond with the vacuum energy namely with $\sim 1.4 \times 10^{16}$ kJ/m^3.

For multiple proton nuclei, the spherical shock wave construction shall be changed to differently formed ones,

state n_i state n_{i+1}
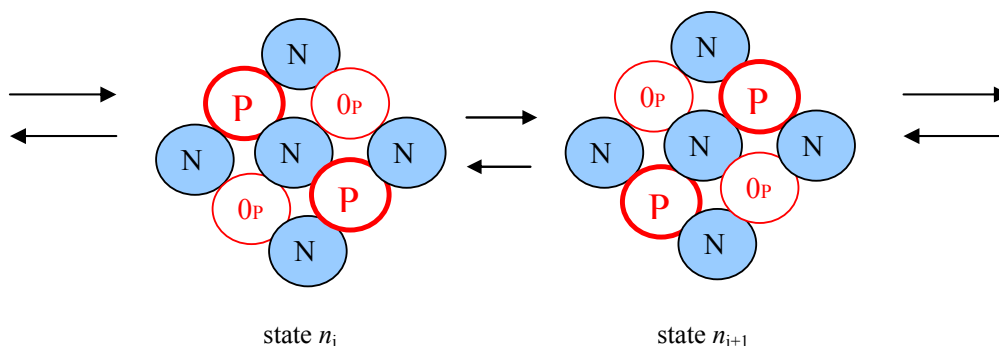
Figure 7. Statistical model for the nucleus formation of beryllium (4 protons (P) and 5 neutrons (N)). P—proton condensed from vacuum, 0p—place of the dissolved proton in vacuum. The most probable states are shown.

Shock wave (electon cloud – orbital) around condensing proton from vacuum

Shock wave evolution (electon cloud – orbital) around dissolving proton in vacuum
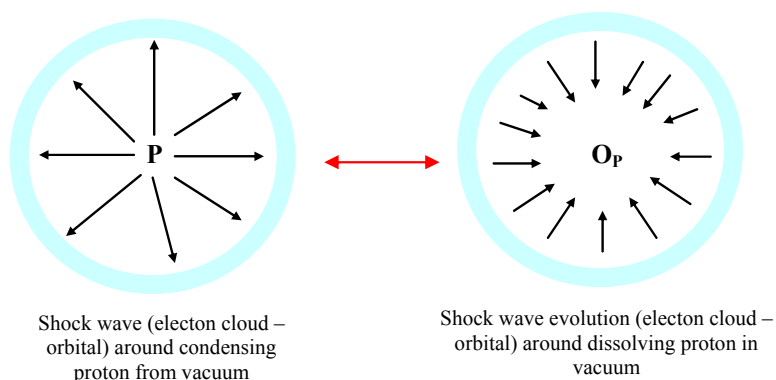
Figure 8. Model for the formation of a spherical electron orbital in the hydrogen atom. This orbital is caused by a shock wave front which arises from the pulsating of the condensing proton from the vacuum (left) and from the front movement at proton dissolving in vacuum (right). The structure and energy of the vacuum are described in [7,9].

known as orbital hybridization in chemistry. Here the hybridization reflects an energy minimization process. On the other side the state of free electrons can be understood as an energy cluster of excited matter from vacuum that exists in the movement form only.

According to this model of nucleus, the molecule is less caused by the unification of nuclei through electron orbitals than by a forced cluster formation of protons in stationary gravitation waves of the space [7]. The concentration of atomic nuclei in a cluster represents a molecule but that one of any molecules a molecule cluster. Starting out from this model the electron orbital can be imagined as a shock wave front in the compressed vacuum being another form of the matter. Under special conditions the shock wave front could be concentrated in a cluster of negative energy-electron-particle. We therefore have to work with two matter forms which aren't mixable with each other, vacuum matter and matter that shall be released or absorbed at condensation/dissolution of a proton.

The GM-spectra observations of water at the period when the Sun is in SPGPR could be an additional proof for the dissolving of the proton and for its existence in two forms (dissolved and condensed). The results of

these observations shall be given in **Figure 9**.

As visible from **Figure 9**, all base skeletal water clusters are present in water of the agarose hydrogel [22]. The GM-spectra are identical up to the entrance of the Sun in SPGPR (13:14) and after its exit from SPGPR (13:18). The molecular clusters are given in their expanded forms indicating a strong inter-cluster interaction through hydrogen bonds. In these bonds, the, by the Paulings so-called, "naked" protons [23] are in the condensed state. At the entrance of the Sun in SPGPR (13:15) the protons disappear, to be explained with their forced dissolution in physical vacuum and the remove to the Sun [7].

Thus, the structure of hydrogen bonds between molecular clusters has been destroyed that means the inter-cluster hydrogen bonds possess the weakest protons that shall be removed to the Sun center first. In the following two minutes in the long–range order of water, another form of hydrogen bonds was observed where water clusters became collapsed (13:16...13:17). A weakened proton is present here in the inter-cluster hydrogen bonds, that return into the normal condition at 13:18 again, the same state before the entrance of the Sun in SPGPR. Therefore, two forms of "naked" protons and a state with-
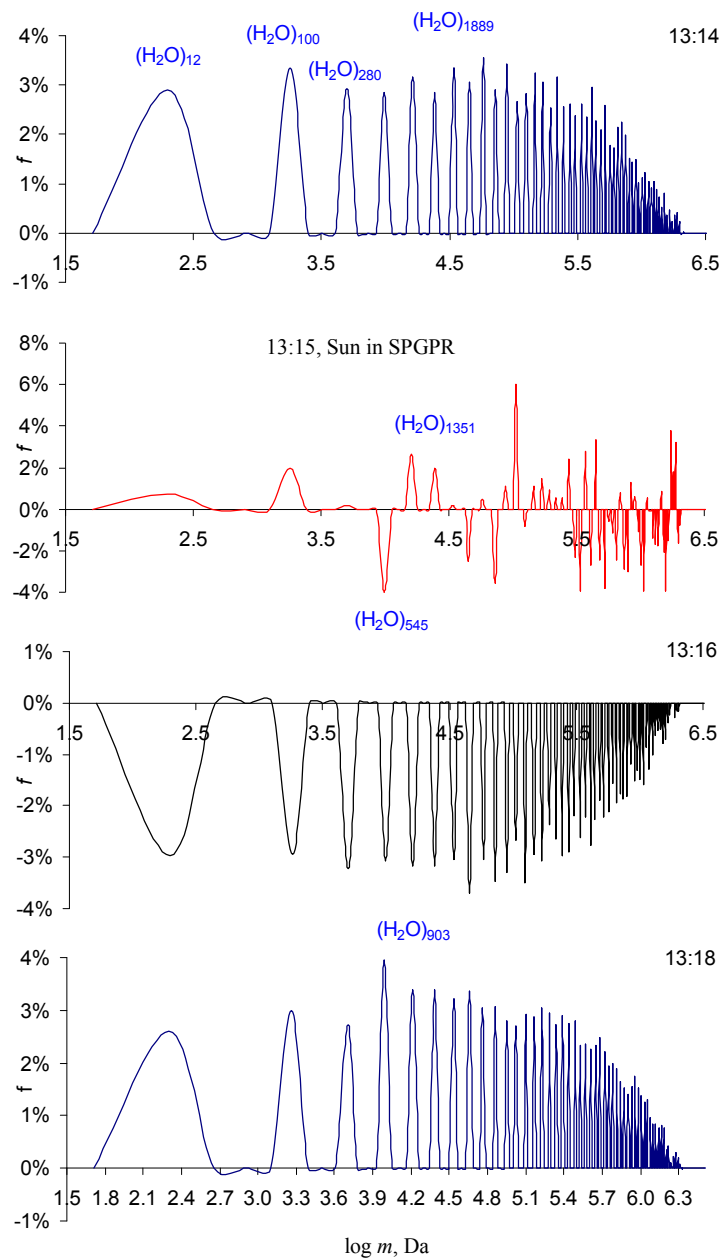
Figure 9. Dynamics of the proton state in hydrogen bonds between water clusters in agarose hydrogel at the period when the Sun is in SPGPR (August 7th 2009).

out any protons were concluded to be present in hydrogen bonds (**Figure 10**).

At this time, to differentiate between the dissolution and condensation state of protons is impossible because they proceed with a super light velocity however, the talk can be on canonical structures in their harmonic resonance. It doesn't have to be excluded that neutrons take place in this family of pendula too. The gravitation strength which holds the nucleus as a unity together is the result of the minimization of the potential energy of this mass ensemble [7].

As shown in **Figure 10** the proton dissolving is accompanied by the disappearance of its electron (stationary front of shock wave). Here in the matter, only one free radical of the so-called "free electron", as it was understood by the nature scientists of the 20th century, remains. If only the proton should dissolve, then the matter should have a gigantic negative charge what isn't the case, however. This simple logic supports the suggested electron model as phenomenon of stationary shock wave front (**Figure 8**). Our universe consists consequently of two not with each other mixable, highly dis-
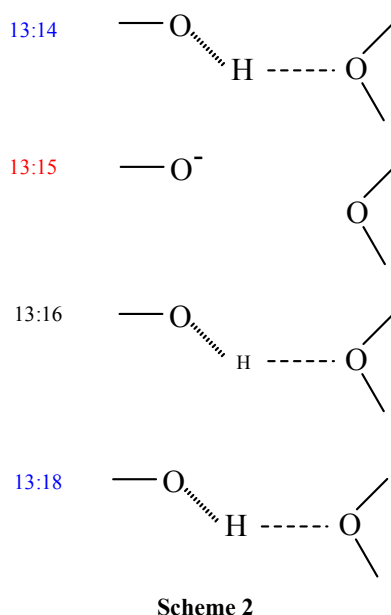
Scheme 2

Figure 10. Scheme illustrating the inter-molecular clusters states of hydrogen bonds when the Sun hits SPGPR.

persed and competitive forms of the matter: mater of vacuum and matter of proton.

4. Conclusions

Thus, the mass transfer of protons of hydrogen bonds or atomic nuclei in vacuum (dissolution) proceeding with a super light velocity as well as the almost simultaneous appearance of protons from vacuum (condensation) at the nearest vacant place of the space were concluded to be the reason for weak gravitation radiation of molecular matter. The structure of the hydrogen atom reflects the surface state between two forms of matter: matter in vacuum and matter consisting of dissolved protons. These two forms could exist independently of each other. The electron orbitals in atoms and molecules are stationary shock waves in vacuum coming from two fast running processes (dissolving/condensing of protons) in atomic nuclei.

5. Acknowledgements

6. References

[1]   A. N. Isaev, "Co-Operation Interactions of Hydrogen Bonds in the Processes with Proton Jumping and Water Molecules Participation. Modelling of Biochemical Systems", *Russian Journal of Chemistry*, Vol. LI, No. 5, 2007, pp. 34-48.

[2]   D. F. Baisa, E. D. Chesnokov, A. I. Ovcharenko and I. G. Vertegel, "NMR Study of Proton Dynamics in Ferroelectric KIO32HIO3 Crystal," *Functional Materials*, Vol. 15, No.1, 2008, pp. 19-22.

[3]   P. Jaque, A. Toro-Labbe, P. Politzer and P. Geerlings, "Reaction Force Constant and Projected Force Constants of Vibrational Modes along the Path of an Intramolecular Proton Transfer Reaction," *Chemical Physics Letters*, Vol. 456, No. 4-6, 2008, pp. 135-140.

[4]   A. V. Zubow, K. V. Zubow and V. A. Zubow, "The Phenomenon of Water Clusters Distribution in Water and Solvated Clusters of Ion Pairs of NaCl in Solution Near the Wall, the Wall Effect," *Journal of Chemical Industry*, Vol. 83, No. 6, 2006, pp 300-306.

[5]   K. V. Zubow, A. V. Zubow and V. A. Zubow, "Using of Flicker Noise Spectroscopy for Non Destroyng Analysis of Nano Structures," *Zavodskaja Laboratorija. Diagnostics of Materials*, Vol. 74, No. 9, 2008, pp. 40-45

[6]   K. V. Zubow, A. V. Zubow and V. A. Zubow, "The Dynamics of Low Frequency Movements of Molecular Clusters in the Hardening Process of Epoxide Resins," *Chem Promislennost Segodnja*, No. 9, 2008, pp. 12-21.

[7]   K. V. Zubow, A. V. Zubow and V. A. Zubow, "Principles of Gravitation Stectroscopy. New Form of Molecular Matter Processes Fields," Aist H & C gmbH, Berlin, 2010, electronic book, www.zubow.de

[8]   K. V. Zubow, A. V. Zubow and V. A. Zubow, "Cluster Structure of Liquid Alcohols, Water and N-Hexane," *Journal of Applied Spectroscopy*, Vol. 72, No. 3, 2005, pp. 321-328.

[9]   K. V. Zubow, A. V. Zubow and V. A. Zubow, "Ensemble of Clusters—New Form of Molecular Matter, Risks and Chances. Zubow Equations," In: F. Columbus, Ed., *Chemical Industry Challenges Issues and Prospects*, Nova Science Publishers, NewYork, 2010.

[10]   W. Horsthemke and R. Lefever, "Noise-Induced Transitions. Theory and Applications in Physics, Chemistry and Biology. Edit. Hermann Haken," Springer-Verlag, Berlin, Heidelberg, Tokio, 1984.

[11]   Hickey, P. Michael and Y. H. Yu, "A full-Wave Investigation of the Use of a "Cancellation Factor" in Gravity Wave-OH Airglow Interaction Studies," *Journal of Geophysical Research*, Vol. 110, No. 1, 2005, pp. 1-15.

[12]   V. N. Smirnov, N. V. Egorov and I. S. Shchedrin, "A New Detector for Pertrubations in Gravitational Field," *Progress in Physics*, Vol. 2, No. 4, April 2008, pp. 129-133.

[13]   E. V. Bogdanov and G. M. Manturova, "Equiclaster Model of Water," *Biomedicinskaja Radioelektronika*, No. 7, 2000, pp. 19-28.

[14]   A. Lenz and L. Ojamäe, "On the Stability of Dence Versus Cage-Shaped Water Clusters: Quantum-Chemical Investigations of Zero-Point Energies, Free Energies, Basis-Set Effects and IR Spectra of $(H_2O)_{12}$ and $(H_2O)_{20}$,"

Chemical Physics Letters, Vol. 418, 2006, pp. 361-367.

[15] "Fisitcheskij Encikloped. Slowar," Moscov, Sovietskaja Enciclopedija, 1984, p. 137.

[16] S. S. Kozlov, A. V. Krivandin, O. V. Shatalova, T. Noda, E. Bertoft, J. Fornal and V. P. Yuryev, "Structure of Starches Extracted from Near-Isogenic Wheat Lines," *Journal of Thermal Analysis and Calorimetry*, Vol. 87, No. 2, 2007, pp. 575-584.

[17] A. Di Virgilio, S. Bigotta, L. Barsotti, *et al.*, "Experimental Upper Limit on the Estimated Thermal Noise at Low Frequencies in a Gravitational Wave Detector," *Physical Review D*: *Particles*, *Fields*, *Gravitation*, *and Cosmology*, Vol. 76, No. 12, 2007, pp. 122004/1-122004/10.

[18] E. Katsavounidis and S. Ballmer, "For How Long will Gravitational Waves Remain Hidden?" *Physics Letters A*, Vol. 347, No. 1-3, 2005, pp. 33-37.

[19] R. T. Stebbins and P. L. Bender, "A Lunar Gravitational Wave Antenna Using a Laser Interferometer," *AIP Conference Proceedings*, Vol. 202. 1990, pp. 188-201.

[20] G.-R. Dorota and L. Francois, "The Final Phase of Inspiral of Strange Quark Star Binaries General Relativity and Quantum Cosmology," Preprint Archive, (Los Alamos National Laboratory, 2008, arXiv: 0801.4829v1), pp.1-13. http://aps.arxiv.org/PS_cache/arxiv/pdf/0801/0801.4829v1.pdf

[21] D. K. Kokkotas, "Gravitational Waves," *Acta Physica Polonica*, Vol. 38, No. 12, 2007, pp. 3891-3923.

[22] A. V. Zubow, K. V. Zubow and V. A. Zubow, "Investigation of the Distribution of Water Clusters in Vegetables, Fruits and Natural Waters by Flicker Noise Spectroscopy," *Biofizika*, Vol. 52, No. 4, 2007, pp. 585-592.

[23] L. Pauling and P. Pauling, "Chemistry," W. H. Freeman and Company, San Francisco, 1975.

Scientific
Research

Scale Invariant Theory of Gravitation in Einstein-Rosen Space-Time

Bivudutta Mishra, Pradyumn Kumar Sahoo, Addepalli Ramu
Mathematics Group, Birla Institute of Technology and Science, Hyderabad Campus, Andhra Pradesh, Pilani, India
E-mail: {bivudutta, addepallir}@gmail.com, sahoomaku@rediffmail.com
Received June 19, 2010; revised July 19, 2010; accepted July 26, 2010

Abstract

In this paper, we have studied the perfect fluid distribution in the scale invariant theory of gravitation, when the space-time described by Einstein-Rosen metric with a time dependent gauge function. The cosmological equations for this space-time with gauge function are solved and some physical properties of the model are studied.

1. Introduction

Several new theories of gravitation have been formulated which are considered to be alternative to Einstein's theory of gravitation. In alternative theories of gravitation, scalar tensor theories proposed by Brans and Dicke [1], Nordvedt [2], Wagoner [3], Ross [4], Dunn [5] and Saez and Ballester [6] are most important among them. In the theory proposed by Brans and Dicke [1] there exists a variable gravitational parameter G. Another theory, which admits a variable G, is the scale covariant theory of Canuto *et al.* [7]. Dirac [8,9] rebuilt the Weyl's unified theory by introducing the notion of two metrics and an additional gauge function β. A scale invariant variation principle was proposed from which gravitational and electromagnetic field equations can be derived. It is concluded that an arbitrary gauge function is necessary in all scale-invariant theories.

It is found that the scale invariant theory of gravitation agrees with general relativity up to the accuracy of observations made up now. Dirac [8,9], Hoyle and Narlikar [10] and Canuto *et al.* [7] have studied several aspects of the scale invariant theory of gravitation. But Wesson's [11,12] formulation is so far the best one to describe all the interactions between matter and gravitation in scale free manner.

Mohanty and Mishra [13] have studied the feasibility of Bianchi type VIII and IX space-times with a time dependent gauge function and a matter field in the form of perfect fluid. In that paper, they have constructed a radiating model of the universe for the feasible Bianchi type VIII space-time. Mishra [14] has constructed the non-static plane symmetric Zeldovich fluid model in this

theory with a time dependent gauge function. Recently, Mishra [15] has constructed static plane symmetric Zeldovich fluid model in scale invariant theory.

Rao *et al.* [16,17] have discussed cylindrically symmetric scalar meson fields and Brans-Dicke scalar fields. It is found from the literature that the scale invariant theory of gravitation has not been studied so far in Einstein-Rosen space-time. Hence, in this paper, we have taken an attempt to study the cylindrically symmetric space-time in the scale invariant theory of gravitation. A cosmological model has been presented.

2. Field Equations

Wesson [11,12] formulated a scale invariant theory of gravitation using a gauge function $\beta(x^i)$, where, $x^i, i = 1,2,3,4$ are coordinates in the four-dimensional space-time and the tensor field is identified with the metric tensor g_{ij}. This theory is both coordinate and scale invariant in nature. The field equations formulated by Wesson [11,12] for the combined scalar and tensor fields are:

$$G_{ij} + 2\frac{\beta_{;ij}}{\beta} - 4\frac{\beta_{,i}\beta_{,j}}{\beta^2} + \left(g^{ab}\frac{\beta_{,a}\beta_{,b}}{\beta^2} - 2g^{ab}\frac{\beta_{;ab}}{\beta} \right)g_{ij} = -\kappa T_{ij}$$

(1)

with

$$G_{ij} \equiv R_{ij} - \frac{1}{2}Rg_{ij}$$

(2)

Here, G_{ij} is the conventional Einstein tensor involving

g_{ij}. Semicolon and comma respectively denote covariant differentiation with respect to g_{ij} and partial differentiation with respect to coordinates. The cosmological term Λg_{ij} of Einstein theory is transformed to $\Lambda_0 \beta^2 g_{ij}$ in scale invariant theory with a dimensionless constant Λ_0. T_{ij} is the energy momentum tensor of the matter field and $\kappa = \dfrac{8\pi G}{c^4}$.

The line element for Einstein- Rosen metric with a gauge function $\beta = \beta(ct)$ is.

$$ds_W^2 = \beta^2 ds_E^2 \qquad (3)$$

with

$$ds_E^2 = e^{2A-2B}\left(c^2 dt^2 - dr^2\right) - r^2 e^{-2B} d\varphi^2 - e^{2B} dz^2 \qquad (4)$$

where A and B are functions of t only, and c is the velocity of light. Here we intend to build cosmological models in this space-time with a perfect fluid having the energy momentum tensor of the form

$$T_{ij}^m = \left(p_m + \rho_m c^2\right) U_i U_j - p_m g_{ij} \qquad (5)$$

together with $g_{ij} U^i U^j = 1$

where U^i is the four-velocity vector of the fluid; p_m and p_m are the proper isotropic pressure and energy density of the matter respectively.

The non – vanishing components of conventional Einstein's tensor (2) for the metric (4) can be obtained as

$$G_{11} = \frac{1}{c^2}\left[B_4^2\right] \qquad (6)$$

$$G_{14} = -\frac{1}{r}\left[A_4\right] \qquad (7)$$

$$G_{22} = \frac{1}{c^2}\left[A_{44} + B_4^2\right] \qquad (8)$$

$$G_{33} = \frac{1}{c^2}\left[A_{44} - 2B_{44} + B_4^2\right] \qquad (9)$$

$$G_{44} = \left[B_4^2\right] \qquad (10)$$

Here afterwards the suffix 4 after a field variable denotes exact differentiation with respect to time t only.

Using the comoving coordinate frame where $U^i = \delta_4^i$, the non-vanishing components of the field Equation (1) for the metric (3) can be written in the following explicit form:

$G_{11} =$

$$-\kappa p_m e^{2A-2B} - \frac{1}{c^2}\left[2\frac{\beta_{44}}{\beta} - \frac{\beta_4^2}{\beta^2} + 2\frac{\beta_4}{\beta}\left(-A_4 + B_4\right) - \Lambda_0 \beta^2 c^2 e^{2A-2B}\right]$$

$$(11)$$

$$G_{14} = 0 \qquad (12)$$

i.e. $A = k_1$, where k_1 is an integrating constant.

$G_{22} =$

$$-\kappa p_m e^{2A-2B} - \frac{1}{c^2}\left[2\frac{\beta_{44}}{\beta} - \frac{\beta_4^2}{\beta^2} + 2\frac{\beta_4}{\beta}\left(B_4\right) - \Lambda_0 \beta^2 c^2 e^{2A-2B}\right]$$

$$(13)$$

$G_{33} =$

$$-\kappa p_m e^{2A-2B} - \frac{1}{c^2}\left[2\frac{\beta_{44}}{\beta} - \frac{\beta_4^2}{\beta^2} - 2\frac{\beta_4}{\beta}\left(B_4\right) - \Lambda_0 \beta^2 c^2 e^{2A-2B}\right]$$

$$(14)$$

$G_{44} =$

$$-\kappa \rho_m c^4 e^{2A-2B} + \left[3\frac{\beta_4^2}{\beta^2} - 2\frac{\beta_4}{\beta}\left(B_4\right) - \Lambda_0 \beta^2 c^2 e^{2A-2B}\right]$$

$$(15)$$

Equation (12) reduces the above set of Equations (11)-(15) as

$G_{11} = G_{22} =$

$$-\kappa p_m e^{2k_1-2B} - \frac{1}{c^2}\left[2\frac{\beta_{44}}{\beta} - \frac{\beta_4^2}{\beta^2} + 2\frac{\beta_4}{\beta}\left(B_4\right) - \Lambda_0 \beta^2 c^2 e^{2k_1-2B}\right]$$

$$(16)$$

$$G_{33} = -\kappa p_m e^{2k_1-2B} -$$
$$\frac{1}{c^2}\left[2\frac{\beta_{44}}{\beta} - \frac{\beta_4^2}{\beta^2} - 2\frac{\beta_4}{\beta}\left(B_4\right) - \Lambda_0 \beta^2 c^2 e^{2k_1-2B}\right] \qquad (17)$$

$$G_{44} = -\kappa \rho_m c^4 e^{2k_1-2B} +$$
$$\left[3\frac{\beta_4^2}{\beta^2} - 2\frac{\beta_4}{\beta}\left(B_4\right) - \Lambda_0 \beta^2 c^2 e^{2k_1-2B}\right] \qquad (18)$$

Now, Equation (1) and Equations (16)-(18) (Wesson [12]) suggest the definitions of quantities p_v (vacuum pressure) and p_v (vacuum density) that involves neither the Einstein tensor of conventional theory nor the properties of conventional matter. These two quantities can be obtained as:

$$2\frac{\beta_{44}}{\beta} - \frac{\beta_4^2}{\beta^2} + 2\frac{\beta_4}{\beta}\left(B_4\right) - \Lambda_0 \beta^2 c^2 e^{2k_1-2B} = \kappa p_v c^2 \quad (19)$$

$$2\frac{\beta_{44}}{\beta} - \frac{\beta_4^2}{\beta^2} - 2\frac{\beta_4}{\beta}\left(B_4\right) - \Lambda_0 \beta^2 c^2 e^{2k_1-2B} = \kappa p_v c^2 \quad (20)$$

$$3\frac{\beta_4^2}{\beta^2} - 2\frac{\beta_4}{\beta}\left(B_4\right) - \Lambda_0 \beta^2 c^2 e^{2k_1-2B} = \kappa \rho_v c^4 \quad (21)$$

It is evident from Equations (19) and (20) that

$$B_4 = 0 \Rightarrow B = k_2 \quad \text{since} \quad \frac{\beta_4}{\beta} \neq 0 \qquad (22)$$

where k_2 is an integrating constant. Using Equation (22) in Equations (19)-(21), the pressure and energy density for vacuum case can be obtained as

$$p_v = \frac{1}{\kappa c^2 e^{2k_1-2k_2}}\left[2\frac{\beta_{44}}{\beta} - \frac{\beta_4^2}{\beta^2} + \Lambda_0\beta^2 c^2 e^{2k_1-2k_2}\right] \quad (23)$$

$$\rho_v = \frac{1}{\kappa c^4 e^{2k_1-2k_2}}\left[3\frac{\beta_4^2}{\beta^2} - \Lambda_0\beta^2 c^2 e^{2k_1-2k_2}\right] \quad (24)$$

Here p_v and p_v relate to the properties of vacuum only in conventional physics. The definition of above quantities is natural as regards to the scale invariant properties of the vacuum. The total pressure and energy density can be defined as

$$p_t \equiv p_m + p_v \quad (25)$$

$$\rho_t \equiv \rho_m + \rho_v \quad (26)$$

Using the aforesaid definitions of p_t and p_t, the field equations in scale invariant theory *i.e.* (16)-(18) can now be written by using the components of Einstein tensor (6)-(10) and the results obtained in Equations (22)-(24) as:

$$B_4^2 = -\kappa p_t c^2 e^{2k_1-2B} \quad (27)$$

$$-2B_{44} + B_4^2 = -\kappa p_t c^2 e^{2k_1-2B} \quad (28)$$

$$B_4^2 = -\kappa\rho_t c^4 e^{2k_1-2B} \quad (29)$$

3. Solution

From Equations (27) and (29), we obtained the equation of state

$$p_t = \rho_t c^2 \quad (30)$$

Using Equation (27) in Equation (28), we obtained

$$B = d_1 t + d_2 \quad (31)$$

where d_1 and d_2 are integrating constants.

Substituting Equation (31) in Equation (27) and Equation (29) respectively, the total pressure 'p_t' and energy density 'ρ_t' can be obtained as:

$$p_t = \rho_t c^2 = \frac{1}{\kappa c^2}\left[-\frac{d_1^2}{qe^{-2d_1 t}}\right] \quad (32)$$

where $q = e^{2k_1-2k_2}$ is a constant. The reality condition demands that $d_1^2 < 0$.

Using Equation (31) in Equations (23) and (24) respectively and taking $\beta = \frac{1}{ct}$, the pressure and energy density corresponding to vacuum case can be calculated as:

$$p_v = -\frac{1}{\kappa c^2 q}\left[\frac{\Lambda_0 q - 1}{t^2}\right] \quad (33)$$

$$\rho_v = \frac{1}{\kappa c^4 q}\left[\frac{\Lambda_0 q - 3}{t^2}\right] \quad (34)$$

In this case, when there is no matter and the gauge function β is a constant, one recovers the relation $c^2\rho_v = c^4\frac{\Lambda_{GR}}{8\pi G} = -p_v$ *i.e.* $c^2\rho_v + p_v = 0$, which is the equation of state for vacuum. Here $\Lambda_{GR} = \Lambda_0\beta^2$ = constant, is the cosmological constant in general relativity. Also p_v being dependent on the constants Λ_{GR}, c and G, is uniform in all directions and hence isotropic in nature. The cosmological model with this equation of state is rare in literature and is known as ρ – vacuum or false vacuum or degenerate vacuum model [18-21], the corresponding model in the static case is a well known de-Sitter model.

Now the matter pressure and density can be obtained as:

$$p_m = p_t - p_v = \frac{1}{\kappa c^2}\left[\frac{\Lambda_0 q - 1}{qt^2} - \frac{d_1^2}{e^{2k_1-2d_1 t - d_2}}\right] \quad (35)$$

$$\rho_m = \rho_t - \rho_v = \frac{1}{\kappa c^4}\left[\frac{3-\Lambda_0 q}{qt^2} - \frac{d_1^2}{e^{2k_1-2d_1 t - d_2}}\right] \quad (36)$$

Now, we have $\rho_m \to \infty$ as $t \to 0$ and $\rho_m \to \infty$ as $t \to \infty$. Also when $t < 0$, $\rho_m \to constant$. It is interesting to note that the model free from singularity.

So, the Einstein-Rosen cylindrically symmetric model in scale invariant theory of gravitation is given by the Equations (12), (31) and (32) and the metric in this case is

$$dS_W^2 =$$
$$\frac{1}{(ct)^2}\left[e^{2k_1-2d_1 t-2d_2}\left(c^2 dt^2 - dr^2\right) - r^2 e^{-2d_1 t-2d_2} d\varphi^2 - e^{2d_1 t+2d_2} dz^2\right]$$
$$(37)$$

4. Some Physical Properties of the Model

The scalar expansion, $\theta = U^i_{;i} = 3\frac{Q_T}{Q}$ for the model given by Equation (37) takes the form

$$\theta = -\frac{1}{c}\left(d_1 e^{d_1 t+d_2-k_1}\right) \quad (38)$$

Thus, we find $\theta \to -\frac{1}{c}(d_1 e^{d_2-k_1})$ as $t \to 0$ and $\theta \to 0$ as $t \to \infty$.

If $c > 0$, $d_1 < 0$ and $d_2 > k_1$ the model represents expanding one for $t < t_1(= \frac{k_1-d_2}{d_1})$.

It is also observed that as $\frac{\rho_m}{\theta^2} \to constant$ as $t \to \infty$ and $\frac{\rho_m}{\theta^2} \to \theta$ as $t \to 0$. Thus the universe confirms the homogeneity nature of the space-time.

Following Raychaudhuri [22], the anisotropy $|\sigma|$ can be defined as

$$\sigma^2 =$$

$$\left[\left(\frac{g_{11,4}}{g_{11}} - \frac{g_{22,4}}{g_{22}}\right)^2 + \left(\frac{g_{22,4}}{g_{22}} - \frac{g_{33,4}}{g_{33}}\right)^2 + \left(\frac{g_{33,4}}{g_{33}} - \frac{g_{11,4}}{g_{11}}\right)^2\right] \tag{39}$$

Consequently for the model (37), $\sigma^2 = \frac{8}{3}(d_1 t + d_2) \neq 0$.

So the shear scalar remains constant for $t \to 0$ and becomes indefinitely large for $t \to \infty$.

The ratio of anisotropy to expansion $\frac{\sigma^2}{\theta^2} = \frac{8c^2}{3}e^{2k_1 - 2d_2} \neq 0$ for $t = 0$. Thus there is a singularity of $t = 0$ for $2k_1 - 2d_2$ is not very large. Moreover, the model is isotropy for finite t and does not approach isotropy for large value of t.

It is observed that the vorticity 'w' vanishes which indicates that u^i is hypersurface orthogonal. As the acceleration $\dot{u}_i$ found to be zero, the matter particle follows geodesic path in this theory.

5. Conclusions

Every physical theory carries its own mathematical structure and the validity of the theory is usually studied through the exact solution of the mathematical structure. In this theory black holes do not appear to exist. If the existence of black holes in nature is confirmed, it will represent a great success of general theory of relativity. Since there is no concrete evidence at present for the existence of black holes, one can take a stand point that black holes represents a familiar concept of space time. Therefore the scale invariant theory involves gauge theories as it relates to gravitational theories with an added scalar field.

The significance of the present work deals with the modification of gravitational and geometrical aspects of Einstein's equations. These are 1) scale invariant theory of gravitation which describes the interaction between matter and gravitation in scale free manner; and 2) the gauge transformation, which represents a change of units of measurements and hence gives a general scaling of physical system. The nature of the cosmological model with modified gravity that would reproduce the kinematical history and evolution of perturbation of the universe is investigated.

Here, cylindrically symmetric static zeldovich fluid model is obtained in the presence of perfect fluid distribution in scale invariant theory of gravitation. As far as matter is concerned the model does not admit either big bang or big crunch during evolution till infinite future. The model appears to be a steady state.

7. References

[1] C. H. Brans and R. H. Dicke, "Mach's Principle and a Relativistic Theory of Gravitation," *Physical Review A*, Vol. 124, No. 3, 1961, pp. 925-935.

[2] K. Nordverdt, Jr., "Post Newtonian Metric for a General Class of Scalar—Tensor Gravitational Theories and Observational Consequences," *The Astrophysical Journal*, Vol. 161, 1970, pp. 1059-1067.

[3] R. V. Wagoner, "Scalar—Tensor Theory and Gravitational Waves", *Physical Review D*, Vol. 1, No. 2, 1970, pp. 3209-3216.

[4] D. K. Ross, "Scalar—Tensor Theory of Gravitation," *Physical Review D*, Vol. 5, No. 2, 1972, pp. 284-192.

[5] K. A. Dunn, "A Scalar—Tensor Theory of Gravitation," *Journal of Mathematical Physics*, Vol. 15, No. 12, 1974, pp. 2229-2231.

[6] D. Saez and V. J. Ballester, "A Simple Coupling with Cosmological Implications," *Physics Letters A*, Vol. A113, No. 9, 1985, pp. 467-470.

[7] V. Canuto, S. H. Hseih and P. J. Adams, "Scale—Covariant Theory of Gravitation and Astrophysical Applications," *Physics Review Letters*, Vol. 39, No. 88, 1977, pp. 429- 432

[8] P. A. M. Dirac, "Long Range Forces and Broken Symmetries," *Proceedings of the Royal Society of London*, Vol. A333, 1973, pp. 403-418.

[9] P. A. M. Dirac, "Cosmological Models and the Large Number Hypothesis," *Proceedings of the Royal Society of London*, Vol. A338, No. 1615, 1974, pp. 439-446.

[10] F. Hoyle and J. V. Narlikar, "Action at a Distance in Physics and Cosmology," W. H. Freeman, San Francisco, 1974.

[11] P. S. Wesson, "Gravity, Particle and Astrophysics," D. Reidel, Dordrecht, 1980.

[12] P. S. Wesson, "Scale—Invariant Gravity—A Reformulation and an Astrophysical Test," *Monthly Notices of the Royal Astronomical Society*, Vol. 197, 1981, pp. 157-165.

[13] G. Mohanty and B. Mishra, "Scale Invariant Theory for Bianchi Type VIII and IX Space-times with Perfect Fluid," *Astrophysics and Space Science*, Vol. 283, No. 1, 2003, pp. 67-74.

[14] B. Mishra, "Non-Static Plane Symmetric Zeldovich Fluid Model in Scale Invariant Theory," *Chinese Physics Letters*, Vol. 21, No. 12, 2004, pp. 2359-2361.

[15] B. Mishra, "Static Plane Symmetric Zeldovich Fluid Model in Scale Invariant Theory," *Turkish Journal of Physics*, Vol. 32, No. 6, 2008, pp. 357-361.

[16] J. R. Rao, A. R. Roy and R. N. Tiwari, "A Class of Exact Solutions for Coupled Electromagnetic and Scalar Fields for Einstein Rosen Metric I," *Annals of Physics*, Vol. 69, No. 2, 1972, pp. 473-486.

[17] J. R. Rao, R. N. Tiwari and K. S. Bhamra, "Cylindrical Symmetric Brans-Dicke Fields II", *Annals of Physics*, Vol. 87, 1974, pp. 480-497.

[18] J. J. Bloome and W. Priester, "Urknall und Evolution Des. Kosmos II," *Naturewissenshaften*, Vol. 2, 1984, pp. 528-531.

[19] P. C. W. Davies, "Mining the Universe," *Physical Review D*, Vol. 30, No. 4, 1984, pp. 737-742.

[20] C. J. Hogan, "Microwave Background Anisotropy and Hydrodynamic Formation of Large-Scale Structure," *Astrophysical Journal*, Vol. 310, 1984, p. 365.

[21] N. Kaiser and A. Stebbins, "Microwave Anisotropy Due to Cosmic Strings," *Nature*, Vol. 310, No. 5976, 1984, pp. 391- 393.

[22] A. Raychaudhuri, Theoretical Cosmology, Oxford University Press, 1979.

Scientific
Research

Kasner Universe in Creation-Field Cosmology

Kishor S. Adhav, Meena V. Dawande, Maya S. Desale, Ranjita B. Raut
Department of Mathematics, Sant Gadge Baba Amravati University, Amravati, India
E-mail: *ati_ksadhav@yahoo.co.in*
Received April 18, 2010; *revised July* 9, 2010; *accepted July* 20, 2010

Abstract

We have studied the Hoyle-Narlikar *C*-field cosmology with Kasner [1,2] space-time. Using methods of Narlikar and Padmanabhan [3], the solutions have been studied when the creation field *C* is a function of time *t* only. The geometrical and physical properties of the models, thus obtained, are also studied.

Keywords: Kasner Space-Time, Creation Field Cosmology, Cosmological Models of Universe.

1. Introduction

The three important observations in astronomy viz., the phenomenon of expanding universe, primordial nucleonsynthesis and the observed isotropy of cosmic microwave background radiation (CMBR) were supposed to be successfully explained by big-bang cosmology which is based on Einstein's field equations. However, Smoot *et al*. [4] revealed that the earlier predictions of the Friedman-Robertson-Walker types of models do not always exactly meet our expectations. Some puzzling results regarding the red shifts from the extra galactic objects continue to contradict the theoretical explanations given from the big bang type of the models. Also, CMBR discovery did not prove it to be an out come of big bang theory. Infact, Narlikar *et al*. [5] proved the possibility of non-relic interpretation of CMBR. To explain such phenomenon, many alternative theories have been proposed from time to time. Hoyle [6], Bondi and Gold [7] proposed steady state theory in which the universe does not have singular beginning nor an end on the cosmic time scale. Moreover, they have shown that the statistical properties of the large scale features of the universe do not change. Further, the constancy of the mass density has been accounted by continuous creation of matter going on in contrast to the one time infinite and explosive creation of matter at *t* = 0 as in the earlier standard models. But, the principle of conservation of matter was violated in this formalism. To overcome this difficulty, Hoyle and Narlikar [8] adopted a field theoretic approach by introducing a massless and chargeless scalar field *C* in the Einstein-Hilbert action to account for the matter creation. In the *C*-field theory introduced by Hoyle and Narlikar there is no big bag type of singularity as in the steady state theory of Bondi and Gold [7].

The solutions of Einstein's field equations admitting radiation with negative energy mass less scalar creation field *C* was obtained by Narlikar and Padmanabhan [3]. The study of Hoyle and Narlikar theory [9,10] and [8] to the space-time of dimensions more than four was carried out by Chatterjee and Banerjee [11]. RajBali and Tikekar [12] studied *C*-field cosmology with variable *G* in the flat Friedmann-Robertson-Walker model. Whereas, *C*-field cosmological models with variable *G* in FRW space-time has been studied by RajBali and Kumawat [13]. Singh and Chaubey [14] studied various Bianchi types models and Kantowski-Sach model in creation field cosmology.

The way in which the Kasner [1,2] metric has played a central role in the elucidation of the existence and structure of anisotropic cosmological models and their singularities in general relativity motivates the authors to study this problem. The Kasner metric is one of the more widely studied metric. Its usefulness for the construction of cosmological models and its utility for certain studies of elementary particles have made it particularly attractive for exploitation. Because of its simplicity it has been "rediscovered" many times and is itself very closely related to metrics given several years earlier by Weyl, Levi-Civita and Wilson. The form in which Kasner presented it has been virtually forgotten in favor of the dynamic form of the synchronous Bianchi I metric. Here, we have considered a spatially homogeneous and anisotropic Kasner form of Bianchi type-I metric in Hoyle and Narlikar *C*-field cosmology. We have assumed that the creation field *C* is a function of time *t* only *i.e.* $C(x,t)$

$$= C(t).$$

2. Hoyle and Narlikar *C*-Field Cosmology

Introducing a massless scalar field called as creation

field viz. C-field, Einstein's field equations are modified. Einstein's field equations modified by Hoyle and Narlikar [8-10] are

$$R_{ij} - \frac{1}{2} g_{ij} R = -8\pi \left({}^m T_{ij} + {}^c T_{ij} \right) \quad (1)$$

where ${}^m T_{ij}$ is matter tensor of Einstein theory and ${}^c T_{ij}$ is matter tensor due to the C-field which is given by

$$ {}^c T_{ij} = -f \left(C_i C_j - \frac{1}{2} g_{ij} C^k C_k \right) \quad (2)$$

where $f > 0$ and $C_i = \dfrac{\partial C}{\partial x^i}$.

Because of the negative value of $T^{00} \left(T^{00} < 0 \right)$, the C-field has negative energy density producing repulsive gravitational field which causes the expansion of the universe. Hence, the energy conservation equation reduces to

$$ {}^m T^{ij}_{;j} = - {}^c T^{ij}_{;j} = f C^i C^j_{;j} \quad (3)$$

i.e. matter creation through non-zero left hand side is possible while conserving the over all energy and momentum.

[Here semicolon (;) denotes covariant derivative]. Above equation is similar to

$$ mg_{ij} \frac{dx^i}{ds} - C_j = 0 \quad (4)$$

Which implies that the 4-momentum of the created particle is compensated by the 4-momentum of the C-field. In order to maintain the balance, the C-field must have negative energy. Further, the C-field satisfy the source equation $f C^i_{;i} = J^i_{;i}$ and $J^i = \rho \dfrac{dx^i}{ds} = \rho v^i$, where ρ is homogeneous mass density.

3. Metric and Field Equations

We consider an anisotropic [Bianchi type-I] metric in Kasner form as

$$ ds^2 = dt^2 - t^{2q_1} dx^2 - t^{2q_2} dy^2 - t^{2q_3} dz^2 \quad (5)$$

where q_1, q_2 and q_3 are three parameters that we shall require to be constants.

We have assumed that creation field C is function of time t only *i.e.* $C(x,t) = C(t)$ and

$$ {}^m T^i_j = diag \left(\rho, -p, -p, -p \right) \quad (6)$$

We have also assumed that velocity of light and gravitational constant are equal to one unit.

We first find the components of Ricci tensor R_{ij}.

Assuming the metric (5), the non vanishing components of Christoffel's symbols are

$$ \Gamma^0_{ii} = q_i t^{2q_i - 1}, \quad \Gamma^i_{i0} = \frac{q_i}{t}, \quad i=1, 2, 3 .$$

Hence, we calculate

$$ R_{ii} = -q_i \left(q_1 + q_2 + q_3 - 1 \right) t^{2q_i - 2}, \quad i=1, 2, 3.$$

$$ R_{00} = -\left[\left(q_1 + q_2 + q_3 \right) - \left(q_1^2 + q_2^2 + q_3^2 \right) \right] t^{-2} .$$

Let $S = q_1 + q_2 + q_3$ and $\theta = q_1^2 + q_2^2 + q_3^2$, we get

$$ R = \left(S^2 - 2S + \theta \right) t^{-2}$$

Now, the Hoyle-Narlikar field Equations (1) for metric (5) with the help of Equations (2), (3) and (6) can be written as

$$ \left[q_1 (S-1) - \frac{1}{2} \left(S^2 - 2S + \theta \right) \right] t^{-2} = 8\pi \left(p - \frac{1}{2} f \dot{C}^2 \right) \quad (7)$$

$$ \left[q_2 (S-1) - \frac{1}{2} \left(S^2 - 2S + \theta \right) \right] t^{-2} = 8\pi \left(p - \frac{1}{2} f \dot{C}^2 \right) \quad (8)$$

$$ \left[q_3 (S-1) - \frac{1}{2} \left(S^2 - 2S + \theta \right) \right] t^{-2} = 8\pi \left(p - \frac{1}{2} f \dot{C}^2 \right) \quad (9)$$

$$ \left[(S - \theta) + \frac{1}{2} \left(S^2 - 2S + \theta \right) \right] t^{-2} = 8\pi \left(\rho - \frac{1}{2} f \dot{C}^2 \right) \quad (10)$$

$$ \dot{\rho} + \frac{S}{t} (\rho + p) = f \dot{C} \left(\ddot{C} + \dot{C} \frac{S}{t} \right) \quad (11)$$

Now, we assume that

$$ V = t^{(q_1 + q_2 + q_3)} = t^S \quad (12)$$

Above Equation (12) can be written in the form

$$ \frac{d}{dV} (V\rho) + p = f\dot{C}(V) \frac{d}{dV} \left[V\dot{C}(V) \right] \quad (13)$$

In order to obtain a unique solution, one has to satisfy the rate of creation of matter-energy (at the expense of the negative energy of the C-field).

Without loss of generality, we assume that the rate of creation of matter energy density is proportional to the strength of the existing C-field energy-density per unit proper-volume.

This is given by

$$ \frac{d}{dV} (V\rho) + p = \alpha^2 \dot{C}^2 \equiv \alpha^2 g^2 (V) \quad (14)$$

where α is proportionality constant .

Let us define that $\dot{C}(V) \equiv g(V)$.

Substituting it in (13), we get

$$ \frac{d}{dV} (V\rho) + p = fg(V) \frac{d}{dV} (Vg) \quad (15)$$

Comparing right hand sides of (13) and (14), we get

$$g(V)\frac{d}{dV}(gV) = \frac{\alpha^2}{f}g^2(V).\qquad(16)$$

On integrating which gives

$$g(V) = A_1 V^{\left(\frac{\alpha^2}{f}-1\right)}\qquad(17)$$

where A_1 is arbitrary constant of integration.

We consider the equation of state of matter as

$$p = \gamma\rho, \quad 0 \leq \gamma \leq 1\qquad(18)$$

Substituting Equations (17) and (18) in the equation (14), we get

$$\frac{d}{dV}(V\rho) + \gamma\rho = \alpha^2 A^2 V^{2\left(\frac{\alpha^2}{f}-1\right)}\qquad(19)$$

which further yields

$$\rho = \frac{\alpha^2 A_1^2}{\left(2\frac{\alpha^2}{f}-1+\gamma\right)}V^{2\left(\frac{\alpha^2}{f}-1\right)}\qquad(20)$$

Subtracting Equation (7) from Equation (8), we get

$$(q_2 - q_1)(S-1)t^{-2} = 0\qquad(21)$$

Equation (21) can be written as

$$\frac{d}{dt}\left(\frac{q_1}{t} - \frac{q_2}{t}\right) + \left(\frac{q_1}{t} - \frac{q_2}{t}\right)\frac{S}{t} = 0$$

Now, using Equation (12), the above equation becomes

$$\frac{d}{dt}\left(\frac{q_1}{t} - \frac{q_2}{t}\right) + \left(\frac{q_1}{t} - \frac{q_2}{t}\right)\frac{\dot{V}}{V} = 0\qquad(22)$$

This on integration gives

$$\frac{t^{q_1}}{t^{q_2}} = d_1 e^{x_1 \int \frac{dt}{V}}, d_1 = const; \qquad x_1 = const\qquad(23)$$

Subtracting Equation (9) from Equation (8), we get

$$(q_2 - q_3)(S-1)t^{-2} = 0\qquad(24)$$

Equation (24) can be written as

$$\frac{d}{dt}\left(\frac{q_2}{t} - \frac{q_3}{t}\right) + \left(\frac{q_2}{t} - \frac{q_3}{t}\right)\frac{S}{t} = 0$$

Now, using Equations (12) the above equation becomes

$$\frac{d}{dt}\left(\frac{q_2}{t} - \frac{q_3}{t}\right) + \left(\frac{q_2}{t} - \frac{q_3}{t}\right)\frac{\dot{V}}{V} = 0.$$

This on integration gives

$$\frac{t^{q_2}}{t^{q_3}} = d_2 e^{x_2 \int \frac{dt}{V}}; d_2 = const; \qquad x_2 = const\qquad(25)$$

Subtracting Equation (9) from Equation (7), we get

$$(q_1 - q_3)(S-1)t^{-2} = 0\qquad(26)$$

Equation (26) can be written as

$$\frac{d}{dt}\left(\frac{q_1}{t} - \frac{q_3}{t}\right) + \left(\frac{q_1}{t} - \frac{q_3}{t}\right)\frac{S}{t} = 0$$

Now, using Equations (12) the above equation becomes

$$\frac{d}{dt}\left(\frac{q_1}{t} - \frac{q_3}{t}\right) + \left(\frac{q_1}{t} - \frac{q_3}{t}\right)\frac{\dot{V}}{V} = 0$$

This on integration gives

$$\frac{t^{q_1}}{t^{q_3}} = d_3 e^{x_3 \int \frac{dt}{V}} \quad d_3 = const; \qquad x_3 = const\qquad(27)$$

where $d_3 = d_1 d_2$; $x_3 = x_1 + x_2$.

Using Equations (23), (25) and (27), the values of t^{q_1}, t^{q_2} and t^{q_3} can be explicitly written as,

$$t^{q_1} = D_1 V^{1/3} \exp\left(X_1 \int \frac{dt}{V}\right)\qquad(28)$$

$$t^{q_2} = D_2 V^{1/3} \exp\left(X_2 \int \frac{dt}{V}\right)\qquad(29)$$

$$t^{q_3} = D_3 V^{1/3} \exp\left(X_3 \int \frac{dt}{V}\right)\qquad(30)$$

where the relations $D_1 D_2 D_3 = 1$ and $X_1 + X_2 + X_3 = 0$ are satisfied by $D_i (i = 1,2,3)$ and $X_i (i = 1,2,3)$.

Adding Equations (7)-(9) and subtracting from three times Equation (10), we get

$$S(S-1)t^{-2} = 12\pi(\rho - p)\qquad(31)$$

From Equation (12) and (18), we get

$$\frac{\ddot{V}}{V} = 12\pi(1-\gamma)\rho\qquad(32)$$

Substituting Equation (21) in Equation (32), we get

$$\frac{\ddot{V}}{V} = \frac{12\pi(1-\gamma)\alpha^2 A_1^2}{\left(2\frac{\alpha^2}{f}-1+\gamma\right)}V^{2\left(\frac{\alpha^2}{f}-1\right)}\qquad(33)$$

This further gives

$$V = \left\{A_1(f-\alpha^2)\left[\frac{12\pi(1-\gamma)}{(2\alpha^2-f+\gamma f)}\right]^{1/2}\right\}^{\frac{f}{f-\alpha^2}}t^{\frac{f}{f-\alpha^2}}\quad(34)$$

Substituting Equation (34) in Equation (17), we get

$$g = \frac{1}{(f-\alpha^2)}\left[\frac{12\pi(1-\gamma)}{(2\alpha^2-f+\gamma f)}\right]^{-1/2}\frac{1}{t}\qquad(35)$$

Also, from equation $\dot{C}(V) = g(V)$, we get

$$C = \frac{1}{\left(f - \alpha^2\right)} \left[\frac{12\pi\left(1 - \gamma\right)}{\left(2\alpha^2 - f + \gamma f\right)} \right]^{-1/2} \log t \quad (36)$$

Substituting Equation (34) in Equation (21), the homogeneous mass density becomes

$$\rho = \frac{\alpha^2 f}{12\pi\left(1 - \gamma\right)\left(f - \alpha^2\right)^2} \frac{1}{t^2} \quad (37)$$

Using Equation (18), pressure becomes

$$p = \frac{\alpha^2 f \gamma}{12\pi\left(1 - \gamma\right)\left(f - \alpha^2\right)^2} \frac{1}{t^2} \quad (38)$$

From Equations (37) and (38), it is observed that:

When time $t \to \infty$, we get, density and pressure tending to zero *i.e.* the model reduces to vacuum. Also from Equation (31), we can verify that [$p = 0$ and $\rho = 0$ gives] $S = 1$. Which is consistent with the Kasner's condition for vacuum *i.e.* $S \equiv q_1 + q_2 + q_3 = 1$.

When $f = \alpha^2$, there is singularity in density and pressure.

There is also singularity in density and pressure for $\gamma = 1$.

From Equation (18), for $\gamma = 1$, we get $p = \rho$ which further gives [using Equation (31)] $S = 1$. In this case, we can interpret this result as "an anisotropic Kasner type universe can be considered to be filled with an ideal (non-viscous) fluid which has equation of state $p = \rho$ [stiff matter: the velocity of sound coincides with the speed of light].

Using Equation (34) in Equations (28)-(30) we get

$$t^{q_1} = D_1 K^{1/3} t^{\frac{f}{3\left(f - \alpha^2\right)}} \exp\left[\frac{X_1}{K}\left(1 - \frac{f}{\alpha^2}\right) t^{\frac{\alpha^2}{\alpha^2 - f}} \right] \quad (39)$$

$$t^{q_2} = D_2 K^{1/3} t^{\frac{f}{3\left(f - \alpha^2\right)}} \exp\left[\frac{X_2}{K}\left(1 - \frac{f}{\alpha^2}\right) t^{\frac{\alpha^2}{\alpha^2 - f}} \right] \quad (40)$$

$$t^{q_3} = D_3 K^{1/3} t^{\frac{f}{3\left(f - \alpha^2\right)}} \exp\left[\frac{X_3}{K}\left(1 - \frac{f}{\alpha^2}\right) t^{\frac{\alpha^2}{\alpha^2 - f}} \right] \quad (41)$$

where $K = \left\{ A_1\left(f - \alpha^2\right)\left[\frac{12\pi\left(1 - \gamma\right)}{\left(2\alpha^2 - f + \gamma f\right)} \right]^{1/2} \right\}^{\frac{f}{f - \alpha^2}}$ and

D_1, D_2, D_3 and X_1, X_2, X_3 are constants of integration, satisfying the relations $D_1 D_2 D_3 = 1$ and $X_1 + X_2 + X_3 = 0$.

4. Physical Properties

We define $a = \left(t^{q_1} t^{q_2} t^{q_3}\right)^{\frac{1}{3}}$ as the average scale factor so that the Hubble's parameter in our anisotropic models may be defined as

$H = \frac{\dot{a}}{a} = \frac{1}{3}\sum_{i=1}^{3} H_i$, where $H_i = \frac{\dot{a}_i}{a_i}$ are directional

Hubble's factors in the direction of x^i s respectively.

The expansion scalar θ is given by

$$\theta = 3H = \left(\frac{f}{f - \alpha^2} \right)\frac{1}{t} \quad (42)$$

The mean anisotropy parameter is given by

$$A = \frac{1}{3}\sum_{i=1}^{3}\left(\frac{\Delta H_i}{H} \right)^2$$

$$A = \frac{3X^2}{K^2}\left(\frac{f - \alpha^2}{f} \right)^2 t^{2\left(\frac{\alpha^2}{\alpha^2 - f} \right)} \quad (43)$$

The shear scalar σ^2 is given by

$$\sigma^2 = \frac{1}{2}\left(\sum_{i=1}^{3} H_i^2 - 3H^2 \right) = \frac{3}{2} A H^2$$

$$= \frac{X^2}{2K^2} t^{2\left(\frac{f}{\alpha^2 - f} \right)} \quad (44)$$

The deceleration parameter is given by

$$q = \frac{d}{dt}\left(\frac{1}{H} \right) - 1$$

$$q = 2 - \frac{3\alpha^2}{f}, \quad (45)$$

where $X^2 = X_1^2 + X_2^2 + X_3^2$

If $f > \alpha^2$ then for large t, the model tends to isotropic case.

Case I : $\gamma = 0$ **(Dust Universe) :**

In this case, we obtain the values of various parameters as

$$g = \frac{1}{f - \alpha^2}\left[\frac{\left(2\alpha^2 - f\right)}{12\pi} \right]^{1/2} \frac{1}{t}$$

$$C = \frac{1}{f - \alpha^2}\left[\frac{\left(2\alpha^2 - f\right)}{12\pi} \right]^{1/2} \log t$$

$$\rho = \frac{\alpha^2 f}{12\pi\left(f - \alpha^2\right)^2} \frac{1}{t^2},$$

$$t^{q_1} = D_1 K_1^{1/3} t^{\frac{f}{3\left(f-\alpha^2\right)}} \exp\left[\frac{X_1}{K_1}\left(1-\frac{f}{\alpha^2}\right)t^{\frac{\alpha^2}{\alpha^2-f}}\right]$$

$$t^{q_2} = D_2 K_1^{1/3} t^{\frac{f}{3\left(f-\alpha^2\right)}} \exp\left[\frac{X_2}{K_1}\left(1-\frac{f}{\alpha^2}\right)t^{\frac{\alpha^2}{\alpha^2-f}}\right]$$

$$t^{q_3} = D_3 K_1^{1/3} t^{\frac{f}{3\left(f-\alpha^2\right)}} \exp\left[\frac{X_3}{K_1}\left(1-\frac{f}{\alpha^2}\right)t^{\frac{\alpha^2}{\alpha^2-f}}\right]$$

where $K_1 = \left\{A\left(f-\alpha^2\right)\left[\dfrac{12\pi}{\left(2\alpha^2-f\right)}\right]^{1/2}\right\}^{\frac{f}{f-\alpha^2}}$

Here D_1, D_2, D_3 and X_1, X_2, X_3 are constants of integration, satisfying the relations $D_1 D_2 D_3 = 1$ and $X_1 + X_2 + X_3 = 0$.

In this case, the expansion scalar θ is given by

$$\theta = \left(\frac{f}{f-\alpha^2}\right)\frac{1}{t},$$

The mean anisotropy parameter is given by

$$A = \frac{3X^2}{K_1^2}\left(\frac{f-\alpha^2}{f}\right)^2 t^{2\left(\frac{\alpha^2}{\alpha^2-f}\right)}$$

The shear scalar σ^2 is given by

$$\sigma^2 = \frac{X^2}{2K_1^2} t^{2\left(\frac{f}{\alpha^2-f}\right)}$$

The deceleration parameter is given by

$$q = 2 - \frac{3\alpha^2}{f},$$

where $X^2 = X_1^2 + X_2^2 + X_3^2$

If $f > \alpha^2$, this model also tends to isotropy for large t .

Case II : $\gamma = \dfrac{1}{3}$ **(Disordered Radiation Universe)**

In this case, we obtain the values of various parameters as

$$g = \frac{1}{f-\alpha^2}\left[\frac{\left(3\alpha^2-f\right)}{12\pi}\right]^{1/2}\frac{1}{t}$$

$$C = \frac{1}{f-\alpha^2}\left[\frac{\left(3\alpha^2-f\right)}{12\pi}\right]^{1/2}\log t$$

$$\rho = \frac{3\alpha^2 f}{24\pi\left(f-\alpha^2\right)^2}\frac{1}{t^2},$$

$$p = \frac{\alpha^2 f}{24\pi\left(f-\alpha^2\right)^2}\frac{1}{t^2}$$

$$t^{q_1} = D_1 K_2^{1/3} t^{\frac{f}{3\left(f-\alpha^2\right)}} \exp\left[\frac{X_1}{K_2}\left(1-\frac{f}{\alpha^2}\right)t^{\frac{\alpha^2}{\alpha^2-f}}\right]$$

$$t^{q_2} = D_2 K_2^{1/3} t^{\frac{f}{3\left(f-\alpha^2\right)}} \exp\left[\frac{X_2}{K_2}\left(1-\frac{f}{\alpha^2}\right)t^{\frac{\alpha^2}{\alpha^2-f}}\right]$$

$$t^{q_3} = D_3 K_2^{1/3} t^{\frac{f}{3\left(f-\alpha^2\right)}} \exp\left[\frac{X_3}{K_2}\left(1-\frac{f}{\alpha^2}\right)t^{\frac{\alpha^2}{\alpha^2-f}}\right]$$

where $K_2 = \left\{A_1\left(f-\alpha^2\right)\left[\dfrac{12\pi}{\left(\alpha^2-f\right)}\right]^{1/2}\right\}^{\frac{f}{f-\alpha^2}}$.

Here D_1, D_2, D_3 and X_1, X_2, X_3 are constants of integration, satisfying the relations $D_1 D_2 D_3 = 1$ and $X_1 + X_2 + X_3 = 0$.

In this case, the expansion scalar θ is given by

$$\theta = \left(\frac{f}{f-\alpha^2}\right)\frac{1}{t} .$$

The mean anisotropy parameter is given by

$$A = \frac{3X^2}{K_2^2}\left(\frac{f-\alpha^2}{f}\right)^2 t^{2\left(\frac{\alpha^2}{\alpha^2-f}\right)}$$

The shear scalar σ^2 is given by

$$\sigma^2 = \frac{X^2}{2K_2^2} t^{2\left(\frac{f}{\alpha^2-f}\right)}$$

The deceleration parameter is given by

$$q = 2 - \frac{3\alpha^2}{f}$$

where $X^2 = X_1^2 + X_2^2 + X_3^2$ or $f > \alpha^2$, this model also tends to isotropy for large t .

5. Discussion

1) In both cases for $f > \alpha^2$, we get negative deceleration parameter indicating that the universe is accelerating. This observation is consistent with the present day observation.

2) The expansion scalar θ starts with an infinite value at $t = 0$, further gradually decreases & the expansion halts when $t = \infty$.

3) For $f > \alpha^2$, we get $\lim\limits_{t\to\infty}\dfrac{\sigma}{\theta} \neq 0$. Therefore, the models are isotropic for large value of *t*.

4) Also, we have noticed that matter density is inversely proportional to square of time *t*. When $t \to 0$, we

get $\rho \to \infty$ and when $t \to \infty$, we get $\rho \to 0$.

These are all physically valid results indicating that there is a situation where Kasner type *C*-field cosmology starts from infinite mass density.

5) In general, we have observed that the creation field *C* is proportional to time *t*. That is, the creation of matter increases as time increases.

6. References

[1] E. Kasner, "Geometrical Theorem on Einstein's Cosmological Equations," *American Journal of Mathematics*, Vol. 43, No. 2, 1921, pp. 217-221.

[2] E. Kasner, "An Algebraic Solution of the Einstein Equations," *Transactions of the American Mathematical Society*, Vol. 27, No. 1, 1925, pp. 101-105.

[3] J. V. Narlikar and T. Padmanabhan, "Creation-Field Cosmology: A Possible Solution to Singularity, Horizon, and Flatness Problems," *Physical Review D*, Vol. 32, No. 8, 1985, pp. 1928-1934.

[4] G. F. Smoot, *et al.*, "Structure in the COBE Differential Microwave Radiometer First-Year Maps," *Astrophysical Journal*, Vol. 396, No. 1, 1992, pp. 21-25.

[5] J. V. Narlikar, *et al.*, "Inhomogeneities in the Microwave Background Radiation Interpreted within the Framework of the Quasi-Steady State Cosmology," *Astrphysical Journal*, Vol. 585, No. 3, 2003, pp. 1-11.

[6] F. Hoyle, "A New Model for the Expanding Universe," Monthly Notices of the Royal Astronomical Society, Vol. 108, No. 1748, 1948, pp. 372-382.

[7] H. Bondi and T. Gold, "The Steady-State Theory of the Expanding Universe," *Monthly Notices of the Royal Astronomical Society*, Vol. 108, No. 3, 1948, pp. 252-270.

[8] F. Hoyle and J. V. Narlikar, "A Radical Departure from the 'Steady-State' Concept in Cosmology," *Proeedings of Royal Society (London) A*, Vol. 290, No. 1421, 1966, pp. 162-176.

[9] F. Hoyle and J. V. Narlikar, "Mach's Principle and the Creation of Matter," *Proceedings of Royal Society (London) A*, Vol. 273, No. 1352, 1963, pp. 1-11.

[10] F. Hoyle and J. V. Narlikar "The C-Field as a Direct Particle Field," *Proceedings of Royal Society (London) A*, Vol. 282, No. 1389, 1964, pp. 178-183.

[11] S. Chatterjee and A. Banerjee, "C-Field Cosmology in Higher Dimensions," *General Relativity Gravitation*, Vol. 36, No. 2, 2004, pp. 303-313.

[12] R. Bali and R. S. Tikekar, "C-Field Cosmology with Variable G in the Flat Friedmann-Robertson-Walker Model," *Chinese Physics Letters*, Vol. 24, No. 11, 2007, pp. 3290-3292.

[13] R. Bali and M. Kumawat, "C-Field Cosmological Models with Variable G In FRW Space-Time," *International Journal of Theoretical Physics*, Vol. 48, No. 3, 2009, pp. 3410-3415

[14] T. Singh and R. Chaubey, "Bianchi type-I, III, V, VI and Kantowski-Sachs Universes in Creation-Field Cosmology," *Astrophysical Space Scence*, Vol. 321, No. 1, 2009, pp. 5-18.

Scientific Research

A Cooling System with a Fan for Thermal Management of High-Power LEDs

Ruishan Wang[1,2], Junhui Li[1,2,3]

[1]*School of Mechanical and Electronical Engineering, Central South University, Changsha, China*
[2]*Key Laboratory of Modern Complex Equipment Design and Extreme Manufacturing,*
Ministry of Education, Changsha, China
[3]*State Key Lab of Digital Manufacturing Equipment & Technology, Wuhan, China*
E-mail: lijunhui@mail.csu.cn, wangruishan86@126.com
Received May 27, 2010; revised July 18, 2010; accepted July 30, 2010

Abstract

To improve the heat dissipation of high-power light-emitting diodes (LEDs), a cooling system with a fan is proposed. In the experiment, the LEDs array of 18 W composed of 6 LEDs of 3 W is used and the room temperature is 26ºC. Results show that the temperature of the substrate of LEDs reaches 62ºC without the fan, however, it reaches only 32ºC when the best cooling condition appears. The temperature of the LEDs decreases by 30ºC since the heat produced by LEDs is transferred rapidly by the fan. The experiment demonstrates that the cooling system with the fan has good performance.

Keywords: High-Power Leds, Cooling System, Heat Dissipation, The Fan, Data Acquisition Card

1. Introduction

Light emitting diodes (LEDs), generally used for indicator lights, have been developed for the past 50 years. Recently, with the emergence of high power LEDs, they are received more and more attention, and have begun to play an important role in many applications. Typical applications include back lighting for cell phones and other LCD displays, interior and exterior automotive lighting including headlights, large signs and displays, signals and illumination, traffic lights, spot lights, and so on [1,2].The extensive applications are due to the distinctive advantages towards incandescent lamp and daylight lamp, such as high brightness, small size, ease of integration, anti-mechanical damage, all solid-state, environmental protection, lower power cost, long life, and high efficiency, good reliability, variable color, etc. So, LEDs are called the fourth generation light or green light [3,4], and have been foreseen as an "ultimate lamp" for the future [5]. However, based on the current semiconductor manufacture technology, only 5%-10% of the input power will transfer into light energy, the remaining will transfer into heat while the chip size is only 1×1 mm-2.5×2.5 mm, the heat flux is very high. If the heat can not dissipate in short time, it will lead excessive temperature, shorten the life, and thermal stress will damage the LEDs chip. So, effective thermal management is the critical factor for the efficiency, reliability, and life of LEDs, especially for high power LEDs, thermal manage-

ment has become the development bottleneck of LEDs [6-8].

To address the thermal problem of LEDs, many investigators have researched interrelated thermal management of LEDs:

LUO and LIU [9] proposed a closed microjet cooling system for LEDs thermal management. By optimizing the microjet array device's parameters, the cooling system was used for cooling a 220 W LED lamp, and the temperature tests demonstrate it can effectively cool the total system. Zhang *et al.* [10] used MWNT and carbon black to improve the thermal performance of TIM in high-brightness light emitter diode (HB-LED) packaging. Thermal interface material was developed to achieve the thermal conductivity of about 0.6 W/m·K with 2 wt% nitric acid treated CNT and 10 wt% carbon black. The output light power of the 1×1 mm 2 HB-LED device with the developed TIM can achieve 62 mW with the input current of 300 mA. Yuan *et al.* [11] described a process of applying a FEA technique to simulate and analyses a light emitting diode (LED) array integrated in microchannel cooler module. The cooling module with different internal configurations, heat source density, and heat dissipation capacity corresponding with different flow velocity are investigated. From the analysis, the special design of internal staggered fins in microchannel cooler could reduce the average die temperature, the difference in temperature and the flow resistance compared to straight fins in microchannel cooler.

Liu *et al.* [12] introduced a method of thermal design and module of thermal resistance of High-power LED; and describes heat dissipation design for illumination High-power LED arrays. The results proved that the radiator designed can control the maximum junction temperature of LED chip within 70℃ under the condition that all chips work in full-load and the environment temperature is 40℃. Zhang *et al.* [13] studied the effect of thermal conductive coating on the thermal management of LED lamps with different color and packing number used in a close un-der-water environment. Experiment result shows that the thermal conductive coating used on LED integrated circuit board can increase the thermal release efficiency of LED. And the higher the thermal conductivity is, the better the effect of thermal management is.

In this paper, a cooling system with a fan is proposed. Several conditions at different input power of the fan are conducted to investigate its effect on thermal management of high power LEDs. For achieving relatively exact tem-perature in LEDs, a K-type thermocouple is welded into the substrate of LEDs, and its signal is collected by using data acquisition system. Based on the detected temprature, the cooling ability of the system is evaluated.

2. Experimental

Figure 1 demonstrates the cooling system. It composes of a radiator including cooling fins and a fan. In the sys-tem, the LEDs and cooling fins is connected through thermal conductive silicone grease. It can be seen that the system is very simple and convenient, and the room it required is very small.

The light source module is composed of six LEDs in tandem mode. (The LED, which type is XL-HP3WHWC, the diameter of substrate is 20 mm, the emitted color is white, and the limit power is 3 W). The total power con-sumption of the 2×3 array is added up to be 18 W. The radiator is 80 mm $\times$ 95 mm. The fan's model is 3110KL-04W-B50. The temperature of heat dissipation substrate of LEDs is measured by K-type thermocouple, the mea-surement error of which is about 0.5℃ at the temperature range from –30℃ to 150℃.

Experimental system is constructed as shown in **Fig-ure 2** DC power supply of LEDs is special electrical source of LEDs, and its power is $6 \times 3 W = 18 W$. In the experiment, the junction temperature could not be achieved directly, so, the substrate of LEDs is measured. Although there is difference temperature between the heat dissipation substrate of LEDs and the junction tem-perature, it is feasible using the former to check the cooling ability of the proposed concept since it can re-flect the latter intuitively. At the beginning, in order to study the heat dissipation effect of the fan, a couple of comparative experiments are conducted under the condi-tion without the fan and the input power of the fan is
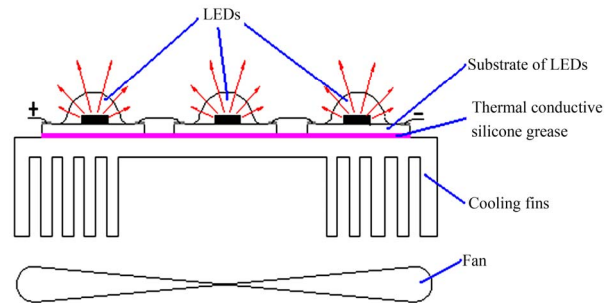
Figure 1. The cooling system.
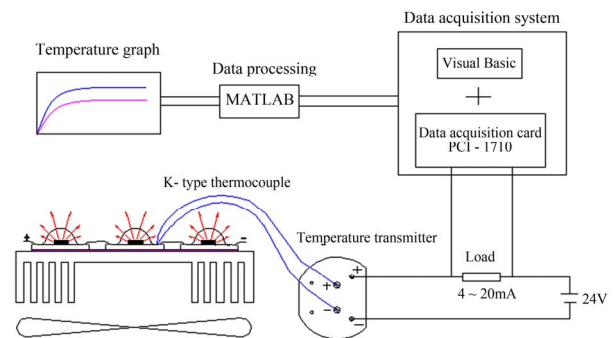
Figure 2. The experimental system.

2.13 W respectively. Then, a set of experiments are con-ducted to study the effect of different input power of the fan on the thermal management of high-power LEDs.

In the experiment, a temperature transmitter is used to transform the signal of temperature from the thermocou-ple into that of voltage which can be acquired by using the data acquisition card (PCI-1710). The acquisition frequency is 0.1 s. Then, the signal of voltage is trans-formed into the signal of temperature through the for-mula describing the relationship between the temperature and the voltage. After the signal of temperature is filtered with the software of MATLAB, the temperature graph can be found which demonstrates the cooling effect of the system.

3. Results and Analysis

After the signature of temperature is filtered with the software of MATLAB, the temperature graphs of LEDs are found as follows:

3.1. Without the Fan and the Input Power of the Fin is 2.13 W

Figure 3 shows the temperature variations of substrate of LEDs with time without the fan and at the input power of the fan 2.13 W. It can be seen that the temperature of substrate of LEDs increases continuously up to 62℃ and still has a rising trend without the fan, however, it reach-es the maximum about 32.5℃ in short time and remains
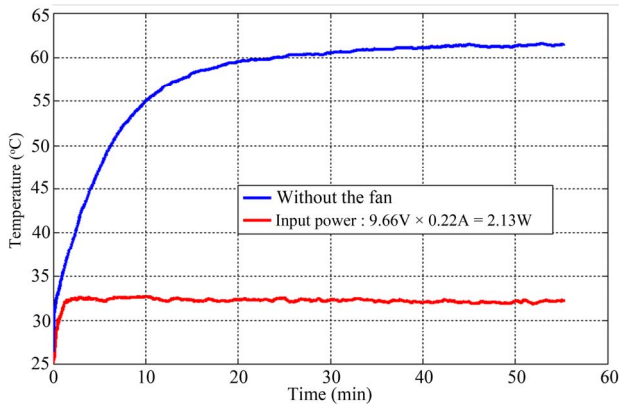
Figure 3. The temperature variations of substrate of LEDs with time without the fan and at the input power of the fan 2.13 W.

steady by using the fan. The above result is easy to understand that the heat generated by LEDs conducts to the cooling fins, if the heat of cooling fins does not released into the environment in time, the temperature of LEDs will increases continually. In the designed system, the main approach of heat exchange between the system and environment is natural convection though cooling fins when the fan is not used. However, when the fan works, it is forced convection, and the effect of heat exchange will be effectively improved. This indicated that the fan has a good performance on the thermal management of high-power LEDs.

3.2. The Different Input Power of the Fan

Figure 4 shows the temperature variations of substrate of LEDs with time at different input power of the fan. It can be seen that the temperature of substrate of LEDs will reach a steady value within 5 mins when the fan is used, and the steady temperatures are different with the different input power of the fan. The maximum and minimum
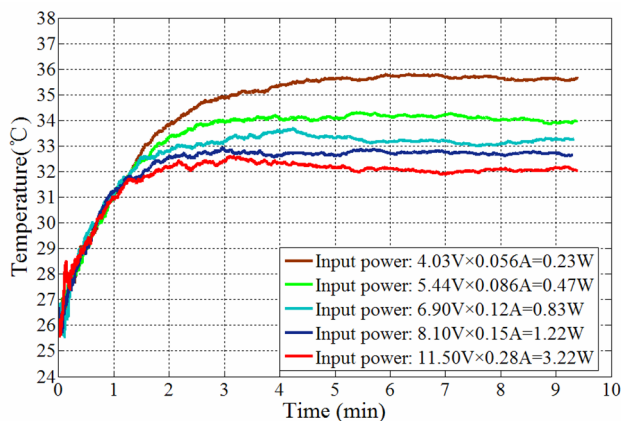
Figure 4. The temperature variations of substrate of LEDs with time at different input power of the fan.

temperature is 35.6°C and 32°C when the input power is 0.23 W and 3.22 W respectively. The higher the input power is, the lower the steady temperature is. As the enlargement of input power, forced convection enhanced, fluid can quickly remove LED heat, leading to the lower temperature of the substrate of LEDs, while the running cost is correspondingly increased. In the practical applications based on the above experiment, a choice should be made to achieve a balance between the cooling effect and the power consumption of the system. **Figure 4** shows that 0.83 W and 1.22 W of the system is appropriated.

4. Conclusions

A cooling system with a fan is presented to improve the heat dissipation of high-power LEDs. Several conditions at different input power of the fan are conducted. The experimental result demonstrates that the cooling system with the fan has a good performance on the thermal management of high-power LEDs. The minimum temperature is only 32°C when the fan is applied and the environment temperature is 26°C, while it reaches 62°C without the fan. With the increasing of the input power, however, the cooling performance improves slightly, so, in practical applications, appropriate input power should be selected to achieve a good balance between the cooling effect and the power consumption of the system.

5. Acknowledgements

6. References

[1] W. H. Chi, T. L. Chou, C. N. Han and K. N. Chiang, "Analysis of Thermal Performance of High Power Light Emitting Diodes Package," *International Conference on Electronics Packaging Technology*, Nanjing, 2008, pp. 533-538.

[2] X. Luo, W. Xiong and S. Liu, "A Simplified Thermal Resistance Network Model for High Power LED Street Lamp," *International Conference on Electronic Packaging Technology & High Density Packaging*, Shanghai, 2008, pp. 1-7.

[3] B. Li, "Lumen Efficiency of 1 W-Level High Power White LED," *Semiconductor Optoelectronics*, Vol. 26, No. 4, 2005, pp. 314-316.

[4]   X. He, B. Cheng, L. Yin and J. Zhang, "Testing System for Thermal Resistance of High-Power LED," *Electronic Measuremient Technology*, Vol. 31, No. 9, 2008, pp. 17-20.

[5]   N. Holonyak, "Is the Light Emitting Diode (LED) an Ultimate Lamp?" *American Journal of Physics*, Vol. 68, No. 9, 2000, pp. 864-868.

[6]   W. Dai, J. Wang and Y. Li, "Transient Thermal Analysis of High-power LED Package," *Semiconductor Optoelectronics*, Vol. 29, No. 3, 2008, pp. 324-328.

[7]   B. Yu and Y. Wang, "Junction Temperature and Thermal Resistance Restrict the Developing of High-power LED," *Chinese Journal of Luminescence*, Vol. 26, No. 6, 2005, pp. 761-766.

[8]   N. Narendran and Y. Gu, "Life of LED-Based White Light Source," *IEEE/OSA Journal of Display Technology*, Vol. 1, No. 1, 2005, pp. 167-171.

[9]   X. Luo and S. Liu, "A Microjet Array Cooling System for Thermal Management of High-Brightness LEDs," *IEEE Transactions on Advanced Packaging*, Vol. 30, No. 3, 2007, pp. 475-484.

[10] K. Zhang, G. Xiao, C. Wong, H. Gu and B. Xu, "Study on Thermal Interface Material with Carbon Nanotubes and Carbon Black in High-Brightness LED Packaging with Flip-Chip Technology," 55*th Electronic Components and Technology Conference*, Lake Buena Vista, 2005, pp. 60-65.

[11] L. Yuan, S. Liu, M. Chen and X. Luo, "Thermal Analysis of High Power LED Array Packaging with Microchannel Cooler," 7*th International Conference on Electronic Packaging Technology* (*ICEPT* '06), Shanghai, 2006, pp. 1-5.

[12] Y. Liu, G. Fu, C. Gao, X. Li and S. Wang, "Thermal Analysis of Illumination High-Power LED," *Chinese Journal of Electron Devices*, Vol. 31, No. 6, 2008, pp. 1716-1719.

[13] S. Zhang, L. Fang, G. Fu, X. Tan, J. Dong, Y. Chen and L. Gao, "Effect of Thermal Conductive Coating on Thermolysis Property of LED," *Semiconductor Optoelectronics*, Vol. 28, No. 6, 2007, pp. 793-796.

Call for Papers

Journal of
Modern Physics

ISSN Print: 2153-1196   ISSN Online: 2153-120X

http://www.scirp.org/journal/jmp/

Journal of Modern Physics(JMP) is an international journal dedicated to the latest advancement of modern physics. The goal of this journal is to provide a platform for scientists and academicians all over the world to promote, share, and discuss various new issues and developments in different areas of modern physics.

Editor-in-Chief

Prof. Victor Yashnikov	Russian Academy of Sciences, Russia

Executive-Editor-in-Chief

Dr. Marko Markov	Erie Community College, USA

Editorial Board

Managing Executive Editor

Prof. Chang Liu	Wuhan University, China

Subject Coverage

Journal of Modern Physics publishes original papers including but not limited to the following fields:

Theoretical High Energy Physics	Materials Sciences and Technology
Biophysics and Medical Physics	Nuclear Science and Engineering
Earth and Planetary Sciences	Computational Physics
Instrumentation and Measurement	Interdisciplinary Physics
Plasma Physics	Other Topics in Physics

We are also interested in: 1) Short Reports—2-5 page papers where an author can either present an idea with theoretical background but has not yet completed the research needed for a complete paper or preliminary data; 2) Book Reviews—Comments and critiques.

Notes for Intending Authors

Submitted papers should not have been previously published nor be currently under consideration for publication elsewhere. Paper submission will be handled electronically through the website. All papers are refereed through a peer review process. For more details about the submissions, please access the website.

Website and E-Mail

http://www.scirp.org/journal/jmp   E-mail: jmp@scirp.org

TABLE OF CONTENTS

Volume 1   Number 3   **August 2010**